EFFECT OF INHALED CORTICOSTEROID ON CT LUNG DENSITY

EFFECT OF INHALED CORTICOSTEROID ON CT-DERIVED LUNG DENSITY IN AN *IN VIVO* ALLERGIC INFLAMMATION MODEL

A Budesonide Dose Response Study

By

Kristi L. Lindsay

B.Sc in Chemistry and Biology

A Thesis

Submitted to the School of Graduate Studies

In Partial Fulfilment of the Requirements for the

Degree Masters of Science

McMaster University

September-25-12

MASTER OF SCIENCE (2012) McMaster University

(Physiology and Pharmacology) Hamilton, Ontario

TITLE: Effect of Inhaled Corticosteroid on CT-derived Lung Density in an *in vivo* Allergic Inflammation Model

AUTHOR: Kristi L. Lindsay, B.Sc. (Georgia Southern University, GA, USA)

SUPERVISOR: Dr. N. R. Labiris

SUPERVISORY COMMITTEE: Dr. N. R. Labiris

Dr. T. H. Farncombe

Dr. M. Jordana

NUMBER of PAGES: xiii, 120

ABSTRACT

Allergic asthma is a disease involving airway inflammation, commonly linked to allergen exposure. Computed tomography (CT) is used to quantitatively assess changes in density, hence inflammation, in the lung. CT imaging provides the ability to non-invasively and longitudinally study disease progression and evaluate treatment efficacy. The objective of this study was to determine the sensitivity of CT to detect the anti-inflammatory effects of budesonide (BUD) by measuring airway tissue density in a rat model of allergic airway disease.

Female Brown Norway rats were exposed intratracheally to house dust mite (HDM) extract (250 μg in 100μL saline) or saline control every other day for a total of five administrations (inflammatory phase). A BUD dose and temporal response study was performed using BUD 0, 10, 100, and 300 μg/kg administered concurrently with HDM for three and six treatments (treatment phase). CT scanning was performed at baseline, post inflammatory phase, and after three and six BUD treatments. From the CT, density was measured in a defined volume of interest surrounding the major airways. Bronchoalveolar lavage (BAL) and histological samples were collected at the same time points.

After the inflammatory phase, a significant increase in peribronchial density was found in the HDM group compared to controls. This corresponded to a significant increase in inflammation by histology and BAL total cell count (TCC), specifically eosinophils. Within the treatment phase after three treatments, BUD 100 and 300 μg/kg led to a significant shift in lung density compared to HDM exposure alone, to a state similar to baseline. All BUD treated groups expressed a significant reduction in peribronchial density after six treatments. However, histology and BAL TCC only showed a significant decrease in inflammation after six treatments for all three BUD doses.

CT densitometry is a sensitive, non-invasive method of evaluating the anti-inflammatory effects of budesonide and can be used for future screening of therapies in allergic lung models. Airway segmentation of CT permits the localized assessment of peribronchial inflammation, while other outcome measurements, such as BAL cytology, provide whole lung assessment which may not accurately reflect important regional changes.

ACKNOWLEDGEMENTS

I would like to thank my family and friends for their encouragement and support through this experience. I would especially like to thank my mother, Kerry Lindsay, and my father, David Lindsay, for encouraging and providing me with the ability to accomplish my goals. Thanks also go to my supervisor, Dr. Renee Labiris, for your time and patience and for teaching me to become a better writer, thinker, and scientist; to my committee members, Dr. Manel Jordana and Dr. Troy Farncombe, for your constructive criticism and intellectual input; to the Small Animal Medical Imaging Facility at McMaster, and to Rod Rhem and Chantal Saab for their assistance and expertise with the CT machine; and finally, to the Labiris lab, Bill Counter and Brian Jobse, for being great mentors and providing an entertaining workplace.

TABLE OF CONTENTS

LIST OF FIGURES

LIST OF TABLES

LIST OF ABBREVIATIONS AND SYMBOLS

1. AHR: Airway hyperresponsiveness
2. FVC: Forced vital capacity
3. FEV_1: Forced expiratory volume in 1 second
4. TLC: Total lung capacity
5. BAL(F): Bronchoalveolar lavage (fluid)
6. HDM: House dust mite
7. OVA: Ovalbumin
8. BN: Brown Norway rat
9. IL: Interleukin
10. TNF-α: Tumor necrosis factor-alpha
11. DPI: Dry powder inhaler
12. BUD: Budesonide
13. MRI: Magnetic resonance imaging
14. CT: Computed tomography
15. HU: Hounsfield units
16. PET: Positron emission tomography
17. SPECT: Single proton emission computed tomography
18. COPD: Chronic obstructive pulmonary disorder
19. IT: Intratracheally
20. BL: Baseline
21. ROI: Region of interest
22. TCC: Total cell counts
23. PBS: Phosphate buffered saline
24. RBG: Red blue green scale
25. ELISA: Enzyme-linked immunosorbent assay
26. ANOVA: Analysis of variance
27. SEM: Standard error of the mean

CHAPTER 1

1 INTRODUCTION

This thesis examined small animal CT imaging as an effective, non-invasive evaluation of biological processes, such as inflammation, without the need for serial sacrifice of animals. It was used in a longitudinal study to characterize asthma progression and evaluate the ability of CT to measure the efficacy of corticosteroids with animals serving as their own controls. This was achieved by comparing CT densitometry of the large airways in a model of allergic airway disease with corticosteroid treatment.

1.1 Asthma

Allergic asthma is a health problem that affects millions worldwide. It is now understood that asthma is a chronic disease caused by many different types of exposures, including allergens, leading to airway hyperresponsiveness (AHR), inflammation, and airway remodelling (Schoor *et al*. 2000, Kasahara *et al.* 2002, Fahy 2009). Asthma is characterized by airway smooth muscle thickening, subepithelial fibrosis, collagen deposition, goblet cell hyperplasia, myofibroblast hyperplasia, and epithelial cell hypertrophy (Elias 2000, Barnes 2008). The specific immune events that can lead to a person becoming asthmatic are not currently understood. What is known is that chronic exposure to common allergens can lead to allergic sensitization causing airway obstruction, which is variable and reversible (Barnes 2008, Bogaert *et al.* 2009).

1.1.1 *Mechanisms of Asthma*

Asthma is an inflammatory disease of the airways defined by physiological changes induced by obstruction, inflammation, and AHR (Barnes 2008, GINA 2009). Early phase

(acute) allergic asthmatic develops an increase in sensitivity and responsiveness to inhaled allergen roughly 10 minutes after exposure. This causes bronchoconstriction with the increase in mucus production, dyspnea, wheezing, and coughing in patients (Bousquet *et al.* 2000, Basdemir *et al.* 2001, Bogaert *et al.* 2009). The early asthmatic response is characterized by the rapid activation of airway mast cells, macrophages, basophils, histamines, proteases, and T-helper lymphocytes. The T-helper lymphocytes lead to the production of cytokines, such as interleukin IL-3, IL-4, IL-5, IL-6, IL-9, IL-10, IL-13, interferon (IFN)-γ, and tumour necrosis factor α (TNF-α) (Holgate 1993, Anderson & Morrision, 1998, Bloemen *et al.* 2007). These activated cells rapidly induce microvascular leakage with exudation of plasma into the airways (Bousquet *et al.* 2000). Additionally the asthmatic response over expresses IgE from B cells and an increase in eosinophils which are present in large numbers in the blood, sputum, and bronchoalveolar lavage fluid (BALF) (Bousquet *et al.* 1990, Anderson & Morrision 1998, Rosi *et al.* 1999). The late phase allergic response occurs anywhere from 3 to 10 hours after the initial allergic reaction. As the asthma attack prolongs, more severe congestion and excessive inflammation of the airways materialize leading to progressive, persistent, and severe airway obstruction than seen in the early phase allergic response (Lancas *et al.* 2005, Bloemen *et al.* 2007). This airway obstruction is due to the thickening of the mucosa, oedema, and infiltration of inflammatory cells into the lungs, including eosinophils, $CD4^+$ T cells, mast cells, fibroblasts, basophils, neutrophils, and macrophages which are released by the bone marrow before being recruited by the airway walls (Drazen *et al.* 1996, Bousquet *et al.* 2000, Basdemir *et al.* 2001, Barnes 2008,

Bogaert *et al.* 2009). Eosinophils continue to release pro-inflammatory mediators, cytotoxic mediators, and cytokines, producing vascular leakage, hypersecretion of mucus, smooth muscle contraction, epithelial shedding, and bronchial hyperresponsiveness (Bousquet *et al.* 2000). Late phase asthma also involves airway inflammation which initiates remodelling if not treated, resulting in decreased lung function (Drazen *et al.* 1996, Bousquet *et al.* 2000, Bloemen *et al.* 2007, Bogaert *et al.* 2009). Remodelling of the airways includes structural changes such as smooth muscle hypertrophy, goblet cell hyperplasia, epithelial and subepithelial fibrosis by deposition of collagen, and increased vascularization (Ahn *et al.* 2007, Bogaert *et al.* 2009).

1.1.2 *Clinical Diagnosis*

Pulmonary function testing is used to measure lung volume, bronchial obstruction, gas exchange, lung compliance, and ventilatory capacity (Behr & Furst, 2008). Spirometry is the main test clinicians administer to measure the mechanical function of the lungs, chest wall, and respiratory muscles by evaluating the forced vital capacity (FVC), forced expiratory volume in 1 second (FEV_1), and the total volume of air exhaled from a full lung (total lung capacity; TLC) to an empty lung (residual volume) (Morris, 1976). A diagnosis of asthma is made based on symptoms presented, such as shortness of breath, cough, and wheezing, in addition to a $\geq$ 20% reduction in FEV_1 after inhaled methacholine, a muscarinic receptor agonist that causes bronchoconstriction ($\leq$ 8 mg/ml) (Rosi *et al.* 1999, Sont *et al*. 1999, Fujimura *et al.* 2005). Impaired lung function does not allow a specific diagnosis to be made, but facilitates the assessment of the presence or absence and the severity of lung disease (Behr & Furst, 2008).

1.1.3 *Animal Asthma Models*

Asthma is not a disease naturally found in rats or mice, but many methods have been developed to stimulate asthma-like response for further investigation into the disease (Johnson *et al.* 2004, Jobse *et al.* 2009, Cates *et al.* 2004). Sensitizing the rat topically, subcutaneous, or sublingually for a specified duration will initiate asthma mechanisms by overexpressing inflammatory mediators while exposure to allergen induces an immune response (Fulkerson *et al*. 2005, Jobse *et al.* 2009, Senti *et al.* 2009, Incorvaia *et al.* 2010). The duration of the sensitization phase differs between models. For intratracheal administration with allergens such as house dust mite (HDM), 7 to 10 days of exposure results in peribronchial, perivascular, and parenchymal inflammation (Johnson, *et al*. 2004, Jobse *et al.* 2009).

To date, most models of allergic asthma have employed ovalbumin (OVA) relying on intraperitoneal delivery and coupling of an adjuvant, such as aluminium hydroxide, to elicit systemic sensitisation followed by an airway challenge to induce an inflammatory response (Cates *et al*. 2007). Not only does respiratory exposure to OVA lead to inhalation tolerance, thus reducing the physiological response and requiring a larger dose to provide the given response, but there have been problems in the assessment of repetition and maintenance of chronic inflammation in the lungs (Ahn *et al*. 2007). Many researchers have looked towards the use of HDM as it has been found to be more successful than OVA at producing a model with concurrent AHR, airway remodelling, and eosinophilic inflammation (Johnson *et al*. 2004). The species *Dermatophagoides pteronyssinus* is a frequently implicated source of mite allergens in subjects with

respiratory allergy. Although whole mite extracts are complex from an immunological perspective, they are ultimately more representative of real-life allergen exposure (Cates *et al*. 2004). Cates *et al*. showed that the intranasal administration of this whole mite extract to mice, in the absence of exogenous adjuvants for 10 consecutive days, leads to a robust inflammatory response (Cates *et al*. 2004). Chronic exposure to HDM has been shown drive airway remodelling, chronic eosinophilic inflammation, and AHR (Whitty 2011, Johnson *et al*. 2004, Southam *et al*. 2008).

Rats are a commonly used species for preclinical studies of pulmonary disease as they provide the ability to study mechanisms of disease that affect lung structure and function (Werner-Klein *et al.* 2008, Jobse *et al.* 2009). The Brown Norway (BN) rat has been used in numerous models of allergic inflammation since this animal develops both early and late airway responses, with increased bronchial hyperresponsiveness, elevated IgE, and airway eosinophilia in response to active immunization to inhaled allergen challenges. (Hylkema *et al.* 2002, Singh *et al.* 2003, Ellis *et al.* 2004, Percy *et al*. 2008, Werner-Klein *et al.* 2008, Jobse *et al.* 2009, Brange *et al*. 2009). These preclinical models are not an identical replication of the human disease, but do impart valuable information regarding the infiltration of specific cell types, changes in lung density, and remodelling in response to allergen exposure.

1.2 Asthma Treatments

Inhaled corticosteroids are the first line therapy for long-term management of asthma (Horvath *et al*. 2006). They have become established as the most potent anti-inflammatory agents in the pharmacotherapy of various chronic inflammatory diseases,

including asthma (Horvath *et al*. 2006). Inhaled corticosteroids have a rapid suppressive effect on airway inflammation, and an increased dose is often used during exacerbations to prevent the increase in airway inflammation (Barnes, 2008). Corticosteroids exert their effects by binding to cytoplasmic glucocorticoid receptors, which are mainly localized in airway epithelial cells and the endothelium of the bronchial vasculature (Goldsmith *et al*. 2004). Stimulation of these receptors leads to down-regulation of pro-inflammatory mediators, such as cytokines interleukin 1 (IL-1), interleukin 6 (IL-6), and tumor necrosis factor-alpha (TNF-α). Corticosteroids also control inflammation by increasing the transcription of anti-inflammatory genes and decreasing the transcription of inflammatory genes (Barnes, 1998). Budesonide (BUD), an inhaled corticosteroid, has been used since 1980 as a dry powder inhaler (DPI) or nebulised suspension (Abdullah *et al*. 2007). Research has shown that budesonide dosing significantly reduces sputum eosinophils clinically and attenuates bronchial inflammation in an allergic rat model (Bandi and Kompella, 2001, Gibson *et al.* 2001, Basdemir *et al.* 2001).

Long-acting bronchodilators are inhaled treatment used simultaneously with inhaled corticosteroids when steroids are unable to completely control asthma symptoms (Kelly, 2008). This combination asthma therapy, such as budesonide and formoterol, works by keeping the airways open and the muscles relaxed (Kelly, 2008). Brange *et al.* has shown clinically that budesonide/formoterol dosing improves the control of asthma exacerbations and inhibited both airway/lung inflammation and increased airway contractility in an allergic Brown Norway rat model (Brange *et al.* 2009). Leukotriene receptor agonists are an asthma therapy that protect against bronchoconstriction (Leff *et*

al. 1998). Additional short-term rescue medications are used to provide quick relief to sudden onset of asthma exacerbations. Short-acting bronchodilators reduce symptoms such as shortness of breath, chest tightness, wheezing, and cough (Reinke and Hoffman, 2000).

1.2.1 *Pharmacology of Corticosteroids*

Corticosteroids are administered by inhalation causing higher concentrations to target the airway mucosa and limiting exposure in the rest of the body. They have a high receptor affinity, first-pass liver and gut inactivation, and prolonged local concentration in the airways (Miller-Larsson *et al.* 1998). Corticosteroids are the most effective drugs to suppress airway inflammation, mainly by down-regulation of pro-inflammatory proteins (Horvath *et al*. 2006). They moreover reverse some components of asthma-induced structural changes, including vascularity of the bronchial wall and collagen deposition(Chanez *et al.* 2004, Horvath *et al*. 2006).

Budesonide is a potent glucocorticosteroid that controls the inflammatory process through its genomic actions on a variety of cells and mediators (Hayashi *et al.* 2004). It has a high affinity for the cytoplasmic glucocorticoid receptors present in airway epithelial cells, the endothelium of the bronchial vasculature, and elsewhere in the lung tissue (Horvath *et al*. 2006, Goldsmith *et al*. 2004). This mechanism alters transcription of pro-inflammatory genes by repression of the transcription factors activator protein-1 (AP-1) and nuclear factor kappa B (NF-κB) by decreasing the expression of various genes that encode for inflammatory mediators, such as IL-6, IL-8, and TNF-α (Bandi *et*

al. 2001, Hayashi *et al.* 2004, Horvath *et al*. 2006, Goldsmith *et al*. 2004). Additionally, as inhaled budesonide saturates these receptors, excess forms esters with long-chain fatty acids, resulting in the formation of inactive budesonide esters (Kelly 2003). This suggests that reversible esterification may lead to the slow release of active budesonide at the targeted site of activity (Tunek *et al.* 1997, Miller-Larsson *et al.* 1998, Kelly 2003). Non-genomic actions are initiated by specific interactions with membrane-bound or cytoplasmic glucocorticoid receptors, or non-specific interactions with the cell (Horvath *et al*. 2006). Potential mechanisms of action include a reduction in the eosinophil infiltrate, inhibition of vascular exudation, and inhibition of mucous secretion (Gibson *et al*. 2001).

Small animal models of pulmonary disease are rapidly developing into the standard for better understanding of disease physiology and new drug development (Farncombe 2008). In an asthma model, inhaled glucocorticoids have been shown to reduce antigen-induced infiltration of BAL fluid eosinophils, lymphocytes, and neutrophils in Brown Norway rats (Xu *et al*. 2000). Budesonide inhibited airway smooth muscle growth and central airway goblet cell hyperplasia following ovalbumin challenges in Brown Norway rats. In addition, budesonide inhibited small but not large airway total wall area smooth muscle growth and central airway goblet cell hyperplasia and did not inhibit airway hyperresponsiveness after repeated challenge (Siddiqui *et al.* 2010). Budesonide also rapidly inhibited the histamine-induced contractions of airway smooth muscle mediated by non-genomic mechanisms using tracheas from albino Hartley guinea pigs (Sun *et al.* 2006). In a radiolabeling study that used intratracheal instillation of tritium-labeled

budesonide and fluticasone in rats, 25% of the budesonide dose and 7% of the fluticasone dose remained in the trachea at 6 hours. After 24 hours, the difference between the two inhaled steroids was 30-fold in favour of budesonide (3.2% vs. 0.09%, respectively, of radioactivity measured at 20 minutes), suggesting prolonged retention of budesonide in the lungs (Kelly, 2003). In Sprague-Dawley rats exposed to bleomycin and assessed by magnetic resonance imaging (MRI), a diffuse signal was associated with induced inflammation and confirmed by histology. Budesonide treatment resulted in decreased MRI signals 24 hours post corticosteroid administration. Conversely, budesonide therapy did not completely resolve the signal but histology did show a decrease in inflammation (Babin *et al.* 2011).

1.2.2 *Clinical Application*

A major goal of asthma treatment is to manage the symptoms with the least amount of treatment mediation (Brange *et al.* 2009). There is evidence that inhaled corticosteroid therapy induces clinically important rapid changes in pulmonary function, whereas systemic corticosteroids probably require >6 h to 24 h to improve pulmonary function (Horvath *et al.* 2006). The aim of inhaled corticosteroid therapy is to employ strong local anti-inflammatory effects in the airways with low risk of unwanted local and systemic effects (Kelly, 2003).

Targeting treatment to the eosinophilic airway inflammatory response in asthma is now a major recommendation of current asthma management guidelines (Gibson *et al*. 2001). Budesonide interacts clinically in patients as ~90% plasma protein bound, with a volume of distribution of ~3 L/kg. It is 90% biotransformed to metabolites in the liver

with a systemic clearance of ~1.2 L/min, and small amounts of budesonide are detected in the urine as it has a short (2-4 hours) elimination half-life (Goldsmith *et al*. 2004). It has been reported to inhibit both early and late airway responses to antigen challenge by reducing airway inflammation in the lungs of asthma patients along with decreasing eosinophilic infiltration, inhibiting vascular exudation and mucous secretion (Gibson *et al.* 2000, Xu *et al*. 2000). Maximum serum concentrations of budesonide occur within 30 minutes after inhalation, with similar absorption characteristics seen in children and adults (Goldsmith *et al*. 2004). Additionally, a study has successfully demonstrated that a single dose of inhaled budesonide significantly reduced sputum eosinophils 6 h after administration (Gibson *et al*. 2001).

1.3 Computed Tomography

Computed tomography (CT) is an important diagnostic tool used for longitudinal non-invasive investigation of pathological lung diseases, though in asthma, CT is not actively used. However, through the use of quantitative measurement of tissue density, CT could be used to study different lung diseases such as emphysema, allergic inflammation, and fibrosis (Ask *et al.* 2008, Jobse *et al.* 2009, Lederlin *et al.* 2010). CT imaging provides high spatial resolution and complete rotation of the gantry. This allows several respiratory cycles to be imaged, supplying information regarding lung densities and volumes at lung expiration and inspiration (Langheinrich *et al.* 2004, Ask *et al*. 2008, Ertel *et al.* 2009). CT analysis is typically used for qualitative purposes in nature, but CT lung density measurements provide an objective qualitative analysis and have been shown to significantly correlate to pulmonary functions tests of airflow obstruction and

hyperinflation (Heremans *et al.* 1992, Carroll *et al.* 2006). Preclinically, CT imaging allows the study of individual animals over time (Langheinrich *et al.* 2004, Artaechevarria *et al.* 2009, Brange *et al.* 2009). This permits the assessment of the progression and severity of pathologies and their resolution with therapy in the same subject, reducing animal numbers and inter-subject variability (Johnson 2007, Jobse *et al.* 2009, Cavigli *et al*. 2009). CT imaging also provides images that can be compared with the biological responses of inflammation seen by BAL and histology to provide complementary information (Johnson 2007, Jobse *et al.* 2009).

1.3.1 *History of Computed Tomography*

Computed tomography was invented by G.N. Hounsfield in the early 1970s. He used X-ray radiation to create non-invasive images of anatomical structures based on differences in tissue densities (Hounsfield, 1973, Poulsen *et al*. 2007). Hounsfield's principles of CT involve multiple planar images taken from 360° around the subject while exposed to a source of X-ray radiation (Figure 1). These projections are acquired with a scintillation crystal or xenon gas detector that converts light energy into an electrical signal which is linked to a computer and reconstructed to create a 3D image (Hounsfield, 1973). Denser materials have a higher electron density, producing an increase in X-ray attenuation. These density differences produce a final image where the denser areas of higher attenuation appear lighter and the less dense areas of lower attenuation regions appear darker (Hounsfield, 1973). Attenuation values are converted to relative density values called Hounsfield Units (HU), where standards are water (0 HU) and air (-1000 HU) (Hounsfield, 1973). The resulting image is comprised of 3D pixels, called voxels,

and provides spatial and volumetric data as well as an average attenuation value determined by the amount of X-rays detected by the detector, measured in CT units (Hounsfield, 1973). CT imaging has become an important tool for the assessment of lung disease.

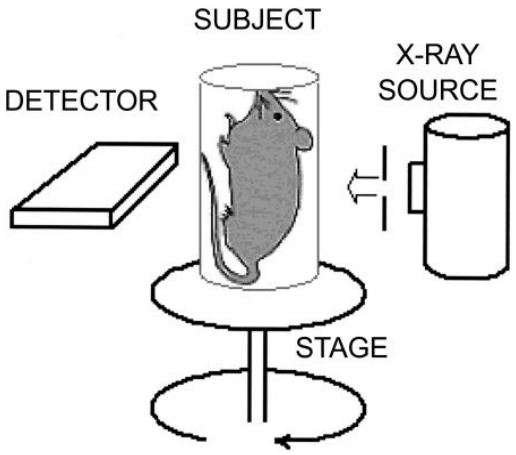

Figure 1. Schematic of a typical CT imaging system with a fixed source and detector and rotating stage (Paulus *et al.* 2000).

1.3.2 *Components of CT Imaging*

X-ray radiation is a form of electromagnetic radiation with a wavelength of 0.01 to 10nm, frequencies from 3×10^{16} Hz to 3×10^{19} Hz, and energies in the range of 120 eV to 120 keV (Koningsberger and Prins, 1987). X-rays are shorter in wavelength than ultra-violet rays and longer than gamma rays (Novelline, 1997). X-rays are generated by an X-ray tube which employs high voltage to accelerate electrons released by a hot cathode to a high velocity. The high velocity electrons collide with the anode, a metal target, which creates the X-rays (Whaites, 2002). CT uses the attenuation of X-rays by tissues as the signal for producing an image (Schuster *et al.* 2004). As attenuation is dependent on the

quantity of X-ray radiation reaching the detector, variability occurs with different X-ray dosages, the durations of scanning, and the use of different machines (Robinson 1979, Levi *et al*. 1982, Cavanaugh *et al.* 2004). A series of planar projection images displays the attenuation of the emitted X-rays as acquired from around the subject at several different angles (Farncombe 2008). The projection images are further reconstructed by a cone beam reconstruction algorithm, which reduces the lateral spread of the electron beam seen by fan-beams providing volumetric data, to determine the 3D anatomical data associated to tissue density (Feldkamp *et al.* 1984, Wang *et al.* 1993, Farncombe 2008). This output data of the image creates a physical map divided into voxels with a precise location and average attenuation value using standards of water (0 HU) and air (-1000 HU), providing regional density measurements of the lung that can be quantified (Hounsfield 1973, Robinson 1979). CT imaging provides high spatial resolution images of small animals (Langheinrich *et al.* 2004). The number of projections obtained for spatial resolution is directly proportional to radiation dose (Farncombe 2008). By knowing the radiation dose administered during a routine CT scan, caution can be taken to avoid significant and potentially lethal doses of radiation, keeping in mind the duration of each scan and the number scans (Obenaus and Smith 2004).

1.3.3 *CT Imaging Improvements*

Numerous CT mechanisms have remained the same since its beginning: the gantry where the energy source and detector are connected on opposite sides and rotated 360 degrees around the object; the platform where the object lies during imaging; and the computer system (Paulus *et al*. 2000). However, several enhancements in CT technology

have been made: continuous spiral acquisitions, increased speed, higher resolution, increased number of detectors, decreased size of the X-ray focal lens, use of cone beam X-rays, gating capabilities, etc. These are just a few of the improvements and advances which have directly improved image quality and led to a reduction in acquisition time, generating high spatial resolution to further explore the fine anatomical structures of numerous rodent organs such as the lungs, heart, and kidneys and to specifically move beyond into non-invasive studies of regional lung physiological function (Paulus *et al*. 2000, Cavanaugh *et al.* 2004, Langheinrich *et al.* 2004, Simon 2004).

Respiratory gating is used to suppress imaging artifacts due to respiration during imaging acquisition (Farncombe 2008). Respiratory gating of CT images are frequently acquired clinically by techniques such as, breath hold at full inspiration and full expiration (Mah *et al.* 2000), forced-shallow breathing technique using a physical plate placed and fixed over the abdominal region (Blomgren *et al.* 1995), and using a marker to generate the respiratory cycle where the gating window can be set to turn the beam ON within and OFF outside the gate (Saw *et al.* 2006). Preclinically, we used the respiratory gating software, *RespGate*, which provides a post acquisition measurement of inhalation and exhalation while the animal is freely breathing (Farncombe 2008). More projections are measured during expiration (gate 1) exhibiting the best contrast to measure emphysema, and fewer projections are measured during inspiration (gate 4) having the greatest contrast for inflammation and fibrosis (Farncombe 2008, Jobse *et al.* 2009). Additionally, other preclinical gating techniques have been used, such as computer-controlled intermittent iso-pressure breath hold (Namati *et al.* 2006), external sensor as a

expiratory cushion that is placed below the chest of the small animal (Bartling *et al.* 2007), and optical systems to deduce the breathing movements (Bartling *et al.* 2008). *RespGate*, is more beneficial than complex external respiratory monitoring devices as it uses projection data to reduce motion artefacts supplying functional information about lung volumes, such as respiratory tidal volume (Farncombe 2008, Ask *et al*. 2008).

1.3.4 *Imaging Lung Inflammation*

Other imaging technologies can be used to measure lung inflammation; however, the function of these techniques to quantify allergic inflammation is limited. Positron Emission Tomography (PET) scans are used to study biological processes, such as inflammation and alveolar ventilation and perfusion, using inhaled or injected radionuclides (e.g. ^{18}F-FDG), but due to its limited spatial resolution, there is limited agreement with suitable biomarkers (Hsia *et al.* 2009, Jannasch, *et al.* 2009). Magnetic Resonance Imaging (MRI) technologies use hyperpolarized gas (e.g. ^{3}He) and are less used in lung studies as this is one of the most challenging organs to image with the low signal content of lung tissue, but for lung diseases involving oedema, fibrosis, and inflammation, MRI easily detects the signal proton density of water (Beckmann *et al.* 2001, Karmouty-Quintana *et al.* 2007, Ask *et al.* 2008, Blamire 2008). Single Proton Emission Computed Tomography (SPECT) imaging also suffers from low spatial resolution, and has long acquisition times, but allows the measurement of regional blood flow and ventilation simultaneously using tracers such as ^{99m}TC and ^{123}I (Levin, 2005, Jannasch *et al.* 2009).

1.3.5 *Quantification vs. Visualization of CT Imaging*

CT imaging is employed as a non-invasive method to analyse anatomical structures within the human body. Clinically, physicians continue to employ visual interpretation of CT images for many disease diagnoses with staging as the principle function to visualize differences in tissue density to differentiate diseased from healthy tissues. The major fault with this process is subjectivity based on the observer (Ng *et al.* 2007). Several benefits of quantifying the image include avoiding biases and variability caused by the interpreter, detecting pathological changes the human eye might not be able to detect, and the ability to measure density changes within a 3D space (Grenier *et al*. 1996, Akira *et al*. 2009, Froese *et al*. 2007). CT densitometry allows for the evaluation of the whole lung in a reasonable amount of time and is more reproducible compared to visual evaluation of the extent of pulmonary diseases. Densitometry may be crucial to detect minor changes in diseased lungs as well as possible successful improvements after medical treatment (Cavigli *et al.* 2009).

1.4 CT Densitometry

CT densitometry is an optimal modality to represent the lung *in vivo* and its morphological changes during the progression of respiratory disease such as asthma, as it creates contrast between air and the surrounding lung tissue (Jannasch *et al.* 2009). The CT image is created of voxels that have values mapped to the density of the tissue being imaged (Johnson 2007). This process creates a CT scale of Hounsfield units (HU) centred on water with a value of zero. Tissues that are less dense than water are negative on the HU scale, while the higher density tissues are positive. Furthermore, the HU scale

provides the ability to quantify density changes in the lungs (Johnson 2007). Therefore, CT imaging has become a useful innovative investigative tool to display the density contrast between lung and the surrounding tissues (Walters *et al.* 2004).

1.4.1 *Clinical CT Densitometry of the Lung*

The application of quantifying pulmonary changes in the lungs has been employed since the early 1960s and CT densitometry specifically has been used since the late 1970s (Wegener 1978, Robinson 1979). As the lung is a mixture of tissue (blood, cells, and fluid) and air, the density of the human lung is said to be less than zero at approximately -700 HU, making it relatively easy to differentiate and segment the lung from the surrounding tissues such as skeletal muscle, bones, and vasculature (Bushberg *et al.* 1994, Johnson 2007). Regions of interest within the lung are regularly utilized in CT densitometry, creating density distribution profiles of the proximal airways (Gupta *et al.* 2010). CT also has the ability to measure lung densities to provide insight into lung function and anatomy, such as gas exchange measured by functional residual capacity (FRC) and lung volume of gas (Schuster *et al.* 2004).

1.4.1.1 Clinical CT Densitometry Studies

Clinically diagnosis of pulmonary diseases is centred on indirect features like pulmonary function tests, clinical examinations, visual assessment by X-rays, and CT images. These tests have limited value as, classically, they neglect the detection of mild or moderate changes in lung tissues (Boehm *et al.* 2008). CT lung densitometry for quantitative analysis is not a widely used method in the clinical practice. There have been

studies evaluating standardizing and validating different pathologies as well as characterizing disease progression in clinical chronic obstructive pulmonary disorder (COPD), asthma, pulmonary oedema, acute respiratory distress syndrome, and pulmonary fibrosis (Garnett *et al.* 1977, Gattinoni *et al.* 2001, Mitsunobu *et al.* 2003, Boehm *et al.* 2008, Akira *et al.* 2009). In the clinic, physicians visually assess CT images by applying a grading system to quantify the severity of the disease, such as fibrosis, emphysema, and inflammation (Gamsu *et al.* 1995, Bankier *et al.* 1999, Ng *et al.* 1999). These results are then correlated to clinical parameters and outcomes of lavage, pulmonary function tests, and/or pathology (Boehm *et al.* 2008).

CT imaging has been used to quantify the degree of airway narrowing induced by inhalation of methacholine in normal and asthmatic subjects (Okazawa *et al*. 1996, Goldin *et al*. 1998, Brown *et al*. 2000). The results visibly demonstrated that the distribution of attenuation values was shifted to higher densities during airway narrowing in intermediate sized airways (Okazawa *et al*. 1996, Goldin *et al*. 1998, Brown *et al*. 2000). CT scans of asthmatic patients show a greater increase in attenuation of CT lung density than controls and patients with stable asthma, with decreased and increased bronchial lumen area, excessive airway narrowing in response to a variety of stimuli and airway wall thickening, as well as mosaic perfusion and gas trapping on expiration (Mitsunobu *et al.*, 2003 Jong *et al.* 2005). Furthermore, increased attenuation in patients with an asthma exacerbation could be improved by systemic glucocorticoid therapy (Mitsunobu *et al.* 2003). Additionally, the lowest 5-10% of the density histogram based

on HUs (-900 to -1000 HU) was discovered and used for automated evaluation of emphysema (Coxson *et al.* 2005, Boehm *et al.* 2008).

1.4.2.2 Preclinical CT Densitometry Studies

Non-invasive imaging has become a novel method where animal models are used for experimentation on respiratory disorders, thus aiding in "proof-of-principle" and efficacy studies (Poulsen and Simonsen 2006, Ask *et al.* 2008). In addition to the anatomical assessment of the lungs, changes in lung density by repeated *in vivo* CT image acquisition can measure pulmonary disease progression and the severity of destruction in parenchyma tissue, inflammation, and fibrosis in rodent models (Froese *et al.* 2007, Labiris *et al.* 2008, Ask *et al.* 2008, Jobse *et al.* 2009, Jannasch *et al*. 2009, Whitty 2011). Jobse *et al.* demonstrated that an allergic airway model induced by exposure to HDM for a 7 to 10 day period in Brown Norway rats caused a significant increase in lung densities, depicted by a rightward shift on the HU scale to higher densities (Jobse *et al*. 2009). Johnson described a correlation between histology and CT results with shifts in density peaks of the histograms to authenticate the change from normal lung tissue to inflammation to fibrosis (Johnson 2007). In addition, regional density measurements of the airways have been studied in a mouse model of asthma characterized by structural airway changes (Lederlin *et al.* 2010). Froese *et al.* (2007) used a mouse model of emphysema to produce regions of increased attenuation. Whitty created density distribution profiles of eosinophilic inflammation, neutrophilic inflammation, fibrosis, and airway remodelling in a mouse study using airway segmentation, which resulted in

defining HU regions of interest that differentiate between the different pathologies (Whitty 2011).

1.5 CT Segmentation Methods

The type of segmentation used for CT quantitative analysis depends on the part of the lung you are trying to assess, whether it be the entire lung, parenchyma, or large airways. The different segmentation types are created using density thresholds to define the region of interest, producing a histogram that can be interpreted in many ways (Hangartner, 2007). Using segmentation provides a consistent analysis method used to measure disease progression and regression based on density changes.

Different segmentation protocols have been used for preclinical analysis in rat and mouse models of pulmonary disease, including thorax, lung, and airway segmentation. Lung segmentation was used by Froese *et al.* (2007) in a model of emphysema, while different studies in asthma have used thoracic segmentation (Jobse *et al*. 2009) and airway segmentation (Lederlin *et al.* 2010, Whitty 2011). Studies of pulmonary fibrosis have used the thoracic segmentation method to assess and quantify lung damage by the disease in humans (Cavanaugh *et al.* 2006, Ask *et al.* 2008) and in rat models of asthma (Jobse *et al*. 2009). The thoracic segmentation is a broad method and requires severe damage to the lung tissues to measure changes in disease (Whitty 2011), but is very useful in measuring changes in lung function in models of asthma by changes in tidal volume (Jobse *et al.* 2009). Lung segmentation is ideal for measuring changes in the lung periphery seen in emphysema and other interstitial lung diseases. Lung segmentation can be applied by using a semi-automated program that isolates the lung based on a specific

density range. It is the least variable, most representative image of a lung, and provides better measurements of the average lung, slice density maps, and 3D volume maps, but is time consuming and requires an increase in user input and knowledge of lung anatomy (Froese *et al*. 2007, Jobse *et al.* 2009). Thoracic segmentation includes more than the lung, such as the heart, diaphragm, and ribs. It is a quick method requiring less user manipulation, can be used on low-quality CT images, and can measure volume changes in the lung (Cavanaugh *et al*. 2006, Ask *et al*. 2008, Jobse *et al*. 2009, Rodt *et al.* 2010). Airway segmentation is limited to the tissues surrounding the major airways, ideal for diseases such as asthma, where inflammation is more focused around the airways (Carroll *et al.* 2006, Artaechevarria *et al.* 2009). Airway segmentation is preferred in asthma models as peribronchial inflammation is a major identifier of this disease; therefore, it is a specific investigative tool to quantify asthma progression and regression (Whitty *et al.* 2011).

CT segmentation data are presented in histograms that express bin volumes as a percentage of the total volume. This provides a means to quantify data and compare it at multiple time points within the study. Changes from baseline measurements can also be used to assess the progression and regression of disease within the same animal over time. Segmentations supply data with better agreement within an experiment, as differences between animals, such as total volume or the baseline state of the lung are partially resolved, therefore producing longitudinal studies with a smaller sample size (Johnson 2007, Froese *et al.* 2007, Jobse *et al.* 2009).

1.6 Purpose of the thesis

The purpose of my thesis was to determine whether CT densitometry is sensitive to inflammatory changes mediated by budesonide in a rat model of allergic airway inflammation.

1.7 Hypothesis

An animal model of allergic airway inflammation will produce denser lung profiles compared to healthy controls due to the presence of inflammation caused by exposure to HDM. Inflammation can be distinguished from controls based on CT densitometry and disease progression can be quantified using CT densitometry.

The resolution of inflammation will occur with corticosteroid treatment using inhaled BUD. Reductions in inflammation can be distinguished from HDM controls based on CT densitometry and disease resolution can be quantified using CT densitometry. A dose and temporal response study of budesonide will demonstrate a reduction in inflammation proportional to the BUD dose.

1.8 Specific Objectives

The Objectives of this thesis are:

1. To determine the intra-subject variability of CT densitometry within the thoracic, lung, and airway segmentations.
2. To investigate the use of CT imaging to further understand how allergic inflammation is associated with allergen exposure. To achieve this, it will be determined if CT densitometry can detect the impact of corticosteroid therapy

on established inflammation as a standard for other novel intervention strategies. The densitometry data will be compared to the traditional method of evaluation, histology and BAL cytology.

CHAPTER 2

2 MATERIALS AND METHODS

2.1 Animals

Female Brown Norway (BN) rats, approximately 6 to 8 weeks old weighing 80-100 g, were purchased from Charles River Laboratories (n=180, strain BN/Crl, Saint-Constant, QC, Canada) and Harlan Global Headquarters (n=56, strain BN/SsNHsd, Indianapolis, IN, USA). They were housed in microisolator cages (two rats per cage) with Harlan Corncob bedding ⅛ inch thick (Harlan Laboratories Inc., Indianapolis, IN, USA) in a Level 2 biohazard clean room at the Central Animal Facility (McMaster University, Hamilton, ON, Canada). The animal room was maintained at 25°C with a daily 12 hour light-dark cycle. The animals had ad libitum access to food and water. The animals were acclimatized to housing conditions for one week prior to experimentation. All experiments were approved by the Animal Research Ethics Board of McMaster University (Hamilton, ON, Canada) and were conducted in accordance with the Canadian Council on Animal Care guidelines (Ottawa, ON, Canada).

2.2 Allergen and Drug Preparations

2.2.1 *House dust mite (HDM) Suspension*

The HDM allergen extract, *Dermatophagoides pteronyssinus*, (Greer Laboratories, Lenoir, NC, USA) was suspended in sterile saline to produce doses of 150 or 250 µg per 100 µL of saline, based on the protein content of HDM. The suspension was prepared in advance and aliquots kept at -80°C until needed. Sterile saline was used as the vehicle control and also kept at -80°C until needed.

2.2.2 *Budesonide (BUD) Suspension*

Budesonide was prepared according to the following method (C. Hjelm, AstraZeneca R&D Lund, Sodertalje, Sweden). A vehicle stock solution was prepared by combining sodium chloride (NaCl, 4.25 g, Bioshop Canada Inc., Burlington, ON, Canada), ethylenediaminetetracetic acid disodium dihydrate (EDTA, 50 mg, EM Industries Inc., Gibbstown, NJ, USA), anhydrous citric acid (75mg, Sigma-Aldrich, Steinheim, Germany), and sodium citrate dihydrate (250 mg, EM Chemical Inc., Gibbstown, NJ, USA) in sterile deionized water (100 ml, Millipore, Billerica, MA, USA). A polysorbate solution was prepared by adding polysorbate-80 (100 mg, Sigma-Aldrich, St. Louis, MO, USA) to sterile deionized water (50 mL). Budesonide (60 mg, Sigma-Aldrich, Oakville, ON, Canada) was dispersed in 5 mL of the polysorbate solution and then added to 10mL of the vehicle stock solution and 35 mL of sterile deionized water. Budesonide was diluted to concentrations of 10, 100, and 300 µg/kg. The budesonide vehicle control was produced by adding 10 mL of vehicle stock, 5 mL of the polysorbate solutions to 35 mL of sterile deionized water. All mixtures were stored at 4-8°C and protected from the light with aluminum foil until needed.

2.3 Development of the Allergic Airway Inflammatory Model

2.3.1 *Dose and Temporal Response of HDM*

A dose and temporal response to HDM were determined in 24 female BN rats (Table 1). Four groups were studied:

Table 1. Inflammatory Phase: HDM Dose and Temporal Response Experimental Groups. Note: Day10 = 5 HDM exposures; Day16 = 8 HDM exposures.

Group	n	Exposures	Endpoint (# animals)
Inflammatory Phase			
Naive	4	Animals left untouched and not imaged. Animals used for biological data only.	Day10 (4)
Veh_{HDM}	4	100 µL of sterile saline every other day for 5 doses. Animals used for biological data only.	Day10 (4)
HDM_{150}	8	HDM 150 µg in 100 mL every other day for 5 doses and 8 doses.	Day10 (4) Day16 (4)
HDM_{250}	8	HDM 250 µg in 100 mL every other day for 5 doses and 8 doses.	Day10 (4) Day16 (4)

Animals were anaesthetized using 1.5% isoflurane (Baxter Corporation, Mississauga, ON, Canada) and 2.0L/minute oxygen (VitalAire Canada Inc., Mississauga, ON, Canada) while HDM or the vehicle control was delivered intratracheally (IT). IT delivery was performed by fastening the animals by their front teeth on an in-house built intubation platform at 35° angle from horizontal plane. Forceps were used to move the tongue in order to expose the trachea. Using a laryngoscope (Welch Allyn, Skaneateles Falls, NY, USA), the trachea was visualized and a 25⅝ gauge needle (Becton Dickinson and Company, Franklin Lakes, NJ, USA) fitted to 3.5 cm PE20 polyethylene endotracheal tubing (0.38 mm inner and 1.09 mm outer diameter and 15 mm in length; Becton Dickinson and Co., Sparks, MD, USA) was inserted in the trachea. HDM or the vehicle control (100 µL) was then instilled IT through the endotracheal tube.

Prior to receiving HDM, a baseline CT was acquired for the $HDM_{150\ \mu g}$ (n=4) and $HDM_{250\ \mu g}$ (n=4) groups. CT scans were performed 24 hours post the fifth dose (Day 10) and a subset of animals (n=4 per group including naïve) were sacrificed to obtain BAL and histological data. The remaining animals received an additional three doses of HDM delivered every-other-day for a total of eight doses. CT scans were performed on the $HDM_{150\ \mu g}$ (n=4) and $HDM_{250\ \mu g}$ (n=4) groups 24 hours post the eight doses (Day16) and all animals were sacrificed. BAL and histological samples were acquired (Figure 2).

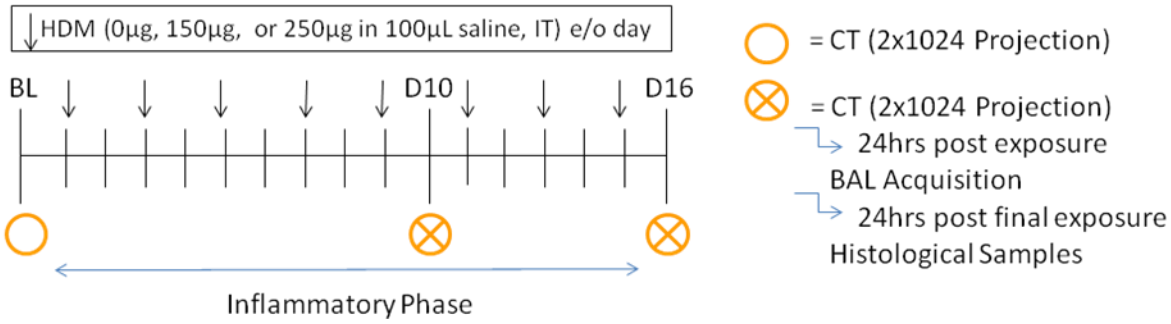

Figure 2. Inflammatory Phase: Allergic Airway Inflammatory Model in Female BN Rats. A baseline CT scan was acquired prior to exposure in the HDM groups. HDM or the vehicle control was delivered every other day for 5 doses. On Day10, CT scans were acquired for HDM groups and a subset of animals was sacrificed including vehicle controls and naïve for BAL and histological data. An additional 3 doses of HDM or the vehicle control were delivered every-other-day followed by CT acquisition of HDM groups on Day16. All remaining animals were sacrificed and BAL and histological data were collected.

2.4 Budesonide Dose and Temporal Response Study

Allergic airway disease was induced using the method outlined in section 2.3.1 using five doses of HDM 250 µg or the vehicle control in 56 female BN rats in eight experimental groups (inflammatory phase). A BUD dose and temporal response study

was performed using BUD 0, 10, 100, and 300 µg/kg administered concurrently with HDM for three and six treatments (treatment phase) (Table 2, Figure 3).

Table 2. Treatment Phase: Budesonide Dose and Temporal Response Experimental Groups. Note: Day16 = 3 treatments BUD; Day22 = 6 treatments BUD

Group	n	Exposures	Endpoint (# animals)
Inflammatory Phase			
Veh_{HDM} alone	4	100 mL saline every other day for 5 doses	Day10
HDM alone	4	HDM 250 µg in 100 mL every other day for 5 doses	Day10
Treatment Phase			
HDM+Veh_{BUD}	8	100 µL vehicle BUD every other day for 3 or 6 treatments delivered 1 hour post HDM exposure	Day16 (4) Day22 (4)
HDM+BUD_{10}	8	BUD 10 µg/kg (100 mL) every other day for 3 or 6 treatments delivered 1 hour post HDM exposure	Day16 (4) Day22 (4)
HDM+BUD_{100}	8	BUD 100 µg/kg (100 mL) every other day for 3 or 6 treatments delivered 1 hour post HDM exposure	Day16 (4) Day22 (4)
HDM+BUD_{300}	8	BUD 300 µg/kg (100 mL) every other day for 3 or 6 treatments delivered 1 hour post HDM exposure	Day16 (4) Day22 (4)
Veh_{HDM}+Veh_{BUD}	8	100 µL vehicle BUD every other day for 3 or 6 treatments delivered 1 hour post HDM vehicle control exposure	Day16 (4) Day22 (4)
Veh_{HDM}+BUD_{300}	8	BUD 300 µg/kg (100 mL) every other day for 3 or 6 treatments delivered 1 hour post HDM vehicle control exposure	Day16 (4) Day22 (4)

Following the five doses of HDM or the vehicle control, 100 µL of BUD (0, 10, 100, or 300 µg/kg) were administered IT 1 hour post HDM exposure, in the same every other day sequence, for a total of six doses. CT scans were performed at baseline (n=4 per group), during the inflammatory phase (n=4 per group), and 24 hours after three (n=4

per treatment group) and six doses (n=4 per treatment group) of BUD (Figure 3). The animals from the HDM (n=4) and vehicle alone (n=4) groups were sacrificed 24 hours post CT scan concluding the inflammatory phase. A subset of animals were sacrificed 24 hours after three (n=4 per treatment group) and six doses (n=4 per treatment group) of BUD. BAL and histological samples were acquired from all animals.

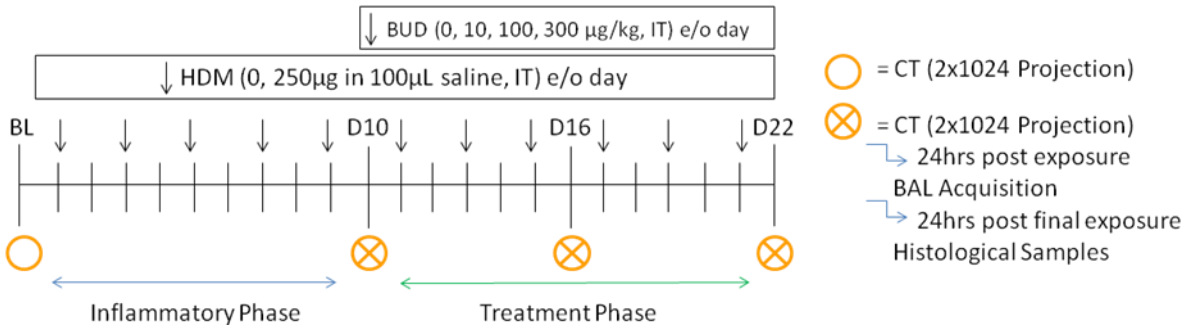

Figure 3. Treatment Phase: Budesonide Dose and Temporal Response Study. A baseline CT scan was acquired prior to HDM or vehicle control exposures. HDM or the vehicle control was delivered every other day for 5 doses. On Day10, CT scans were acquired from each group and HDM and vehicle alone groups were sacrificed for BAL and histological data. BUD dose response of 0, 10, 100, and 300 µg/kg concentrations were delivered every other day for 3 and 6 doses, 1 hour post exposure to HDM. On Day16 and Day 22; CT scans, BAL, and histological data were collected.

2.5 CT Acquisition and Image Reconstruction

CT images of the lung were acquired using two rotations of 1024 projections each at a voltage of 75 kVp and a current of 220 µA on an SPECT/CT (X-SPECT, *Gamma Medica*-Ideas, Northridge, CA, USA) in the McMaster Centre for Pre-Clinical and Translational Imaging. Animals were freely breathing under 1.5% isoflurane and 2.0 L/minute oxygen in HEPA-filter rat holding tubes used to remove smaller airborne particles. Data collected were then reconstructed using a Feldkamp cone beam back projection algorithm into a 512x512x512 matrix (0.115mm isotropic voxels). CT units

were converted to Hounsfield Units (HU) (Hounsfield, 1973) using a water tube as a standard for water (0 HU) and air (-1000HU). Data from the summed images were used in the analysis of the CT images. The absorbed radiation dose per CT was estimated to be 166 mGy (Jobse *et al.* 2009).

2.6 CT Densitometry Validation Study

A validation study was performed to determine the intra-subject variability in CT densitometry and establish the variability of the three different segmentation methods: thoracic, lung, and airway segmentations as outlined below (Section 2.6.1 to 2.6.3). CT images were acquired in three female BN rats daily for 3 days, at the same time of day, using the method outlined in section 2.5.

2.6.1 *Thoracic Segmentation*

Thoracic segmentation is a manual sampling method for tissue densities in a defined thoracic cavity region of interest (ROI) which includes the lungs, heart, ribs, and diaphragm. The segmentation was performed by identifying three anatomical landmarks: the first rib, mediastinum, and full view of the diaphragm. The thoracic cavity was segmented by interpolating between these three points using Amira 5.2.1 software (Visage Imaging, Andover, MA, USA) with a Gaussian 3D filter, sigma value of 0.9, and kernel value of 4. It is important to note that non-lung tissues in the thorax region, for instance the heart, the ribs, and the diaphragm, were included in this analysis (Appendix I-9.1, Figure 24).

2.6.2 *Lung Segmentation*

Lung segmentation is a semi-automatic sampling method for assessing tissue densities in the whole lung and eliminates the other components of the thoracic cavity, such as the ribs, heart, and diaphragm. The lung was segmented using a density threshold of -1000 to -100HU. If necessary, manual alterations were performed to include all lung regions by growing and filling in the lungs as described by Jobse and colleagues, using Amira 5.2.1 software with a Gaussian 3D filter, sigma value of 0.9, and kernel value of 4 (Jobse *et al.* 2009). This lung segmentation included blood vessels and small volumes of tissue immediately surrounding the lung, but excluded the heart, ribs, and diaphragm (Appendix I-9.1, Figure 25).

2.6.3 *Large Airway Segmentation*

Airway segmentation is a manual sampling method for tissue densities in a defined ROI surrounding the large airways. The segmentation started at approximately the seventh rib, the major bronchial trifurcation in the right lung, where a peribronchial ROI, with a diameter of roughly 3.5 mm, was centred on the lumen of the descending bronchi in both lungs using a segmentation length of approximately 6.9 mm (61 slices). Segmentation used Amira 5.2.1 software with a Gaussian 3D filter, sigma value of 0.9, and kernel value of 4. This airway segmentation included any blood vessels and smaller airways within the 3.5 mm x 6.9 mm ROI cylinder (Figure 4).

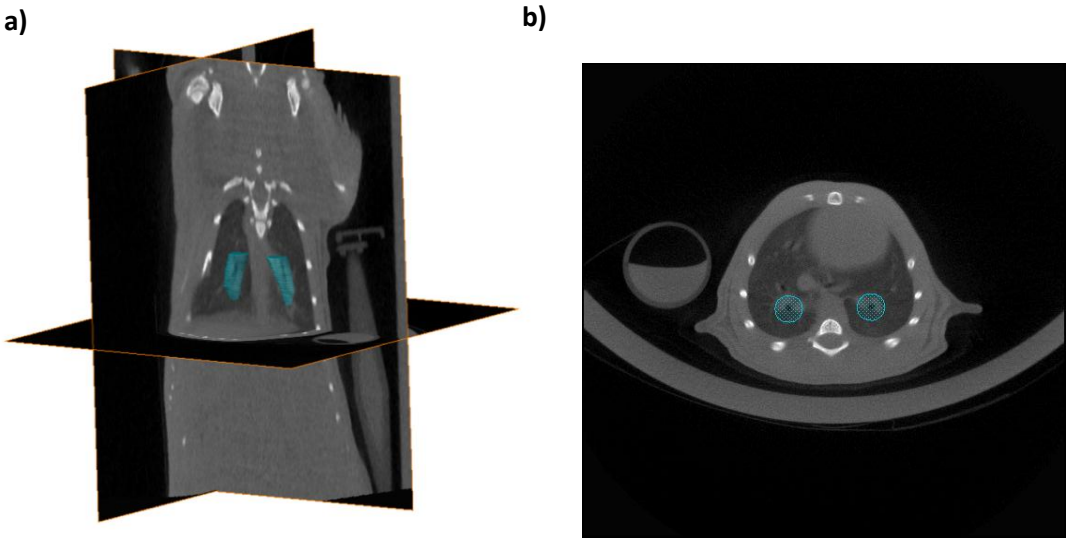

Figure 4. Large Airway Segmentation. The blue regions illustrate the location and relative size of the segmentation. **a)** 3D representation and **b)** cross-sectional slice.

2.7 CT Densitometry

Thoracic, lung, and airway segmentations were each applied to the CT images as described in section 2.6. For the segmentations, the frequency of voxels in the density interval of -1025 and 250 HU was determined. The density interval was divided into 26 bins of 49.04 HU each. Densities were plotted as a percentage of total segmented voxels for lung and airway segmentation (Figure 5a). For thoracic segmentation, air volumes were calculated by determining the air volume in each bin based on the HU value (e.g. -500HU ≈ 50% air) and densities plotted as a percentage of total air in the segmented region (Jobse *et al.* 2009).

CT results will be presented in this thesis using airway segmentation. This segmentation best suited the study since the allergic airway inflammatory model presented increased CT densities by inflammatory processes and was localized

peribronchially, i.e around the major airways of the lungs. To quantify peribronchial density changes, cumulative density distributions were produced for each animal at baseline from the airway segmentation to identify the density at which 90% of the volume is represented (Figure 5b). This is similar to the methods used to identify emphysema, where a decrease in tissue (increase in air volume) lowers the lung density, and emphysema is defined as the lowest 5-10% in density histograms (-900 to -1000 HU) (Coxson *et al.* 2005, Boehm *et al.* 2008). The average of all baseline density values at 90% was then used to analyse all further time points within the experiments. The density threshold was identified to be -100 HU; the assumption was that densities above -100 HU represent inflammatory processes (Figure 5c). To control for the inter-subject variability at baseline, data were analyzed as percent change from baseline (Figure 5d). The mean percent voxels above the density threshold (-100 HU) was calculated per experimental group.

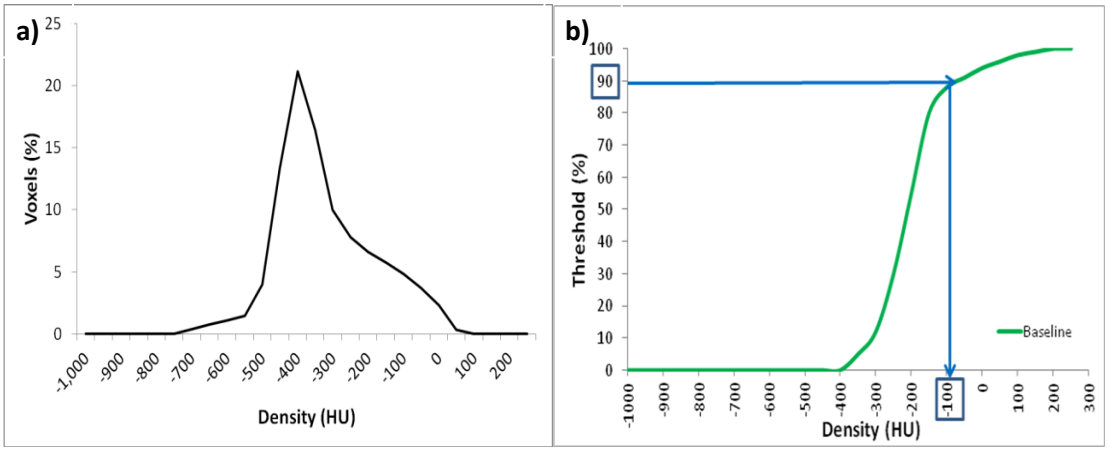

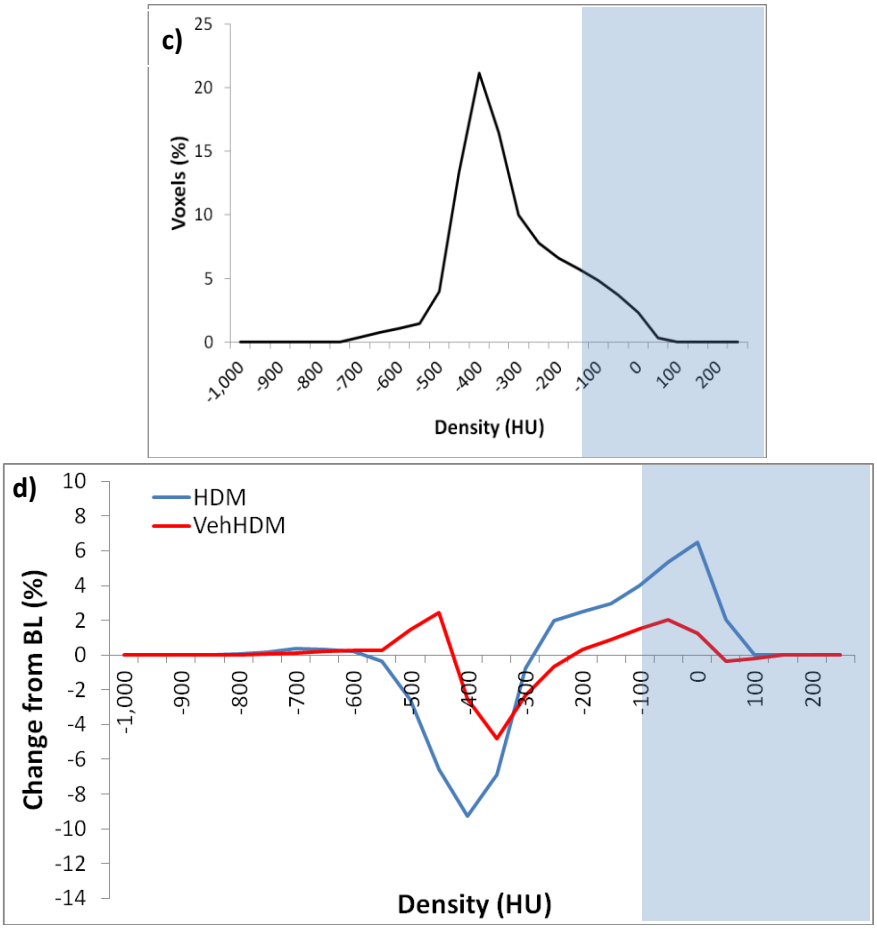

Figure 5. Airway Segmentation CT Densitometry Analysis. a) Representative large airway segmentation density histogram from a control rat, **b)** Cumulative density distributions from baseline CT scans were used to identify the density which 90% of the voxels fell below. A density of -100 HU was measured, **c)** Representative histogram where the blue box is the 90% density threshold being measured. Percent voxels was calculated above this threshold, and **d)** Representative percent change from baseline (BL) demonstrating the changes in density from one time point to another.

2.8 Total and Differential Cell Counts in Bronchoalveolar Lavage (BAL)

Animals were euthanized by exsanguination 24 hours post final exposure to treatment. BAL was performed IT using two washes of 1.5 mL of phosphate buffered saline (PBS) with a 25⅝ gauge needle attached to approximately 4.5 cm of Butterfly-19 tubing (Venisystems, Lake Forest, IL, USA). Approximately 1.0-1.5 mL of BAL fluid

was recovered and kept on ice. Total cell counts (TCC) were determined by a hemocytometer (Bright-Line, Horsham, USA) with a 6:1 Turk (Ricca Chemical Company, Arlington, TX, USA) to BAL ratio. BAL fluid was then centrifuged at 15,000g for 2 min (Hermle model Z233M, Germany), and the supernatant was extracted and stored at -20°C. The cell pellet was resuspended in 1000 µL of PBS and slides were prepared by centrifugation in a Shandon Cytospin3 (Shandon Inc., Pittsburgh, USA) using 100 µL of final resuspended cells and spun for 3 min at 300 rpm. Slides were stained using Hema3 (Fisher Scientific Co., Kalamazoo, MI, USA) to distinguish differential cell types present. Differential cell counts (DCC) were acquired by randomly counting 500 cells from the BAL using an Olympus CX41 microscope (Markham, ON, Canada). Eosinophils were measured as a percent of the total cells from the BAL.

2.9 Histology

2.9.1 *Tissue Collection*

Lungs were removed from the thoracic cavity and inflated with 10% formalin at a pressure of 30 cmH_2O. Lungs were stored in 10% formalin for a minimum of 24 hours before histology preparation. Histology was taken from the left lung as it clearly followed the major airway. It was cut using a sterile stainless steel surgical blade (Magna, Montreal, Canada) into four sections and dehydrated in 50% ethanol for 10 min then placed in 75% ethanol. The lungs were embedded in paraffin and sectioned (3 µm thick) using a RM2255 microtome (Leica, Richmond Hill, ON, Canada) and stained with Hematoxylin and Eosin (H&E) (Fisher Scientific Co., Kalamazoo, MI, USA).

2.9.2 *Quantitative Histology*

Quantitative analysis of peribronchial inflammation was performed on airway histology slices. The appropriate histological ROI was determined by first measuring the CT airway segmentation diameter and airway lumen diameter (n=24) to calculate the mean distance from the outer segment boundary to the lumen wall. This measure was then multiplied by the CT voxel size (0.115 mm) to determine the ROI (2240 μm). In order to apply to histological images, the CT ROI was converted to pixels by dividing the ROI in voxels by pixel size (1 pixel = 6.1 μm) to obtain an area of interest of 183.6 μm^2. This ROI was applied the large airway in each histological image.

Histology pictures were taken using OpenLab software version 5.5.0 (Improvision, Guelph, ON, Canada) via a Leica camera and microscope (Leica Microsystems Wetzlar GmbH, Wetzlar, Germany) attached to a Macintosh computer (Mac OS X operating system, version 10.6.8). Microscope settings were set to 1.6X magnification, light level of 8.8 V with the red setting at 49%, the green setting at 33%, and the blue setting at 48%. Additionally, the aperture was set to 2, the focuser was out, and all the filters were on. Pictures were taken for all four slices centering on the large airway. Images were converted from RBG values to greyscale. This was done by forming a weighted sum of the R, G, and B components using Matlab software version r2001b (MathWorks, Inc., USA). Images were uploaded into Amira software where a brush size of 45 (183.6 μm^2) traced around the large airway and was filled as described above (Figure 6a&b). A intensity histogram was produced displaying the grey intensity per bin with an interval range of -251.5 units (white) to -3.5 (black) divided into 32 bins, 7.75 units in width.

From a cumulative intensity graph, the threshold at which 90% of the pixels were below was determined by the method described in section 2.6.1 and was found to be -187.5 units for control animals (Figure 6c).

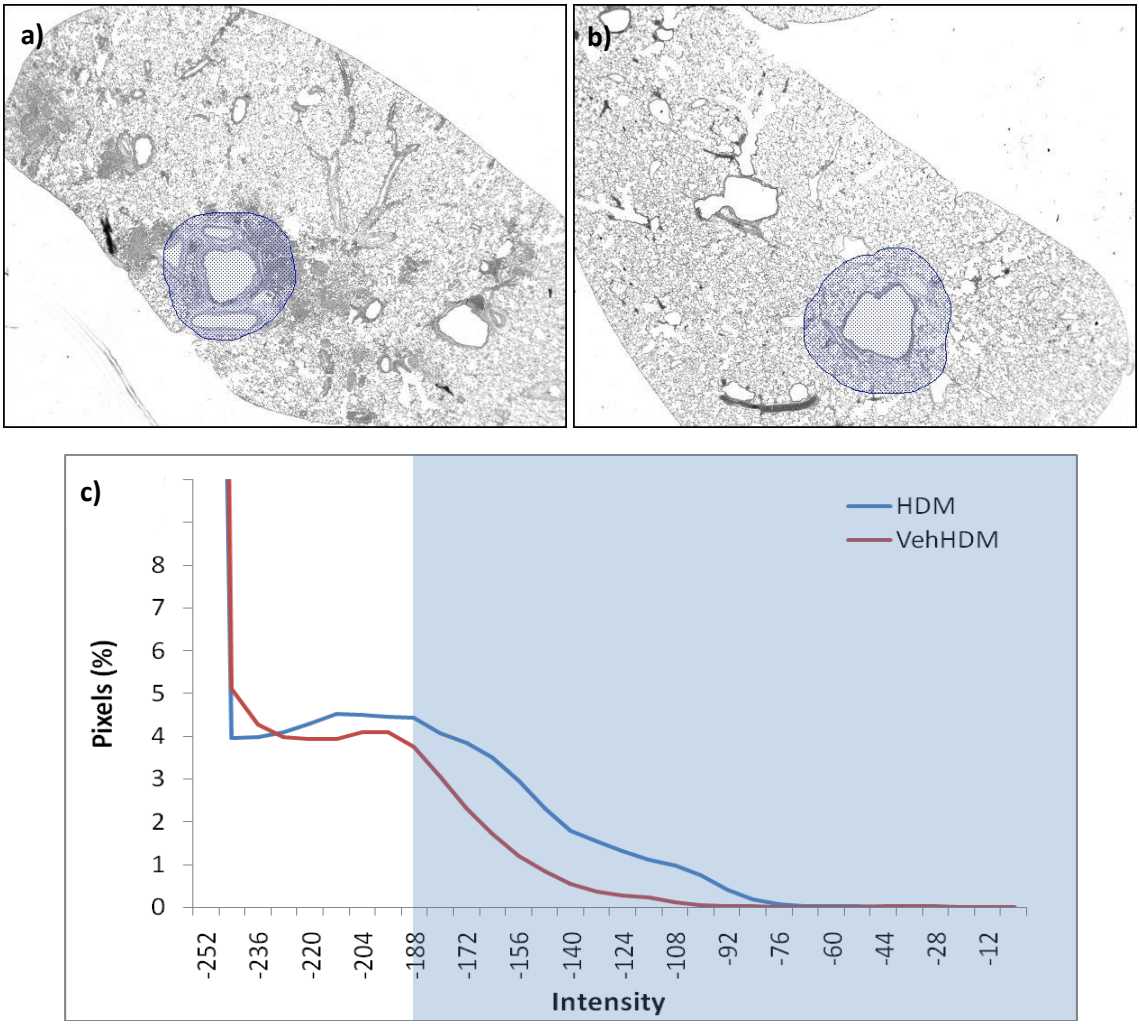

Figure 6. Representative Airway Histology Analysis. The blue shaded area represents the area of interest measured in **a)** An HDM animal and **b)** A VehHDM animal. At 90% the grey intensity profile distribution from vehicle control, an intensity of -187.5 units was measured. **c)** Representative percent intensity histogram where the blue box is the 90% threshold being measured.

2.10 Albumin Concentrations in BAL

Since pulmonary oedema is commonly observed in allergic lung models, the albumin concentration in the BAL supernatant was measured using an ELSIA to study the effect of BUD in oedema.

A rat albumin ELISA (ALPCO Diagnostics, Salem, NH, USA) was performed on supernatant from the BAL fluid of all BUD dose response animals and time points except for HDM+BUD_{10} and HDM+BUD_{100}. Samples (4 µL) were added to the plate wells and the specific anti-albumin antibody was added (100 µL), forming an albumin anti-albumin complex. The plate was washed, removing the unbound sample proteins. A second antibody, anti-albumin-HRP, was added (100 µL) and bound to the antibody-antigen complex. The plate was again washed, removing excess unbound proteins. A chromogenic substrate was added (100 µL) and the measurement of absorbance by the degree of colour change provided the results. The absorbance at 450 nm was measured using an ELx800 Automated Microplate Reader (Bio-Tek Instruments, Inc., Winooski, VT, USA) and the total concentration in µg/mL was calculated from the standard curve.

2.11 Statistical Analysis

The CT validation density thresholds for the individual segmentations were determined by the method described in section 2.7. The 90% density threshold of -250 HU was determined for the thoracic segmentation, and -100 HU for the lung and airway segmentations. The CT variability of each segmentation method was measured by

averaging the standard deviations of the three CTs of each animal. The results were expressed as $\bar{x}$ ± standard deviation (SD) where $\bar{x}$ was predefined as 2SD of the error.

For the HDM dose and temporal response study, a two-tailed independent t-test was used to compare the HDM exposed animals to the vehicle control animals using GraphPad Prism version 5.0 for windows (GraphPad Software Inc., La Jolla, CA, USA). The BUD dose and temporal response results were analysed using a one-way ANOVA to assess if a significant difference existed between BUD doses. A Tukey post-hoc was used to assess possible pair-wise comparisons of the data. Additionally, a Dunnett post-hoc was used to compare group means holding HDM+Veh_{BUD} as the reference group. A two-tailed t-test was performed to determine temporal response of each BUD dose. Data were expressed as mean ± standard error of the mean (SEM) and a statistical significance was determined at $p<0.05$.

CHAPTER 3

3 RESULTS

3.1 CT Validation Study

The CT validation study was performed to determine the intra-subject variability of CT densitometry using three different segmentation methods: thoracic, lung, and airway.

3.1.1 *Thoracic Segmentation*

The intra-subject variability in CT density was slight with a measured error of 1.44 ± 0.70 associated with the thoracic segmentation method (Figure 7). In addition to statistical significance being achieved, a minimal difference of 2.86 must be present for a change in density to be considered significant (Table 3).

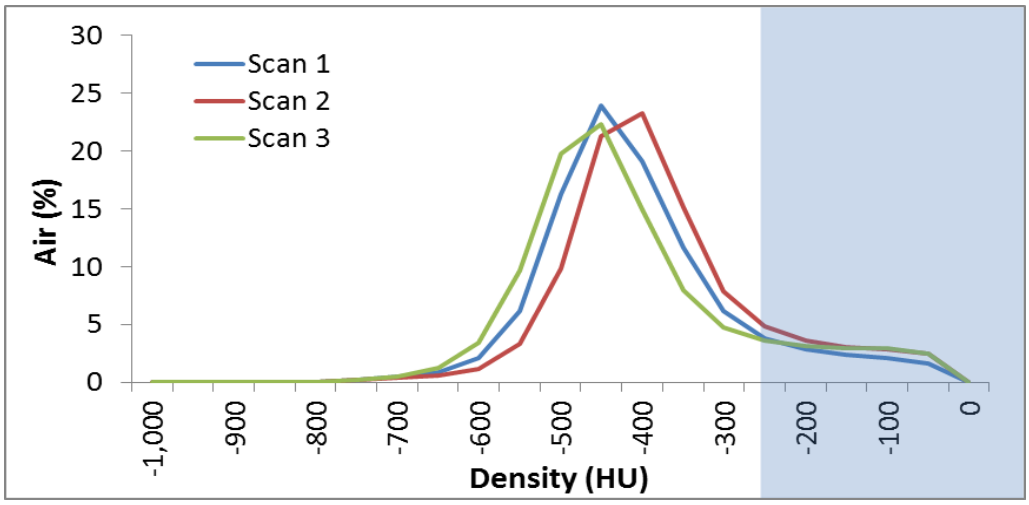

Figure 7. Representative Thoracic Cavity CT Density Distribution. The CT thoracic segmentation analysis of three CT images 24 hours apart of the same animal. Percent of total air was measured at each density bin within the segmentation volume. HU: Hounsfield units.

3.1.2 *Lung Segmentation*

CT densitometry varied slightly within the same animal with a measured error of 0.40 ± 0.09 associated with the lung segmentation method (Figure 8). Thus, a minimal difference of 0.58 must be present for a change in density to be considered significant with this segmentation method (Table 3).

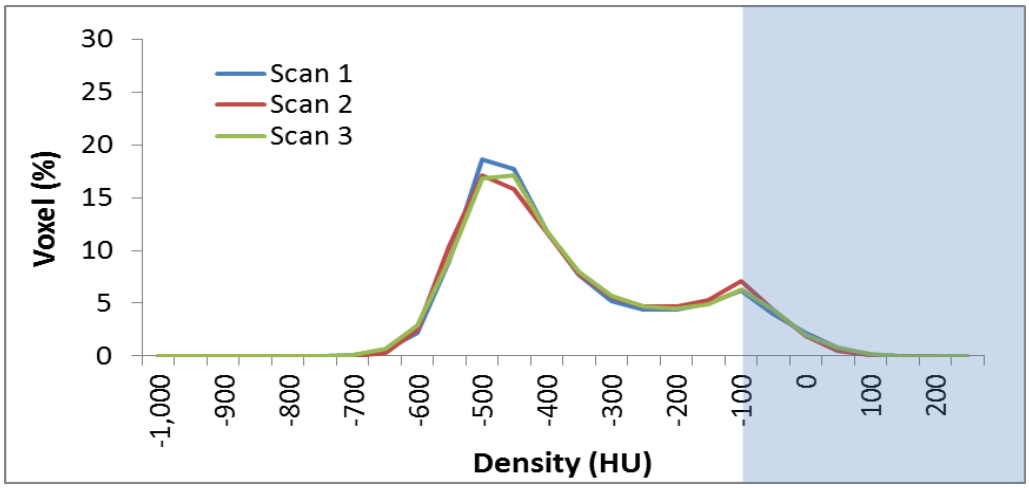

Figure 8. **Representative Lung CT Density Distribution**. The CT lung segmentation analysis of three CT images of the same animal taken 24 hours apart. Percent of total voxels was measured at each density bin within the segmentation volume. HU: Hounsfield units.

3.1.3 *Airway Segmentation*

The CT densitometry varied slightly with a measured error of 2.10 ± 1.86 associated with the airway segmentation method (Figure 9). A minimal difference of 5.82 must be present for a change in density to be considered significant for this segmentation method (Table 3).

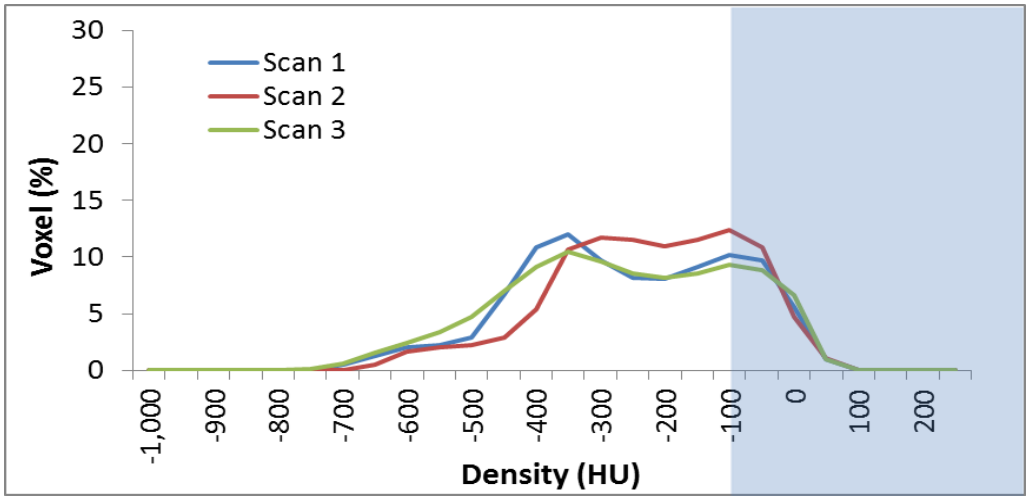

Figure 9. Representative Airway CT Density Distribution. The CT airway segmentation analysis of three CT images, 24 hours apart, of the same animal. Percent of total voxels was measured at each density bin within the segmentation volume. HU: Hounsfield units.

Table 3. Intra-Subject Variability in Thoracic, Lung, and Airway Segmentation CT Density Distributions.

Thoracic Segmentation	**%Air > -250HU**						
Rat #	**CT_1**	**CT_2**	**CT_3**	**Mean**	**SD**	**$\bar{x}$**	**SD**
1	12.87	16.94	15.16	14.99	2.04	1.44	0.70
2	9.91	12.86	12.52	11.76	1.61		
3	N/A	17.61	18.55	18.08	0.66		
Lung Segmentation	**%Voxels > -100HU**						
Rat #	**CT_1**	**CT_2**	**CT_3**	**Mean**	**SD**	**$\bar{x}$**	**SD**
1	14.54	15.45	14.64	14.88	0.50	0.40	0.09
2	13.28	14.04	13.71	13.68	0.38		
3	N/A	15.39	14.94	15.16	0.32		
Airway Segmentation	**%Voxels > -100HU**						
Rat #	**CT_1**	**CT_2**	**CT_3**	**Mean**	**SD**	**$\bar{x}$**	**SD**
1	16.20	16.58	16.42	16.40	0.19	2.10	1.86
2	21.49	17.64	21.41	20.18	2.20		
3	N/A	22.94	17.41	20.17	3.91		

3.2 Development of an Allergic Inflammatory Model: Dose and Temporal Response to HDM

3.2.1 *Peribronchial CT Densitometry*

Exposure to HDM caused a significant rightward shift in the density distribution from 6.5±2.7% at baseline to 20.9±7.2% and 23.1±6.7% of the total peribronchial voxels above -100 HU after five and eight HDM doses, respectively, regardless of dosage (150 and 250 µg) ($p<0.05$, Figure 10a&b). No difference in the CT density distribution was found between HDM_{150} and HDM_{250} at five or eight doses, nor was there a difference within the dose groups (Appendix II-9.2.1, Figure 26).

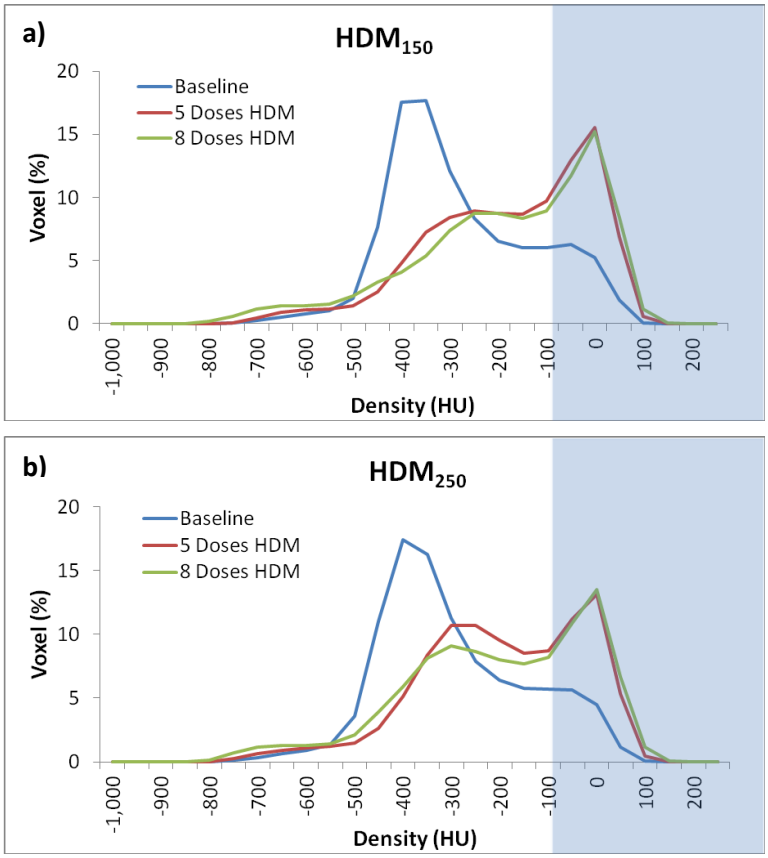

Figure 10. Comparative Peribronchial CT Density Distribution – Dose and Temporal Response to HDM a) HDM 150 µg and **b)** HDM 250 µg. Mean data are shown. Blue box: Density threshold. HU: Hounsfield units.

3.2.2 *BAL Total Cell Count and Percent Eosinophils*

HDM exposure induced a significantly higher TCC and percent eosinophils compared to the vehicle control and naïve groups after five and eight administrations ($p<0.001$, Figure 11a&b). No differences in TCC and percent eosinophils were observed between the vehicle controls and naïve groups. There were also no differences in TCC and percent eosinophils between HDM doses and the duration of exposure (Figure 11a&b).

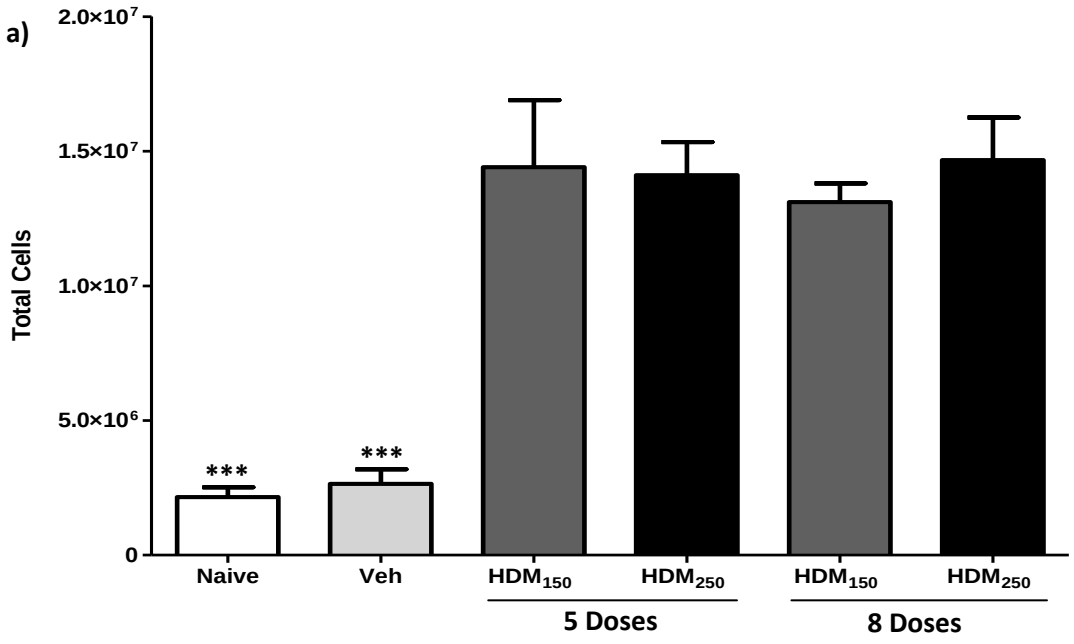

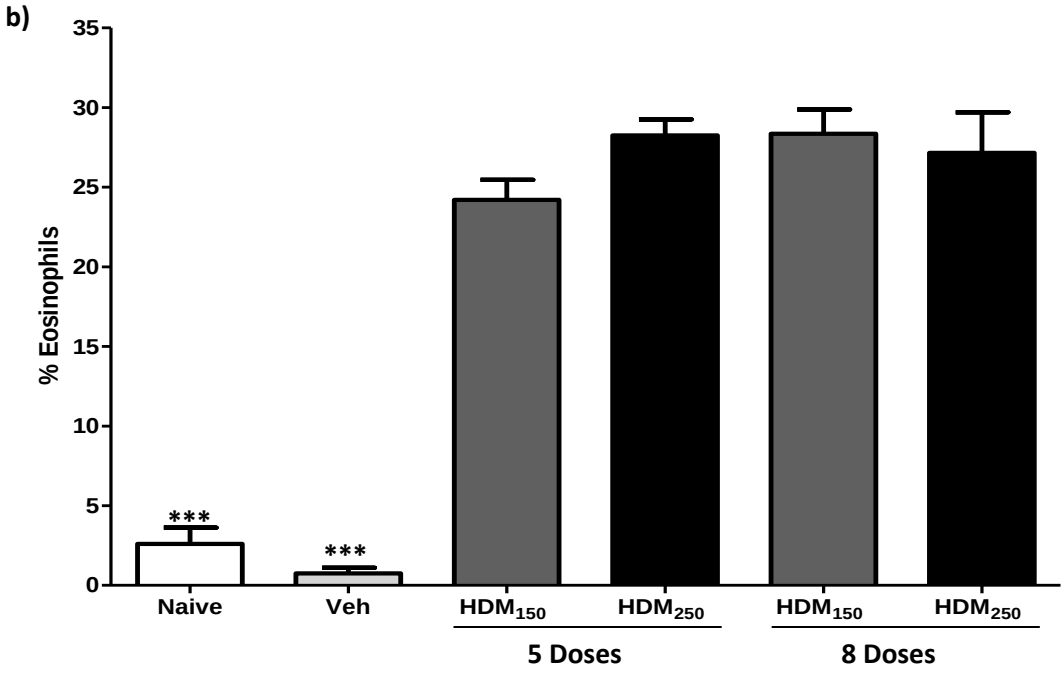

Figure 11. BAL Total Cell Count and Percent Eosinophils in the Allergic Airway Inflammatory Model. Samples were collected 24 hours after the final HDM exposure. **a)** TCC in the BAL and **b)** eosinophils expressed a percent of total cells from the BAL. Data are expressed as mean ± SEM. ***p<0.001 (vs. HDM groups), by a one-way ANOVA with a Tukey post-hoc test. Veh = vehicle control.

3.2.3 *Histology*

Inflammation was present around the major airways after five and eight doses for both HDM 150 and 250 µg compared to the vehicle control and naïve groups (Figure 12). Quantification of the peribronchial inflammation showed a significant increase in inflammation after five administrations of HDM_{150} (33.51±3.41%) and HDM_{250} (41.14.22±6.34%) compared to the vehicle (19.12±2.25%) and naïve (14.48±1.17%) groups ($p<0.05$, Figure 13). There was no difference in peribronchial inflammation

between HDM_{150} and HDM_{250} after either five or eight doses, nor was there a difference within a dose group (Figure 13).

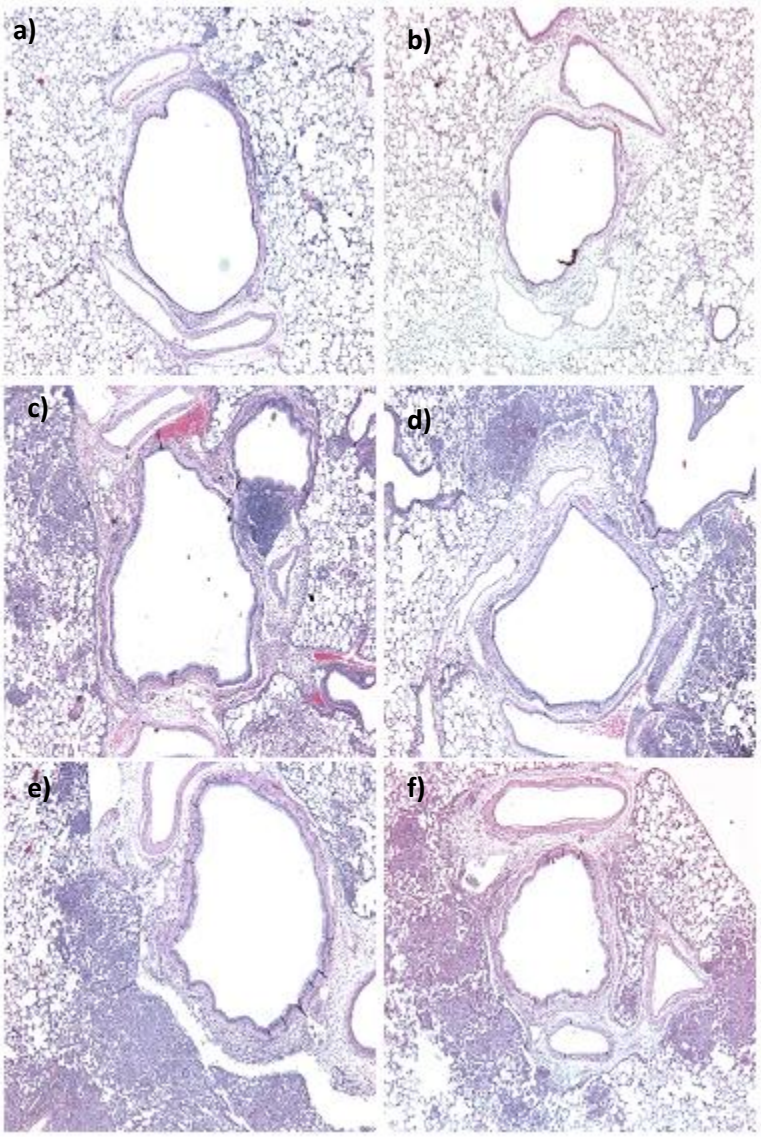

Figure 12. Representative Lung Sections from the Allergic Airway Inflammatory Model. a) Naïve, **b)** Vehicle control after five doses, **c)** HDM 150 µg after five doses, **d)** HDM 150 µg after eight doses, **e)** HDM 250 µg after five doses, and **f)** HDM 250 µg after eight doses.

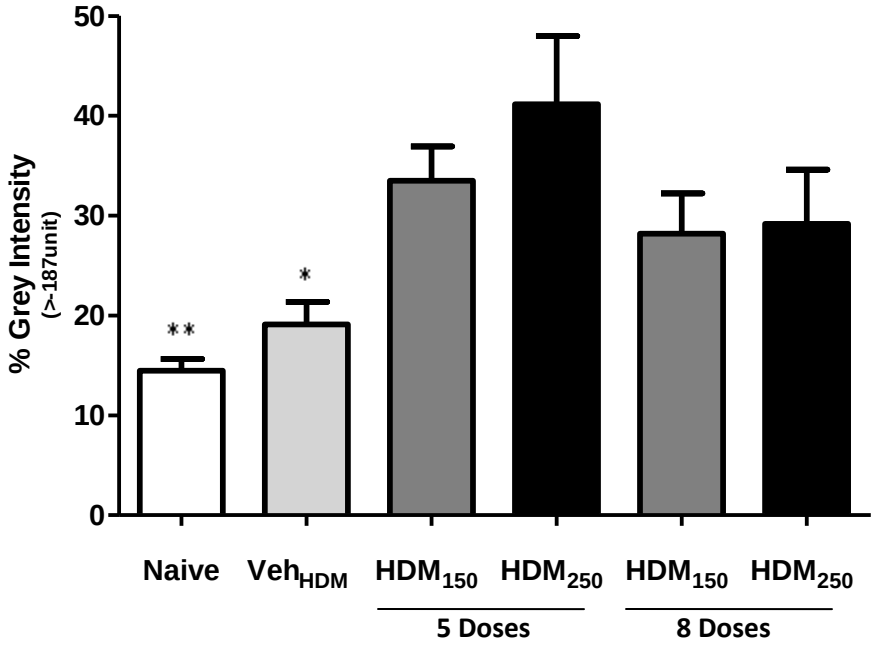

Figure 13. Quantitative Histological Analysis of Peribronchial Inflammation. Data are expressed as mean ± SEM. *$p<0.05$ and **$p<0.01$ (vs. HDM_{150} and HDM_{250} at 5 and 8 doses) by a one-way ANOVA with a Tukey post-hoc test. Intensity threshold defined as grey intensity at which 90% of the area is below.

Based on the CT, BAL, and histological findings, the inflammatory phase of all subsequent experiments used five doses of HDM 250 µg every other day. Typically, HDM 150 µg would be selected, but the HDM concentration of 250 µg was chosen to ensure a robust inflammatory response since previous studies have shown variable responses with a lower dose (Jobse *et al.* 2009).

3.3 Dose and Temporal Response to Budesonide

3.3.1 *Allergic Inflammatory Phase*

3.3.1.1 *CT Densitometry*

The combined CT densitometry profiles of the inflammatory phase from the HDM and BUD dose response studies showed a significant increase in the percent voxels above the -100 HU density threshold of 19.65±1.37% from baseline after HDM exposure compared to 5.47±2.23% in the vehicle controls ($p<0.001$, Figure 14a&b).

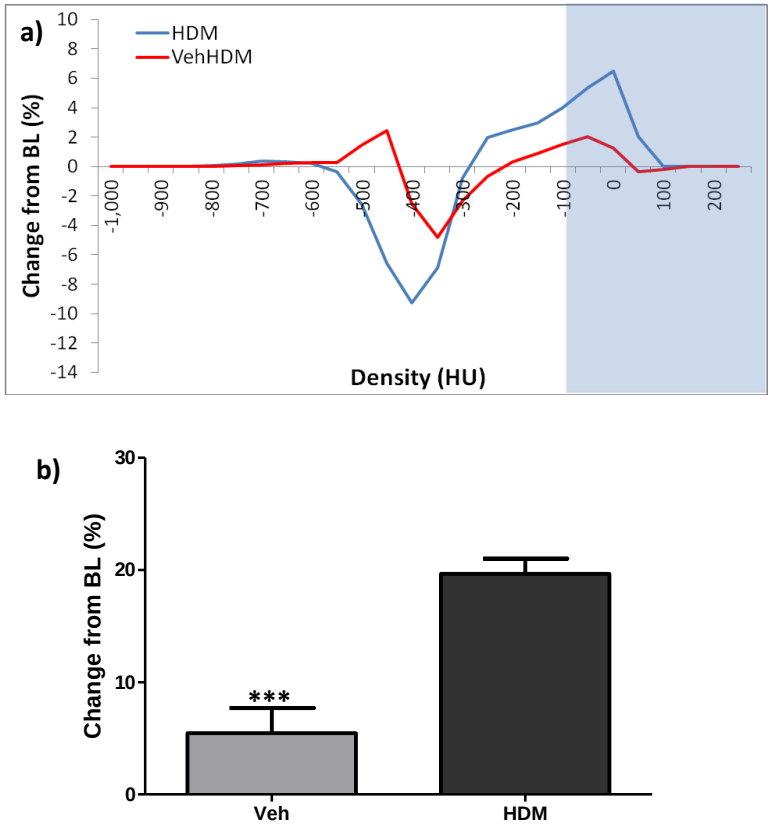

Figure 14. Change from Baseline (BL) in Peribronchial CT Density Distribution. **a)** Comparative change from baseline histogram after five doses of HDM 250 µg and **b)** Change from baseline of the percent voxels above the density threshold of -100 HU. Data are expressed as mean ± SEM. *******$p<0.001$, by a two-tailed independent t-test. Blue box: Density threshold. HU: Hounsfield units.

3.3.1.2 *BAL Total and Differential Cell Counts – Inflammatory Phase*

Animals exposed to HDM 250 µg had significantly greater total cell counts with a significantly higher percent eosinophils compared to the vehicle control after five exposures ($p<0.001$, Figure 15a&b).

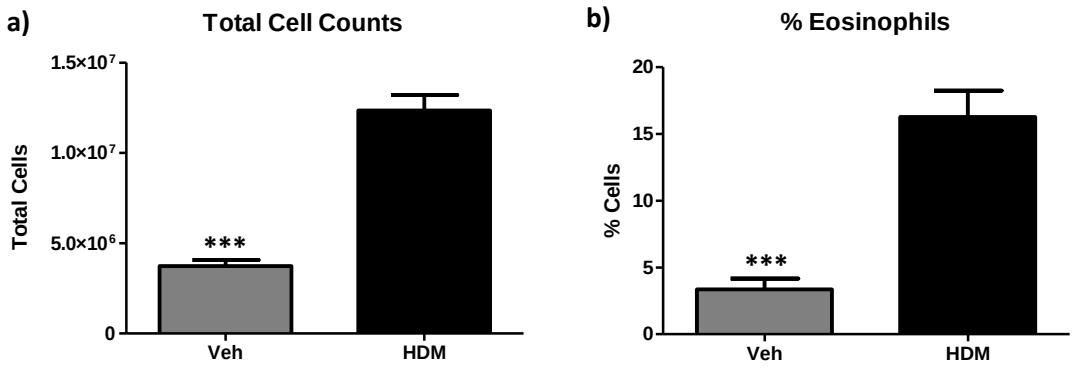

Figure 15. BAL Total Cell Count and Percent Eosinophils in an Allergic Airway Inflammatory Model. a) TCC and **b)** Eosinophils expressed a percent of total cells. Data are expressed as mean ± SEM. *******$p<0.001$, by a two-tailed independent t-test.

3.3.1.3 *Histology*

Inflammation was present around the major airways post five doses of HDM 250 µg compared to the vehicle control (Figure 16). There was a significant difference in the percent intensity around the major airways between HDM animals and vehicle controls (24.22± 2.72% vs. 11.35±0.96%, $p<0.001$) (Figure 17).

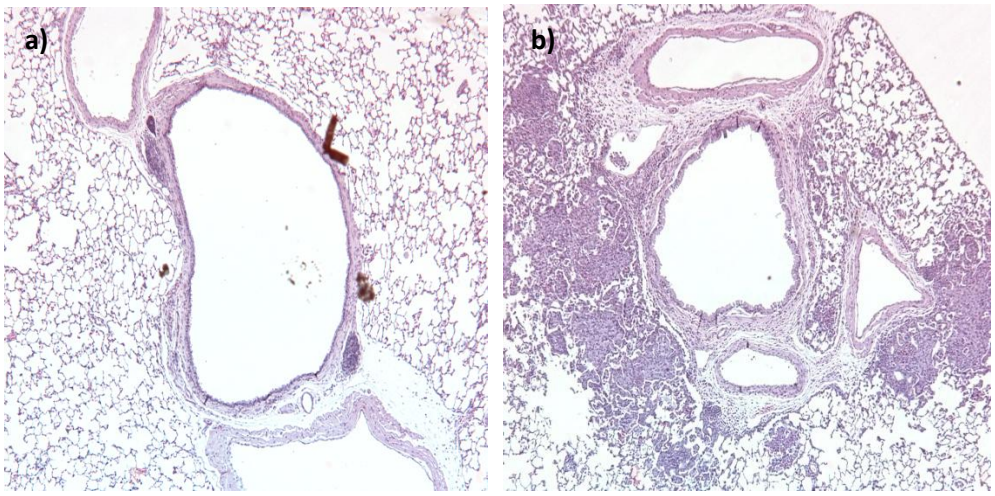

Figure 16. Representative Lung Sections from the Allergic Airway Inflammatory Model. a) Vehicle control and **b)** after five doses of HDM 250 µg.

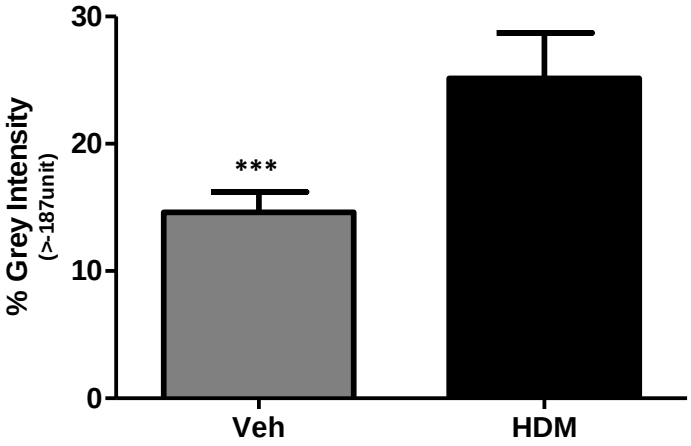

Figure 17. Quantitative Histological Analysis of Peribronchial Inflammation. Histology images acquired in the vehicle control, and after five doses of HDM 250 µg. Data expressed as mean ± SEM. ***$p<0.001$, by a two-tailed independent t-test. Intensity threshold defined as grey intensity at which 90% of area is below.

3.3.2 *Dose Response Effect of Budesonide on HDM Induced Airway Inflammation*

3.3.2.1 *Representative CT Images*

At baseline, there was little to no presence of higher tissue densities (>-100 HU) around the major airways. After five exposures of HDM 250 µg, an increase in peribronchial density was observed. With the administration of BUD_{300}, a decrease in density around the airways was seen in HDM exposed animals (Figure 18).

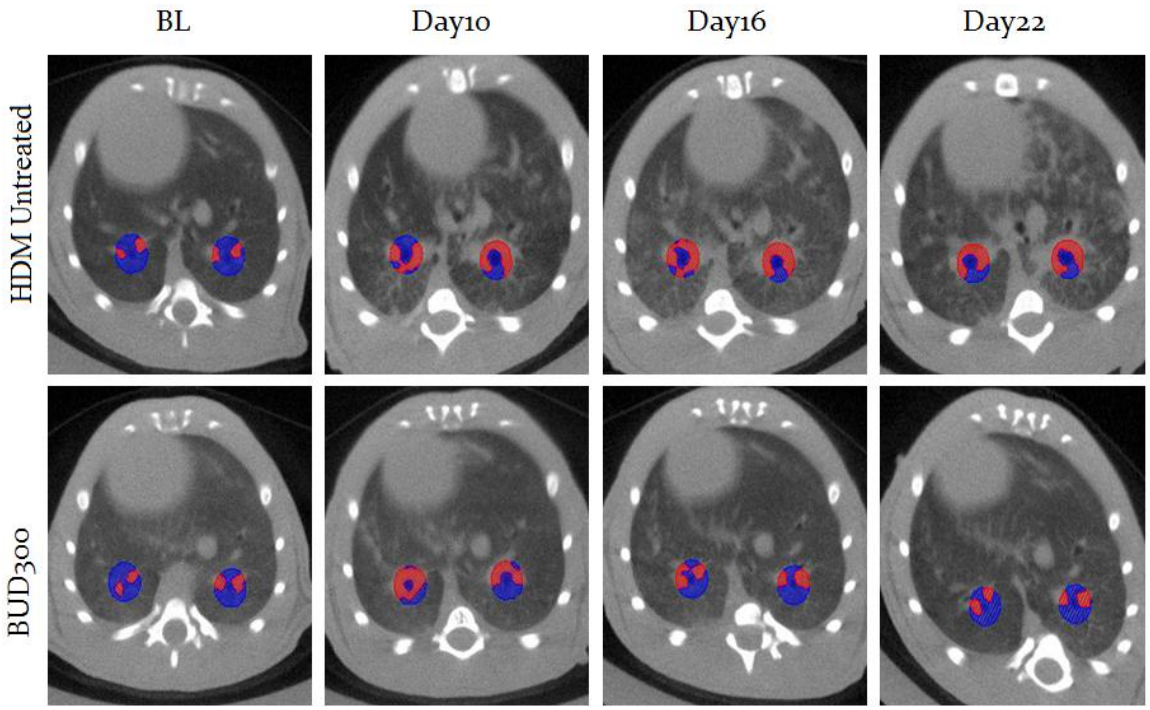

Figure 18. Representative Axial CT Slices. Baseline (**BL**), **Day10** after five HDM doses, after three doses of BUD 300 µg/kg (**Day16**), and after six doses of BUD 300 µg/kg (**Day22**). Blue shades denote values between -100 HU and -200 HU while red shades denote values >-100 HU.

3.3.2.2 *CT Densitometry – Effect of Budesonide on Peribronchial Density*

After three doses of 10 µg/kg BUD, no significant change in peribronchial density was observed compared to HDM+Veh_{BUD}. After three treatments of BUD 100 and 300 µg/kg, a significant reduction in density compared to HDM+Veh_{BUD} was noted, with densities returning to baseline levels ($p<0.05$, Figure 19a&c). There were no statistical differences between the BUD doses after three administrations, although a trend for a reduction in density relative to BUD dose was observed (Figure 19a&c). After six doses of BUD 10, 100, and 300 µg/kg, peribronchial densities returned to baseline levels for all BUD dosages compared to HDM+Veh_{BUD} ($p<0.01$, Figure 19b&d). Again, there was no statistical difference between the BUD doses after six administrations. No significant difference was observed within the BUD dose groups between three and six administrations (Appendix II-9.3.1, Figure 27). Peribronchial density was significantly less in Veh_{HDM}+BUD and Veh_{HDM}+Veh_{BUD} compared to HDM+Veh_{BUD} throughout the treatment phase ($p<0.05$).

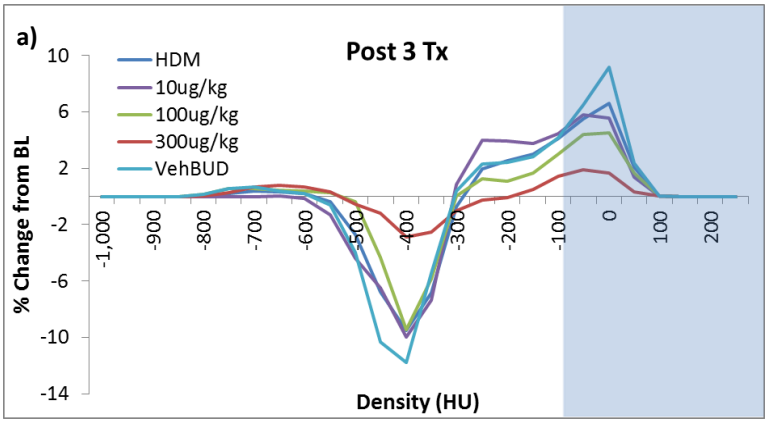

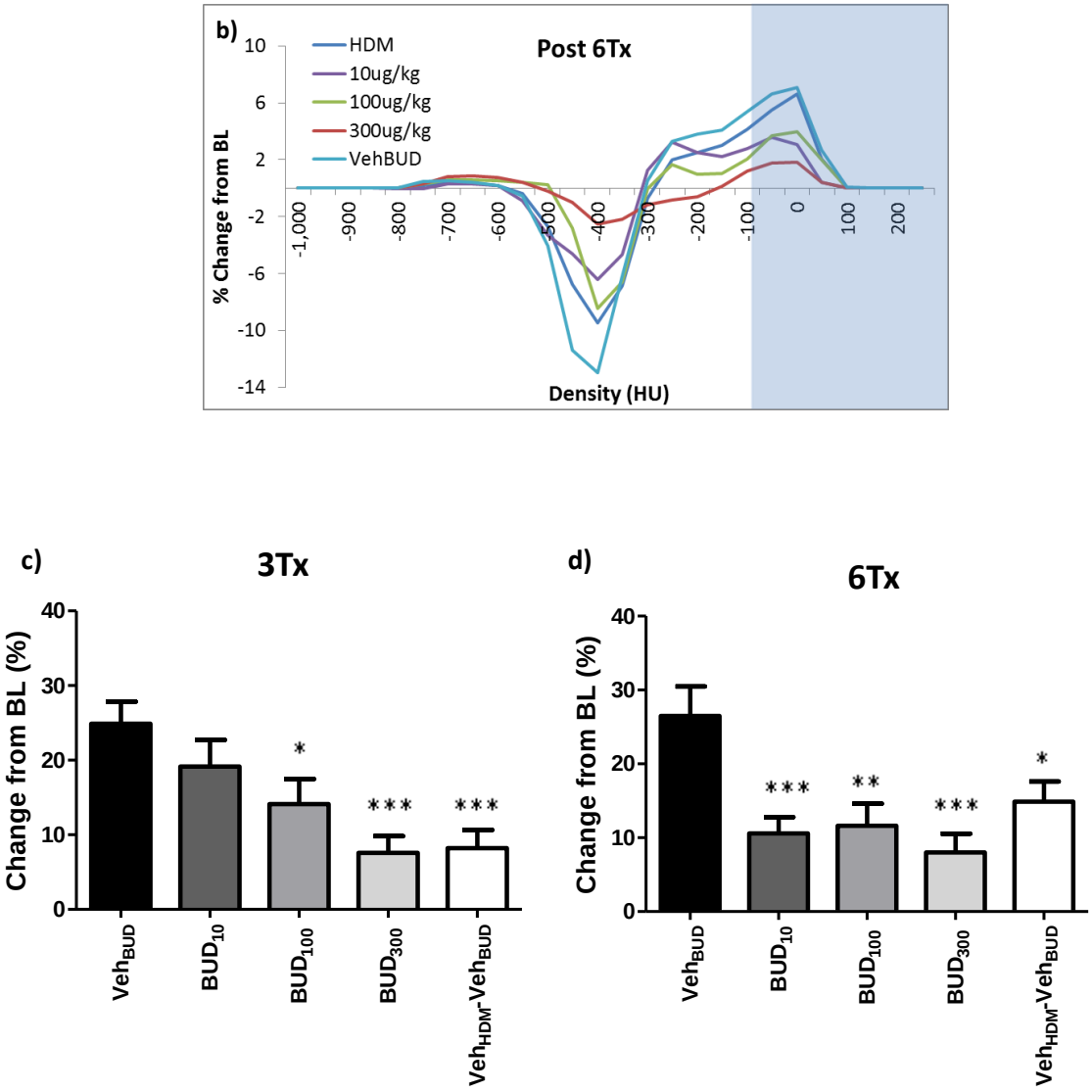

Figure 19. Change from Baseline in Peribronchial CT Density with Budesonide Treatment. **a)** After three doses BUD and **b)** after six doses BUD. Change from baseline of the percent voxels above the density threshold of -100 HU. **c)** After three doses BUD and **d)** after six doses BUD. Data are expressed as mean ± SEM. *p<0.05, **p<0.01, and ***p<0.001 (vs. Veh_{BUD}) by a one-way ANOVA with a Dunnett post-hoc test. Blue box: Density threshold. HU: Hounsfield units.

3.3.2.3 *BAL Total Cell Count and Percent Eosinophils*

No significant difference in TCC between the BUD treated groups and HDM+Veh_{BUD} were observed after three doses of BUD (Figure 20a). The Veh_{HDM}+BUD and Veh_{HDM}+Veh_{BUD} had significantly lower TCC compared to HDM+Veh_{BUD} and HDM+BUD_{300} ($p<0.05$). Additionally, there were no statistical differences between the BUD concentrations after three administrations. After six administrations, BUD 100 and 300 µg/kg led to significantly lower TCC compared to HDM+Veh_{BUD} ($p<0.05$, Figure 20b). The Veh_{HDM}+BUD and Veh_{HDM}+Veh_{BUD} groups had significantly lower TCC compared all treatment groups ($p<0.001$). No statistical differences were observed between the treatment concentrations after six BUD administrations. In the BUD 10 µg/kg group, TCC significantly increased from three to six treatments, while the remaining BUD groups showed no significant effect of treatment duration ($p<0.05$, Appendix II-9.3.2, Figure 28).

No significant differences were observed in percent eosinophils between HDM+Veh_{BUD} and all BUD doses after three doses (Figure 20c). Additionally, there were no statistical differences between BUD doses after three administrations. After six doses of BUD, only BUD 10 and 100 µg/kg induced a significant decrease in the percent eosinophils compared to HDM+Veh_{BUD} ($p<0.05$, Figure 20d). Again, there were no statistical differences between dosages after six BUD administrations. BUD 10 µg/kg did significantly decrease the percent eosinophils between three and six doses, while the remaining groups showed no significant difference ($p<0.05$, Appendix II-9.3.2, Figure 29).

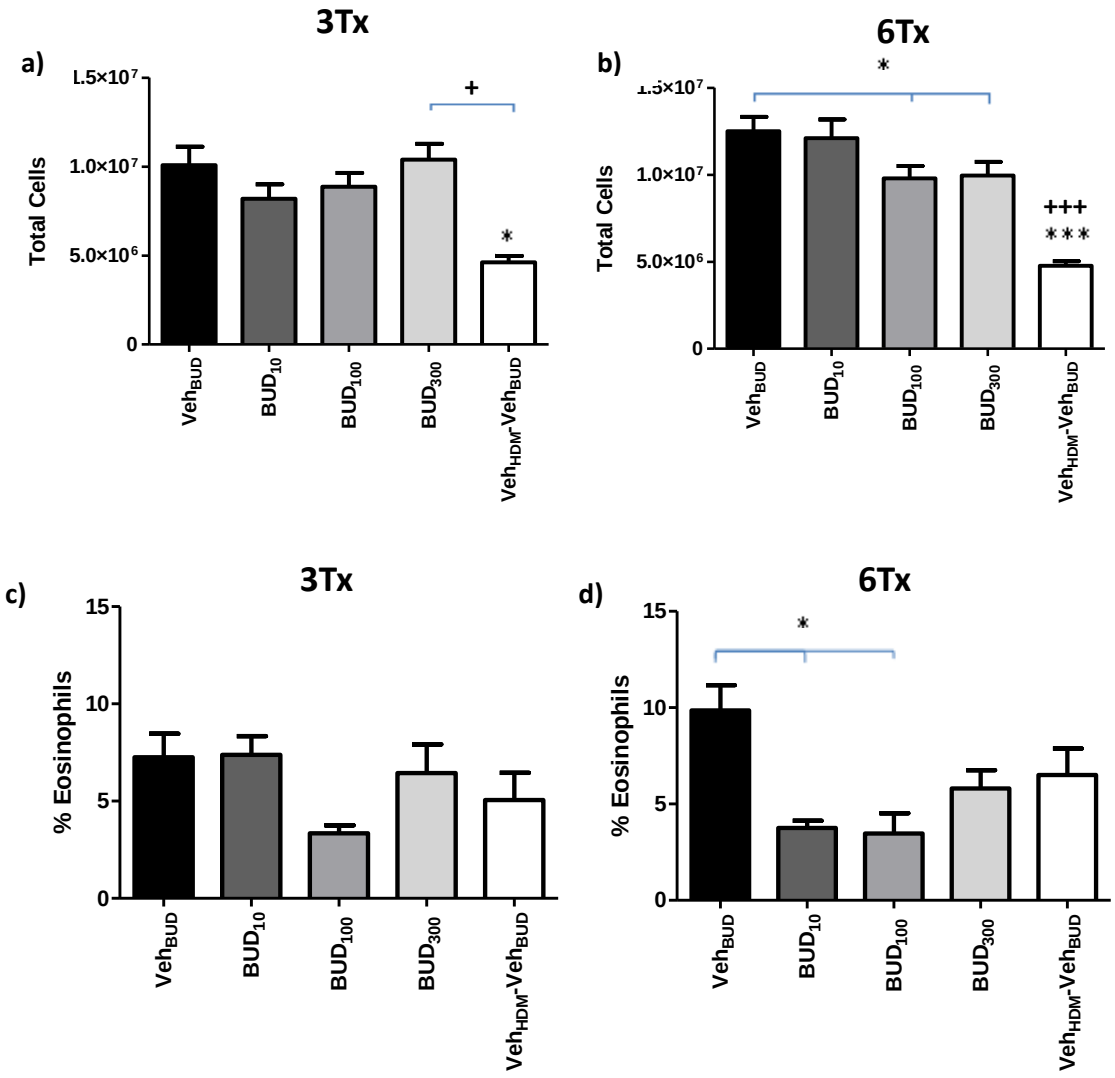

Figure 20. BAL Total Cell Counts and Percent Eosinophils with Budesonide Treatment. TCC in BAL **a)** After three BUD doses and **b)** after six BUD doses. Eosinophils expressed a percent of total cells from the BAL **c)** After three BUD doses and **d)** after six BUD doses. Data are expressed as mean ± SEM. *p<0.05 and ***p<0.001 (vs. Veh_{BUD}) by a one-way ANOVA with a Dunnett post-hoc test. +p<0.05 and +++p<0.001 (vs. Veh_{HDM}+Veh_{BUD}) by a one-way ANOVA with a Tukey post-hoc test.

3.3.2.4 *Histology*

After three and six administrations of BUD, inflammation was reduced around the major airways compared to HDM+Veh_{BUD} (Figure. 21). Quantitative analysis showed the degree of inflammation within the region of interest (ROI) around the major airways significantly decreased after three treatments of BUD 300 μg/kg (13.41±1.99%) compared to the HDM+Veh_{BUD} group (23.48±3.13%, $p<0.01$). No significant change in inflammation within the ROI was observed in the 10 μg/kg and 100 μg/kg BUD groups. Furthermore, there was no dose response observed after three administrations of BUD (Figure 22a). After six doses of BUD 100μg/kg (10.69±0.59%) and 300 μg/kg (12.26±1.66%), a significant decrease in inflammation was observed within the ROI compared to the HDM+Veh_{BUD} (23.27±4.28%) ($p<0.05$, Figure 22b). No significant change in inflammation was seen in the BUD 10μg/kg group. Again, no dose response was observed after six BUD administrations. The Veh_{HDM}+BUD and Veh_{HDM}+Veh_{BUD} were significantly different from HDM+Veh_{BUD} throughout the treatment phase ($p<0.001$). A temporal response was only observed in the HDM+BUD_{100} group. The remaining groups, HDM+Veh_{BUD}, HDM+BUD_{10}, and HDM+$BUD_{300,}$ showed no significant differences between three and six administrations (Appendix II-9.3.3, Figure 30).

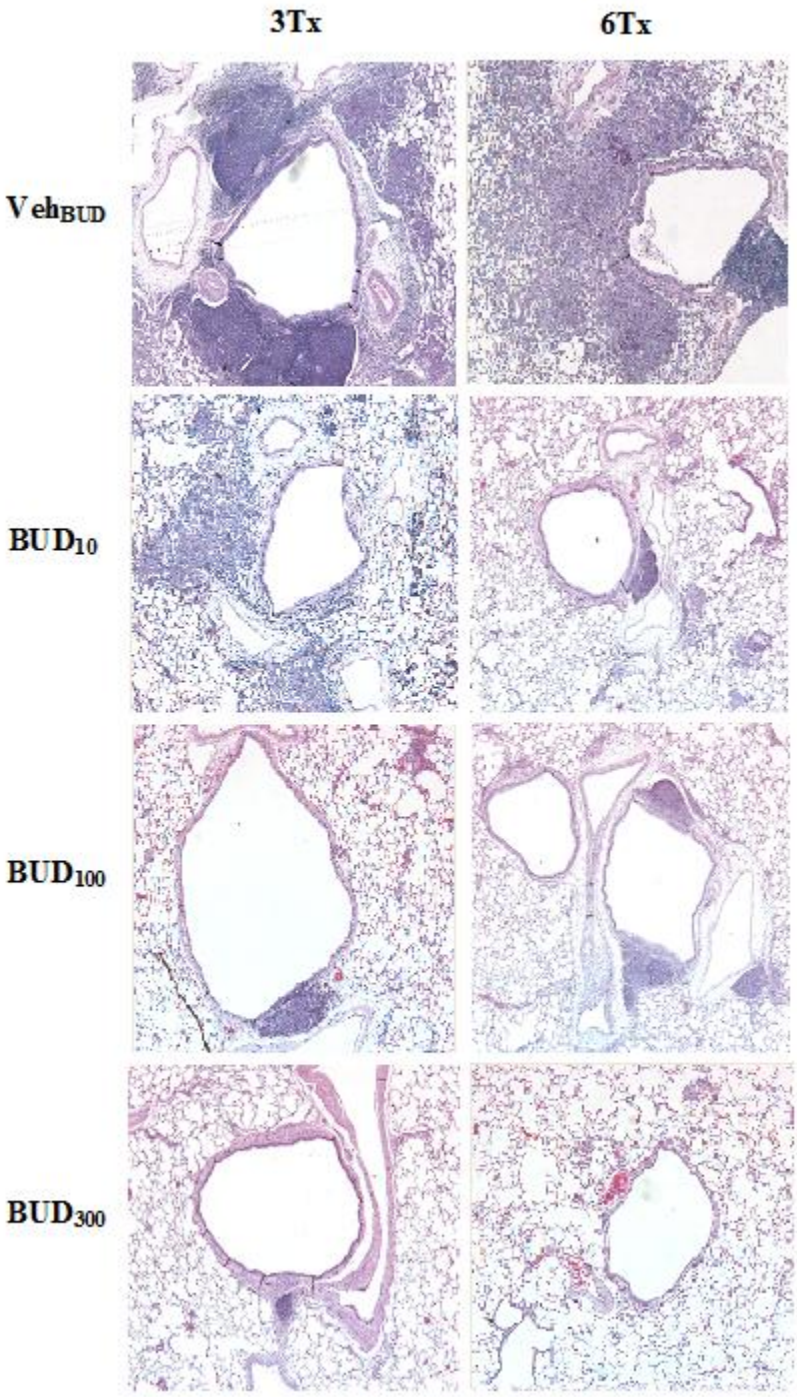

Figure 21. Representative Histological Lungs Slices of Budesonide 10, 100, 300 µg/kg Treated Animals in an Allergic Airway Model. After three (**3Tx)** and six (**6Tx)** administrations.

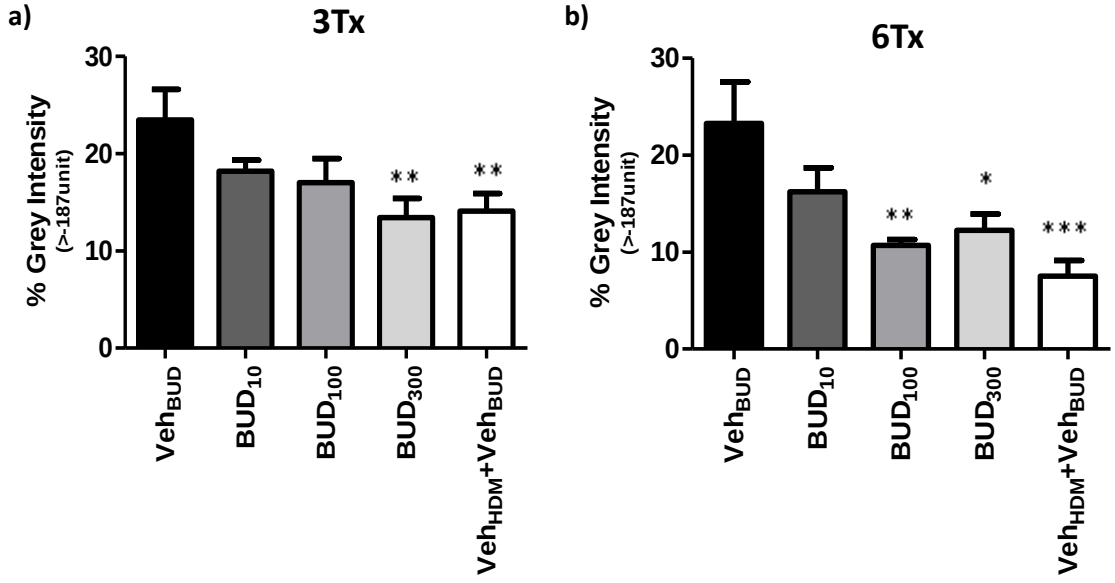

Figure 22. Quantitative Histological Analysis of Peribronchial Inflammation. Inflammation measured as percent of total area of interest above the grey intensity threshold of -187 HU. **a)** After three doses BUD and **b)** after six doses BUD. Data are expressed as mean ± SEM. *p<0.05, **p<0.01, and ***p<0.001 (vs. Veh_{BUD}) by a one-way ANOVA with a Dunnett post-hoc test.

3.4 BAL Albumin Concentration

A significantly higher concentration of albumin was found in the BAL supernatant of animals exposed to five doses of HDM 250 µg compared to naive and the vehicle control animals ($p<0.05$, Figure 23a). After six doses of BUD 300 µg/kg, a significant decrease in the BAL albumin concentration was observed ($p<0.001$). Interestingly, the control group ($Veh_{HDM}+Veh_{BUD}$) showed no difference in albumin concentration compared to $HDM+Veh_{BUD}$ and had a significantly higher concentration of albumin compared to $HDM+BUD_{300}$ ($p<0.05$, Figure 23b).

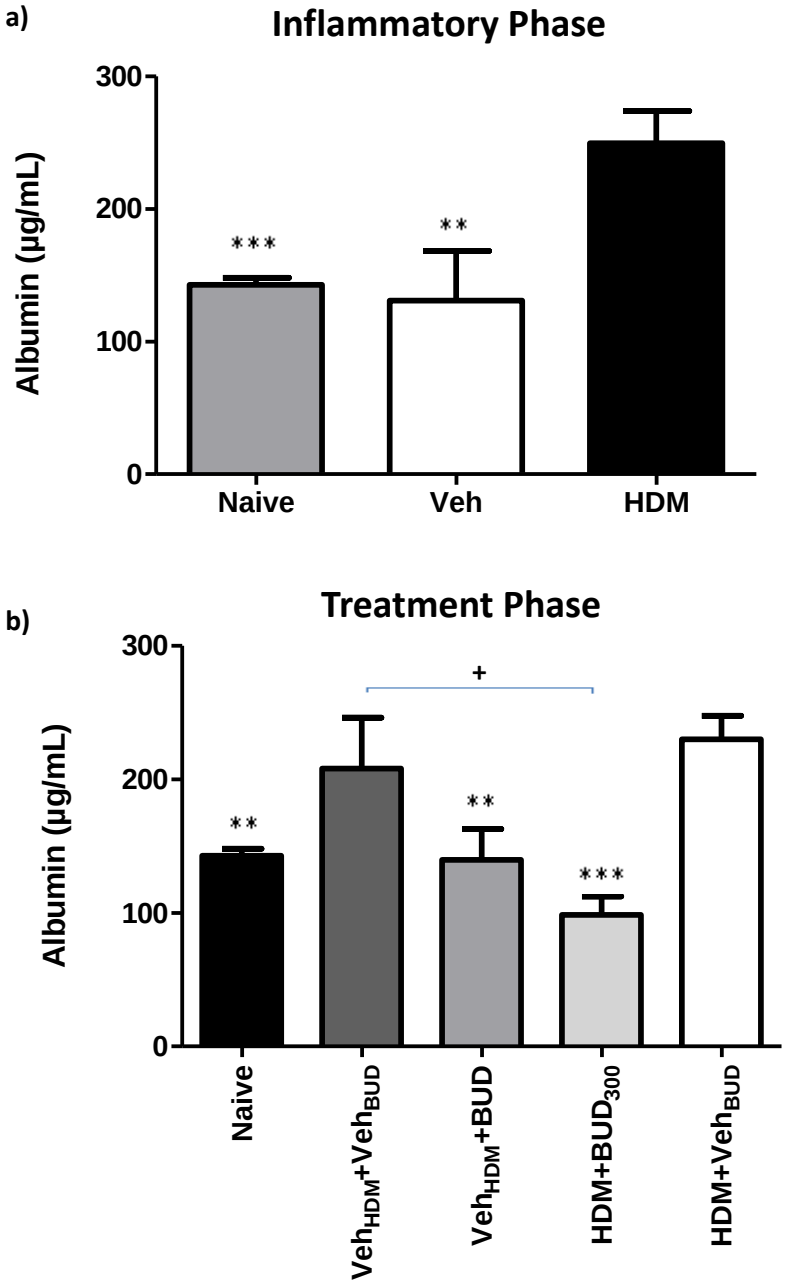

Figure 23. Albumin Concentration in BAL fluid. a) After five doses HDM and **b)** after six doses of BUD. Data are expressed as mean ± SEM. **p<0.01 and ***p<0.001 (vs. Veh_{BUD}) by a one-way ANOVA with a Dunnett post-hoc test. +p<0.05 by a one-way ANOVA with a Tukey post-hoc test.

CHAPTER 4

4 DISCUSSION

The objectives of this study were to investigate the use of CT imaging to further understand how allergic events lead to asthma, in particular airway inflammation, and to determine if CT densitometry can detect the impact of corticosteroid therapy on established inflammation, as a standard for novel intervention strategies. This was accomplished by evaluating peribronchial changes in the progression and regression of inflammation in a rat model of allergic airway disease.

The CT validation study evaluated the intra-subject variability in CT densities of the three different segmentation methods. We showed that lung segmentation had the lowest intra-subject variability followed by the thoracic and airway segmentations. This error measured was applied when analyzing peribronchial density changes to determine whether the changes were due to the effects of the treatment and not a result of variability in the segmentation method. The CT validation study demonstrated that the three different segmentation methods were reproducible. Thoracic segmentation is beneficial for measuring lung volume and tidal volumes. It included tissues such as the heart and ribs in the analysis, but required regular user manipulation and was time efficient (~10 min). The thoracic segmentation had an intra-subject variability of 2.86%. Lung segmentation is the best representative segmentation type for measuring pulmonary diseases and the most concise method in measuring the lung with the lowest intra-subject variability of 0.58% and user manipulation. However, it took the longest to perform (~15 min). Airway segmentation provided large airway density profiles important for studying

airway pathologies such as inflammation, was the most time efficient (~5 min), but required a large amount of user manipulation and had the largest intra-subject variability at 5.82%. The ability to perform these different segmentations is important as they can provide whole lung and airway analysis and lung volumes as a standardized investigative tools used for CT analysis (Jobse *et al*. 2009).

In the allergic inflammatory model, CT was sensitive for the detection of inflammation around the major airways depicted by an increase in density values around -100 HU or greater. The biological data confirmed these findings as total cell counts, eosinophils, and inflammation by quantitative histology measurements had increased. Furthermore, a dose and temporal response to steroid therapy with budesonide was observed with CT densitometry, suggesting that CT was sensitive in detecting the reduction in inflammation proportional to budesonide concentration and the duration of treatment as the density profiles returned to a state similar to baseline. Histology confirmed a dose and treatment duration dependency of budesonide, since a significant reduction in grey intensity (e.g. inflammation) around the major airways was observed. However, BAL TCC and eosinophils did not mimic these results.

CT has been employed in several animal models of lung disease, but there is limited concurrence in the segmentation methods used to quantify the data. Different research groups have created automated programs clinically for patients with emphysema (Boehm *et al.* 2008), preclinically using porcine lungs (Carroll *et al.* 2006), and mouse models of emphysema and asthma (Artaechevarria *et al.* 2009, Lederlin *et al.* 2010) to segment the airways. In addition, user-dependent clinical lung segmentations have been created in

emphysematous patients (Cavigli *et al.* 2009) and preclinically in rat models of asthma (Jobse *et al.* 2009). There are methodological discrepancies that can be reduced by employing standard user-dependent segmentation techniques, thus allowing better study comparisons (Jobse *et al.* 2009). This user-based thoracic, lung and airway segmentation method are suited for quantification of different lung diseases.

Traditionally, invasive outcome measures have been used to study allergic airway disease and effect of therapy. Serial sacrifice is most common amongst researchers to measure fundamental biological information of the inflammatory response to allergen exposure in *in vivo* rat and mice models of allergic airway disease (Singh *et al.* 2002, Johnson *et al.* 2004, Ahn *et al.* 2007, Werner-Klein *et al.* 2008, Turi *et al.* 2010, Botelho *et al.* 2011, etc.), but limited use of imaging techniques, such as the CT, has been used for analysis and quantification of the disease. In the inflammatory phase of our model, CT densitometry revealed an influx in peribronchial inflammation with the increase in density values above the 90% density threshold; the assumption is that changes in density above -100 HU represent the inflammatory processes. The 250 µg concentration of HDM allergen delivered in five doses every other day significantly increased the density distributions, shifting the histogram curve to the right, independent of the dosage and number of HDM administrations. Jobse *et al.*, using a similar model, found comparable results using HDM 150 µg delivered IT for 7 and 10 exposures using both a lung and thoracic segmentation method. BAL cytology confirmed these findings, as they showed robust and statistically significant eosinophilic inflammation and increased TCC in HDM exposed animals compared to controls. After sensitization to HDM, Brown Norway rats

have been shown to develop an immediate airway response to HDM challenge compared to controls with an increase in BAL eosinophils after two IT exposures to HDM 10 µg (Singh *et al.* 2002). Additionally, mouse models of allergen exposure to HDM express sustained airway eosinophilic inflammation in the BAL (Johnson *et al.* 2004).

Visually, an increase in inflammatory cells was observed histologically in the HDM exposed animals compared to controls. Quantitative histology confirmed lung inflammation as the HE-stained sections from animals exposed to 250 µg HDM had significantly greater percent grey intensity depicted as an influx in inflammatory cells around the major airways compared to vehicle controls. Similar results showed severe inflammatory lesions after HDM exposure with an increase in inflammatory cells around blood vessels, as well as the major and peripheral airways (Singh *et al.* 2002, Jobse *et al.* 2009). Taylor *et al.* demonstrated that antigen challenge of sensitized BN rats results in loosely packed fibrous tissue, an influx of inflammatory cells, and thickened alveolar walls which was evidence of injury due to leakage of plasma from the vessels. This structural damage was observed in the present model as an increase in albumin in the BAL supernatant of HDM animals compared to vehicle controls and naïve animals. These histological results furthermore confirm the CT finding of increased densities around the major airways was due to increased inflammatory cells and oedema. Although this method of analysing histology is novel and does not employ traditionally used scoring, it mimics the airway segmentation and analysis used for CT densitometry.

Asthma management and regulation guidelines state that a major aim is to treat eosinophilic airway inflammation and the use of inhaled corticosteroids is recommended

as treatment for asthma exacerbations (Gibson *et al.* 2000). Research has already shown that the use of inhaled steroids in the management of asthma results in decreased infiltration of inflammatory cells, decreased airway hyperresponsiveness, and inhibition of vascular exudation and mucous secretion (Gibson *et al.* 2000, Goldsmith *et al.* 2004, Horvath *et al.* 2006). CT visualization and quantification of these effects has been limited. With this study, we have that shown CT densitometry was sensitive in detecting a reduction in inflammation around the major airways after budesonide treatment. It showed that BUD 100 and 300 µg/kg reduced inflammation to a state similar to baseline after three doses every other day with the continuance of allergen exposure. After six treatments, BUD 10 to 300 µg/kg showed the resolution of higher CT densities around the airways. BAL cytology results did not confirm these findings, as there were no differences in total cell counts and eosinophil counts after three BUD doses in the treatment groups compared to HDM exposed rats. Not until six administrations did the 100 and 300 µg/kg doses reduce total cell counts and the 10 and 100 µg/kg reduce eosinophil counts in the BAL. We believe the effects on BAL inflammatory cells did not follow similar trends observed with our CT densitometry because BAL extracts cells from the entire lung, while our CT analysis focused directly on the major airways. However, a visual assessment of the histological lung slices showed a decrease in the apparent inflammation around the airways (Figure 21). Therefore, quantification of histology was performed to measure the change in peribronchial inflammation with BUD treatment. The histology results correlated with CT in terms of the reduction in peribronchial inflammation with steroid treatment. After three doses of BUD 300 µg/kg and six doses

of BUD 100 µg/kg, the percent grey intensity was significantly reduced, indicating fewer cells in the airway ROI compared to the HDM exposed group.

Delivering BUD after allergen challenge was performed to evaluate its role in reducing established inflammation, whereas previous studies gave BUD prior to allergen challenge as preventative therapy (Xu *et al.* 2000, Basdemir *et al.* 2001, Shen *et al.* 2005). The acute effect of short-term inhaled budesonide 2 and 4 hours prior to OVA challenge in Sprague Dawley rats led to reduced inflammatory cells in asthmatic rats and no severe inflammation present around the major airways (Basdemir *et al.* 2001). In BN rats given BUD 2.5 mg/kg initially, again after 17 hours, then exposed to OVA, total cell counts in the BAL were reduced in the BUD treated group. The authors hypothesized that this was due to the significant decrease in macrophages in BUD treated animals compared to controls, with little effect on the number of eosinophils (Xu *et al.* 2000). Johnson *et al.* chronically exposed mice to HDM 25 µg for 5 or 7 weeks, initiating robust airway inflammation, then treated the mice with BUD/Formoterol (Symbicort™) immediately prior to allergen challenge for 2 weeks, which led to a significant decrease in both total cellular airway inflammation in histology and BAL eosinophilia (Johnson *et al.* 2008). Their results were confirmed with histopathology, demonstrating that the treatment reduced inflammation in the whole lung. These findings were similar to those found using our method of quantitative histology.

CT densitometry and histological analysis are in agreement that BUD reduced density changes and cellular influx brought on by allergen challenge. However, there is literature stating that these changes may be due to the effect of BUD on oedema induced

by the challenge and not directly to the reduction in inflammatory cells (Tigani *et al.* 2003, Horvath and Wanner, 2006). Tigani *et al.* showed, 24 hours after OVA administration, significant oedema depicted by MRI. BUD was administered 24 hours later and the histological results showed a decrease in oedema and BAL protein concentrations. These data correspond with our results showing that BUD treated groups had significantly lower concentrations of albumin in the supernatant, thus less oedema, compared to animals with continued to HDM exposure but not treated with BUD.

The experimental control groups of this study, Veh_{HDM}+BUD and Veh_{HDM}+Veh_{BUD}, showed mixed results. The CT density distributions and BAL total cell counts indicated healthy lungs, but the percent eosinophils, quantitative histology, and albumin concentration results indicated otherwise. CT densitometry showed significantly fewer change from baseline compared to the HDM exposed group and lower BAL TCC after three and six treatments. The control group's percent eosinophils remained high and albumin analysis showed high concentrations in the Veh_{HDM}+Veh_{BUD}, not different from HDM exposed animals. The quantitative histological results posed even more confusion as the percent grey intensity significantly decreased throughout the treatment phase, not corresponding to the imaging and biological results. The cause for this discrepancy is unclear, and the examination and evaluation of possible reasons needs to be investigated; excipients in the budesonide vehicle control, animal bedding, and the BN phenomenon of spontaneous severe eosinophil-rich multisystemic granulomatosis could be responsible (See Study Limitations).

This study possesses benefits that are clinically associated with the timing and dose of budesonide in an allergic airway model. Additionally, this model has demonstrated similarities in the allergic initiation and inflammatory effects seen clinically by methacholine, mannitol, and fractional exhaled nitric oxide challenges (Anderson and Lipworth, 2012) and eosinophil reduction seen clinically to make it a valid preclinical model to measure the efficacy of lung-directed therapies (Gauvreau *et al.* 1996, Gibson *et al.* 2000). The results of this study are consistent with clinical results published by Gauvreau *et al.* demonstrating that seven doses of budesonide (400 µg) can attenuate the magnitude of the asthmatic response and reduce airway responsiveness and eosinophils induced by allergen challenge. Gibson *et al*. (2000) successfully showed that a single dose of budesonide (2400 µg) could reduce sputum eosinophils and slightly increase FEV_1 after treatment.

It has been documented that CT densitometry is more sensitive to assess the progression of pulmonary diseases, such as emphysema, asthma, and fibrosis, than lung function tests (Biernacki *et al.* 1997, Goris *et al.* 2003, Stoel & Stolk, 2004). It has not, however, been employed as a diagnostic tool or used to evaluate the efficacy of treatment in asthma (Stoel & Stolk, 2004). CT densitometry in this current study was used to measure the extent of the allergic airway inflammation after exposure to an allergen and the anti-inflammatory effects of corticosteroid therapy. The CT airway densitometry had the ability to correctly identify those animals with increased density due to airway inflammation and decreased density by steroid therapy. The specificity of CT densitometry did not, however, correctly identify all the control animals without the

disease resulting in false positives. This model provides a standard measurement tool with an optimized CT acquisition protocol and densitometric technique to use allowing a standardized and reproducible result, especially useful for new drug trials.

CT densitometry was shown to be a sensitive, non-invasive method of evaluating the anti-inflammatory effects of budesonide and can be used for screening therapies in allergic lung models. It allows for a localized assessment of peribronchial inflammation and appears to be a more precise measure of airway inflammation than BAL, which provides a global assessment of the inflammatory state of the lung.

CHAPTER 5

5 LIMITATIONS OF THE STUDY

There are a number of potential limitations of this study, starting with the airway segmentation method. While it focused around the major airways, the primary region affected in asthma, and excluded the rest of the lung, the user manipulation required for this segmentation method required a certain level of expertise in identifying the region of interest. Potential variability between and within animals themselves was observed and illustrated by the CT validation study. The landmark of the seventh rib and region of interest of 3.5 mm diameter centred on the lumen and 6.9 mm in length were chosen to reduce the subjectivity of selecting the airways. The fact that the BAL analysis of the TCC and percent eosinophils did not correlate with CT densitometry was probably due to the different sampling areas; CT densitometry included tissues surrounding the major airways and BAL fluid from the whole lung.

Budesonide was chosen due to its potent anti-asthma effects as it has shown high receptor affinity, airway selectivity, prolonged tissue retention, and inhibition of inflammatory symptoms such as oedema and vascular hyperpermeability (Bandi *et al*. 2001). The CT results showed decreased densities and quantitative histology showed a reduction in grey intensity after three and six treatments of budesonide compared to HDM exposed, but the BAL findings did not correlate. While one factor may be the sampling area, it may also be that budesonide did not reduce inflammation but only acted on oedema caused by the allergen exposures. Even after the continuance of HDM and BUD exposures for three more administrations, the resolution seen at the lowest budesonide

concentration was not observed in the biological results, indicating the possibility that a higher concentration of budesonide is required to reduce oedema and persist to reducing inflammation.

Another potential limitation is the budesonide formulation used and the possible effects caused by the excipients within the vehicle (Veh_{BUD}). The control group exposed to the vehicle formulation (Veh_{HDM}+Veh_{BUD}) showed an increase in BAL albumin concentration over time, suggesting that the excipients in the vehicle may cause harm to the lung structure. It has been documented by Gao *et al.* and Hirama *et al.* that EDTA at a concentration of 2.0 mM and polysorbate-80 at a concentration above 300 µg/mL may modify lung membranes by damaging the wall junctions causing pulmonary microvascular permeability and thus "leaky lungs". The amounts of EDTA (0.1 mM) and polysorbate-80 (20 µg/mL) within the BUD vehicle did not reach these destructive concentrations, but with repeated exposure (six doses), it is plausible to deduce that they may in fact be increasing lung permeability in the control animals, thus resulting in a detectable rightward shift in CT density due to oedema.

Other factors that may have contributed to the abnormal results of the control animals are the animal corncob bedding type and strain of rat. Researchers have attempted to create animal protocols where all possible variables are controlled. It is easy, however, to dismiss simple elements, such as the type of animal bedding which may contain harmful endotoxins and affect study results, especially for lung inflammation studies. D.A. Schwartz *et al.* researched, in the early 1990s, the effect of the endotoxin lipopolysaccharide (LPS) found in corn dust extract (CDE) within human and mouse

inhalation studies. They discovered that endotoxins present in corncob dust are responsible for inflammatory response seen within the lungs (Schwartz *et al.* 1994, Schwartz *et al.* 1995, Jagielo *et al.* 1996, Schwartz 1996). Further investigations by Kaliste *et al.* compared the percentage of airborne dust and endotoxin in clean and soiled animal bedding, and discovered that the bedding contained biologically active compounds (Kaliste *et al.* 2004). The dust and endotoxin affect both the staff as well as the animals, resulting in the incidence of airway obstruction and immunologic responses; increased BALF TCC, neutrophils, and TNF-α (Schwartz *et al.* 1994, Kaliste *et al.* 2004). The CAF uses autoclaved corncob bedding, which has been shown by Whiteside *et al.* to contain the highest level of endotoxins and coliform counts of all animal bedding types (Whiteside *et al.* 2010). These studies provide a potential explanation that the inhaled endotoxins found in the corncob bedding may have caused inflammatory damage to the control animals, increasing BAL eosinophils, neutrophils, and albumin concentration. This suggestion would have to be examined further to be conclusive.

The use of female Brown Norway rats may itself be a limitation of the study. It has been documented that Brown Norway rats mimic allergic human asthma in several respects, by producing high levels of IgE in response to active immunization and by developing both early and late asthmatic response to allergen challenge, causing airway constriction and an influx of inflammatory cells and mediators (Brange *et al.* 2009, Hylkema *et al.* 2002). The BN rat can also develop spontaneous severe eosinophil-rich multisystemic granulomatosis (Germann *et al.* 1998, Noritake *et al.* 2007, Percy *et al.* 2008). This event is found in both sexes, but predominantly in females of a young age

starting around 8 weeks, the age of the animals used in this present study, with recovery after 15 weeks of age (Percy *et al.* 2008). The lesions are multifocal to diffuse, found in the parenchyma, and characterized by cellular infiltrate consisting of eosinophils and histiocytes with frequent perivascular oedema (Noritake *et al.* 2007, Percy *et al.* 2008). This phenomenon may explain the increase in the percent eosinophils and albumin concentrations in the BAL fluid within the control animals as the samples were obtained from the entire lung. However, the histology and CT analyses of this study focused on the major airways where eosinophil-rich multisystemic granulomatosis was absent. The complete baseline data set of CT airway segmentation analysis was re-examined for the presence of granulomatosis; three rats were eliminated from the data analysis. A preliminary study on this phenomenon is found in Appendix III. With this information regarding the BN rat strain, it is important to non-invasively collect baseline data from a sample to ensure this phenomenon is not present before initiating experimental procedures.

CHAPTER 6

6 CONCLUSIONS

Our study has shown that CT peribronchial densitometry is sensitive to the detection of allergic airway disease and its regression by steroid therapy. This peribronchial region of interest expressed an increased inflammatory change in the density profile with a right shift to a denser region of -100 HU and returned back to a state similar to baseline in a dose response manner to the inhaled corticosteroid, budesonide. Quantitative histology and albumin measurements confirmed the anti-inflammatory effects of budesonide, as seen by CT as decreased inflammation surrounding the major airways. BAL cytology was not representative of local airway changes, suggesting that outcome measures specific to the peribronchial region (used in CT analysis) may be a more accurate depiction of the pathological changes and therapeutic effect of steroids in allergic airway disease.

CT is an important investigative tool, providing a method of analysis that is non-invasive and allows the longitudinal study of structure and function of the lungs. Furthermore, CT allows the translation of preclinical study of disease progression and regression by treatment to clinical application using individual subjects as their own controls. With developed segmentation parameters to assess the extent of airway disease, CT provides the ability to quantify pathologies using density profiles and provides a method to study the efficacy of novel clinical therapies in an allergic airway animal model and can be further applied to new drug trials in patients with asthma. Additionally, this model demonstrated a high sensitivity and specificity of the developed optimized CT

acquisition protocol and densitometric technique, permitting a standardized and reproducible result. Of particular relevance would be the adaptations of this non-invasive technique to better understand disease progression and effectiveness of the anti-inflammatory treatment in patients with asthma.

CHAPTER 7

7 FUTURE DIRECTIONS

Potential studies should investigate a longitudinal evaluation and dose response of other anti-inflammatory treatments using this model to explore their therapeutic effects as measured by CT densitometry. This would provide important information that may assist clinical research. Additionally, the lung and thoracic segmentation methods could be investigated in the context of different lung disease studies, as they may better represent that disease. Discovering CT density thresholds pertaining to individual lung diseases and their treatments would be extremely valuable for measuring the initiation, progression and possible regression of the disease.

The pilot CT validation study provides useful preliminary information regarding the random error associated within the airway, thoracic, and lung segmentations. Further investigation is still required to provide more concrete findings. Analysis should continue using a greater number of animals with CT imaging every day, every other day, and every week representing different imaging time-points of individual investigative models. Additionally, different rodent species, primarily rats and mice, should be investigated to determine the specific error associated within each species using the different segmentation methods. Segmentation analysis of these studies should also be performed by multiple users to include user subjectivity in the error. With the results of these investigations, it will be easy for investigators to select a segmentation method and associate a concrete error to that specific analysis based on the criteria of the experiment.

CHAPTER 8

8 BIBLIOGRAPHY

Abdullah, K.A. & Khan, S. (2007). Evidence-Based Selection of Inhaled Corticosteroid for Treatment of Chronic Asthma. *Journal of Asthma 44,* 1-12

Ahn, J.H., Kim, C.H., Kim, S.J., Lee, S.Y., Kim, Y.K., Kim, K.H., Moon, H.S., Song, J.S., Park, S.H., & Kwon, S.S. (2007). Inflammatory and Remodeling Events in Asthma with Chronic Exposure to House Dust Mites: A Murine Model. *Journal of Korean Medical Science, 22(6),* 1026-1033

Akira, M., Toyokawa, K., Inoue, Y., & Arai, T. (2009). Quantitative CT in Chronic Obstructive Pulmonary Disease: Inspiratory and Expiratory Assessment. *Cardiopulmonary Imaging*. AJR *192:*267-272

Allen, J.E., Bischof, R.J., Chang, H-Y. S., Hirota, J.A., Hirst, S.J., Inman, M.D., Mitzner, W. & Sutherland, T.E. (2009). Animal Models of Airway Inflammation and Airway Smooth Muscle Remodelling in Asthma. *Pulmonary Pharmacology & Therapeutics*, *22,* 455-465

Anderson, G.G. & Morrison, J.F.J. (1998). Molecular biology and genetics of allergy and asthma. *Arch Dis Child,* 78, 488-496

Anderson, W.J. & Lipworth, B.J. (2012). Relationship of Mannitol Challenge to Methacholine Challenge and Inflammatory Markers in Persistent Asthmatics Receiving Inhaled Corticosteroids. *Lung* (Epub ahead of print)

Artaechevarria, X, Pérez-Martin, D., Ceresa, M., de Biurrun, G., Blanco, D., Montuenga, L.M., van Ginneken, B., Ortiz-de-Solorzano, C. & Muñoz-Barrutia, A. (2009). Airway Segmentation and Analysis for the Study of Mouse Models of Lung Disease Using Micro-CT. *Physics in Medicine and Biology, 54,* 7009-7024

Ask, K., Moeller, A., Gauldie, J., Farncombe, T.H., Labiris, R., & Kolb, M.R.J. (2008). The Use of Small Animal Imaging in Respiratory Disease Drug Discovery. *Drug Discovery Today: Therapeutic Strategies, 30(20),* 1-5

Auffray, C., Adcock, I.M., Chung, K.F., Djukanovic, R., Pison, C., & Sterk, P.J. (2010). An Integrative Systems Biology Approach to Understanding Pulmonary Diseases. *American College of Chest Physicians, 137,* 1410-1416

Babin, A.L., Cannet, C., Gerard, C., Wyss, D., Page, C.P., & Beckmann, N. (2011). Noninvasive Assessment of Bleomycin-induced Lung Injury and the Effects of Short-term Glucocorticosteroid Treatment in Rats using MRI. *Journal of Magnetic Resonance Imaging, 33(3),* 603-614.

Bandi, N., & Kompella, U.B. (2001). Budesonide Reduces Vascular Endothelial Growth Factor Secretion and Expression in Airway (Calu-1) and Alveolar (A549) Epithelial Cells. *European Journal of Pharmacology, 425,* 109-116

Bankier, A.A., De Maertelaer, V., Keyzer, C., & Gevenois, P.A. (1999). Pulmonary Emphysema: Subjective Visual Grading versus Objective Quantification with Macroscopic Morphometry and Thin-Section CT Densitometry. *Radiology, 211,* 851-858

Barnes, P.J. (2008). Immunology of Asthma and Chronic Obstructive Pulmonary Disease. *Nature, 8,* 183-192

Barnes, J.P. (1998). Anti-inflammatory Actions of Glucocorticoids: Molecular Mechanisms. *Clinical Science 94,* 557-572

Barnes, J.P. (1998). Efficacy of Inhaled Corticosteroids in Asthma. *Journal of Allergy and Clinical Immunology 102,* 531-538

Bartling, S.H., Dinkel, J., Stiller, W., Grasruck, M., Madisch, I., Kauczor, H.U., Semmler, H., Gupta, R., & Kiessling, F. (2008). Intrinsic respiratory gating in small-animal CT. *Eur Radiol, 18,* 1375-1384

Basdemir, D., Nuhoglu, Y., Bahceciler, N.N., Tukenmez, F., Kotiloglu, E., Barlan, I.B., & Basaran, M.M. (2001). Acute Effect of Inhaled Budesonide on Bronchial Inflammation in Asthmatic Rats. *Journal of Asthma, 38(6),* 461-467

Beckmann, N., Tigani, B., Ekatodramis, D., Borer, R., Mazzoni, L., & Fozard, J.R. (2001). Pulmonary Edema Induced by Allergen Challenge in the Rat: Noninvasive

Assessment by Magnetic Resonance Imaging. *Magnetic Resonance in Medicine, 45,* 88-95

Behr, J. & Furst, D.E. (2008). Pulmonary Function Tests. *Rheumatology, 47(Suppl 5),* 65-67

Biernacki, W., Redpath, A.T., Best, J.J., & MacNee, W. (1997). Measurement of CT lung density in patients with chronic asthma. *Eur Respir J,* 10, 2455-2459

Blamire, A.M. (2008). The Technology of MRI--The Next 10 Years? *British Journal of Radiology, 81(968),* 601-17

Bloemen, K., Verstraelen, S., van den Heuvel, R., Witters, H., Nelissen, I., & Schoeters, G. (2007). The allergic casade: Review of the most important molecules in the asthmatic lung. *Immunology Letters, 113,* 6-18

Blomgren, H., Lax, I., Naslund, I. et al. (1995). Stereotactic high dose fractionradiation therapy of extracranial tumours using an accelerator. Clinical experience of the first thirty-one patients. *Acta Oncol,* 34, 861-70

Boehm, H. F., Fink, C., Attenberger, U., Becker, C., Behr, J. & Reiser, M. (2008). Automated Classification of Normal and Pathologic Pulmonary Tissue by Topological Texture Features Extracted from Multi-Detector CT in 3D. *European Society of Radiology, 18 (12),* 2745-2755

Bogaert, P., Tournoy, K.G., Naessens, T., & Grooten, J. (2009). Where Asthma and Hypersensitivity Pneumonitis Meet and Differ. *The American Journal of Pathology, 174*(1), 3-13

Botelho, F.M., Llop-Guevara, A., Trimble, N.J., Nikota, J.K., Bauer, C.M., Lambert, K.N., Kianpour, S., Jordana, M., & Stampfli, M.R. (2011). Cigarette Smoke Differentially Affects Eosinophilia and Remodeling in a Model of House Dust Mite Asthma. *The American Journal of Physiology: Lung Cellular and Molecular Physiology, 45(4),* 753-760

Bousquet, J., Chanez, P., Lacoste, J.Y., Barnéon, G., Ghavanian, N., Enander, I., Venge, P., Ahlstedt, S., Simony-Lafontaine, J., Godard, P., & Michel, F.B. (1990). Eosinophilic Inflammation in Asthma. *The New England Journal of Medicine, 323,* 1033-1039.

Bousquet, J., Peter, K.J., William, W.B., Johnson, M., & Antonio, M.V. (2000). Asthma. From Bronchoconstriction to Airways Inflammation and Remodeling. *American Journal of Respiratory and Critical Care Medicine, 161(5),* 1720-1745.

Brange, C., Smailagic, A., Jansson, A.H., Middleton, B., Miller-Larsson, A., Taylor, J.D., Silberstein, D.S., & Lal, H. (2009). Sensitivity of Disease Parameters to Flexible Budesonide/Formoterol Treatment in an Allergic Rat Model. *Pulmonary Pharmacology & Therapeutics, 22,* 20-26

Brannan, J.D. (2010). Bronchial Hyperresponsiveness in the Assessment of Asthma Control: Airway Hyperresponsiveness in Asthma: Its Measurement and Clinical Significance. *Chest, 138,* 11-17

Brown, R.H., Croisille, P., Mudge, B., Diemer, F.B., Permutt, S., & Togias, A. (2000). Airway Narrowing in Healthy Humans Inhaling Methacholine Without Deep Inspirations Demonstrated by HRCT. *American Journal of Respiratory and Critical Care Medicine, 161,* 1256*–1263.*

Bushberg, J.T., Seibert, J.A., Leidholdt, E.M., & Boone, J.M. (1994). *Essential Physics of Medical Imaging*. (2nd Edition). Williams and Wilkins; Baltimore, MD.

Carroll, J.R.D., Chandra, A., Jones, A.S., Berend, N., Magnussen, J.S., & King, G.G. (2006). Airway Dimensions Measured from Micro-computed Tomography and High Resolution Computed Tomography. *European Respiratory Journal, 28(4),* 712-720

Casado, J.B., Plaza, V., Perpina, M., Picado, C., Bardagi, S., Bru, C.M., & Torrejon, M. (2010). Inflammatory Response of Rapid Onset Asthma Exacerbation. *Archivos De Bronconeumologia, 46(11),* 587-593

Cates, E.C., Fattouh, R., Wattie, J., Inman, D.M., Goncharova, S., Coyle, J.A., Gutierrez-Ramos, C.J., and Jordana, M. (2004). Intranasal Exposure of Mice to House Dust Mite Elicits Allergic Airway Inflammation via a GM-CSF-Mediated Mechanism. *The Journal of Immunology 173,* 6384-6392

Cates, E.C., Fattouh, R., Johnson, J.R., Llop-Guevara, A., & Jordana, M. (2007). Modeling Responses to Respiratory House Dust Mite Exposure. *Contributions to Microbiology 14,* 42-67

Cavanaugh, D., Johnson, E., Price, R.E., Kurie, J., Travis, E.L., & Cody, D.D. (2004). In Vivo Respiratory-Gated Micro-CT Imaging in Small-Animal. *Molecular Imaging, 3(1),* 55-62.

Cavigli, E., Comiciottoli, G., Diciotti, S., Orlandi, I., Spinelli, C.,. Meoni, E., Grassi, L., Farfalla, C., Pistolesi, M., Falaschi, F. & Mascalchi, M. (2009). Whole-Lung Densitometry Versus Visual Assessment of Emphysema. *European Radiology, 19,* 1686-1692

Chanez, P., Bourdin, A., Vachier, I., Godard, P., Bousquet, J., & Vignola, A.M. (2004). Effects of Inhaled Corticosteroids on Pathology in Asthma and Chronic Obstructive Pulmonary Disease. *Proc Am Thorac Soc*, 1(3), 184-190

Cheng, I., Nilufar, S., Flores-Mir, C., & Basu, A. (2007). Airway Segmentation and Measurement in CT Images. Proceedings of the 29th Annual International Conference of the Institute of Electrical and Electronic Engineers.

Cormack, A.M. (1973). Reconstruction of Densities from their Projections, with Applications in Radiological Physics. *Physics in Medicine and Biology, 18* (2), 195-207

De Jong, P.A., Muller, N.L., Pare, P.D., & Coxson, H.O. (2005).Computed Tomographic Imaging of the Airways: Relationship to Structure and Function. *European Respiratory Journal, 26(1),* 140-152

Drazen, J.M., Arm, J.P., & Austen, K.F. (1996). Sorting out the Cytokines of Asthma. *Journal of Experimental Medicine, 183*, 1-5

Elias, J.A. (2000). Airway Remodelling in Asthma: Unanswered Questions. *Am J Respir Crit Care Med*, 161, 168-171

Ellis, K.M., Cannet, C., Mazzoni, L., & Fozard, J.R. (2004). Airway Hyperresponsiveness to Bradykinin by Allergen Challenge in Actively Sensitised Brown Norway Rats. *Naunyn-Schmiedeberg's Articles in Pharmacology, 369,* 166-178

Ertel, D., Kyriakou, Y., Lapp, R. M., & Kalender, W. A. (2009). Respiratory Phase-Correlated Micro-CT Imaging of Free-Breathing Rodents. *Physics in Medicine and Biology, 54,* 3837-3846

Fahy, J.V. (2008). Eosinophilic and Neutrophilic Inflammation in Asthma. *Proceedings of the American Thoracic Society, 6,* 256-259

Farncombe, T.H. (2008), Software-based Respiratory Gating for Small Animal Conebeam CT. *Medical Physics, 35,* 1785-1792

Feldkamp, L., Davis, L., & Kress, J. (1984). Practical Cone-Beam Algorithm. *Journal of the Optical Society of America, 1,* 612-619

Froese, A.R., Ask, K., Labiris, R., Farncombe, T., Warburton, D., Inman, M.D., Gauldie, J., & Kolb, M. (2007). Three-dimensional Computed Tomography Imaging in an Animal Model of Emphysema. *European Respiratory Journal, 30,* 1082-1089.

Fujimura, M., Hara, J., & Myou, S. (2005). Change in Bronchial Responsiveness and Cough Reflex Sensitivity in Patients with Cough Variant Asthma: effect of inhaled corticosteroids. *Cough, 1(5),* 1-8

Gamsu, G., Salmon, C.J., Warnock, M.L., & Blanc, P.D. (1995). CT Quantification of Interstitial Fibrosis in Patients with Asbestosis: a Comparison of Two Methods. *American Journal of Roentgenology, 164(1),* 63-68

Gao, X., Kouklis, P., Xu, N., Minshall, R.D., Sandoval, R. Vogel, S.M.,& Malik, A.B. (2000). Reversibility of Increased Microvessel Permeability in Response to VE-cadherin Disassembly. *The American Journal of Physiology: Lung Cellular and Molecular Physiology, 279,* 1218-1225

Garnett, E. S., Webber, C. E., Coates, G., Cockshott, W. P., Nahmias, C., & Lassen, N. (1977). Lung Density: Clinical Method for Quantitation of Pulmonary Congestion and Edema. *Canadian Medical Association Journal, 116(2),* 153-154

Gattinoni, L., Caironi, P., Pelosi, P., & Lawrence, R.G. (2001). What Has Computed Tomography Taught Us about the Acute Respiratory Distress Syndrome? *American Journal of Respiratory and Critical Care Medicine, 164(9),* 1701-1711

Gauvreau, G.M., Watson, R.M., Jordana, M., & O'Byrne, M. (1996). Inhaled Budesonide on Allergen Induced Airway Responses and Airway Inflammation. *American Journal of Respiratory and Critical Care Medicine, 154,* 1267-1271

Germann, P.G., Hafner, D., Hanauer, G., and Drommer, W. (1998). Incidence and Severity of Granulomatous Pneumonia in Brown Norway (BN) Rats: Breeder Related Variations. *Journal of Experimental Animal Science, 39*: 22-33

Gibson, P.G., Saltos, N., & Fakes, K. (2000). Acute Anti-inflammatory Effects of Inhaled Budesonide in Asthma. *American Journal of Respiratory and Critical Care Medicine, 163,* 32-36

Goldin, J.G., McNitt-Gray, M.F., Sorenson, S.M., Johnson, T.D., Dauphinee, B., Kleerup, E.C., Tashkin, D.P., & Aberle, D.R. (1998). Airway Hyperreactivity: Assessment with Helical Thin-Section CT. *Radiology, 208,* 321-329

Goldsmith, D.R., & Keating, G.M. (2004). Budesonide/Formoterol : A Review of its Use in Asthma. *Adis Drug Evaluation, 64(14),* 1597-1618

Goris, M.L., Zhu, H.J., Blankenberg, F., Chan, F., & Robinson, T.E. (2003). An automated approach to quantitative air trapping measurements in mild cystic fibrosis. *Chest,* 123, 1655-1663

Grenier, P., Mourey-Gerosa, I., Benali, K., Brauner, M. W., Leung, A. N., Lenoir, S., Cordeau, M.P., & Mazoyer, B. (1996). Abnormalities of the Airways and Lung Parenchyma in Asthmatics: CT Observations in 50 Patients and Inter- and Intraobserver Variability. *European Radiology, 6,* 199-206

Groch, M.W., & Erwin, W.D. (2001). Single-Photon Emission Computed Tomography in the Year 2001: Instrumentation and Quality Control. *Journal of Nuclear Medicine Technology, 29,* 12-18

Gupta, S., Siddiqui, S., Haldar, P., Entwisle, J.J., Mawby, D., Wardlaw, A.J., Bradding, P., Pavord, I.D., Green, R.H., & Brightling, C.E. (2010). Quantitative Analysis of High-resolution Computed Tomography Scans in Severe Asthma Subphenotypes. *Thorax, 65,* 775-781

Hangartner, T.N. (2007). Thresholding Technique for Accurate Analysis of Density and Geometry in QCT, pQCT and ÌCT Images. *Journal of Musculoskeletal and Neuronal Interactions, 7(1),* 9-16

Hayashi, R., Wada, H., Ito, K., & Adcock, I.M. (2004). Effects of Glucocorticoids on Gene Transcription. *European Journal of Pharmacology, 500,* 51–62

Heremans, A., Verschakelen, J.A., Van Fraeyenhoven, L., & Demedts, M. (1992). Measurement of Lung Density by Means of Quantitative CT Scanning: A Study of Correlations with Pulmonary Function Tests. *Chest, 102(3),* 805-811

Hirama, S., Tatsuishi, T., Iwase, K., Nakao, H., Umebayashi, C., Nishizaki, Y., Kobayashi, M., Ishida, S., Okano, Y., & Oyama, Y. (2004). Flow-cytometric Analysis of Adverse Effects of Polysorbate 80 in Rat Thymocytes. *Toxicology, 199,* 137-143

Holgate, S.T. (1993). Asthma: past, present and future. *Eur J Respir Dis,* 6, 1507–1520

Horvath, G., & Wanner, A. (2006). Inhaled Corticosteroids: Effects on the Airway Vasculature in Bronchial Asthma. *European Respiratory Journal, 27,* 172-187

Hounsfield, G.N. (1973). Computerized Transverse Axial Scanning (Tomography): Part 1. Description of System. *British Journal of Radiology, 46,* 1016-1022

Hsia, C.C.W., Hyde, D.M., Ochs, M., & Weibel, E.R. (2010). An Official Research Policy Statement of the American Thoracic Society/European Respiratory Society: Standards for Quantitative Assessment of Lung Structure. *American Journal of Respiratory and Critical Care Medicine, 181,* 394-418

Hylkema, M.N., Hoekstra, M.O., Luinge, M., & Timens, W. (2002). The Strength of the OVA-induced Airway Inflammation in Rats is Strain Dependent. *Clinical and Experimental Immunology, 129(3),* 390-396

Incorvaia, C., Riario-Sforza, G.G, Incorvaia, S., & Frati, F. (2010). Sublingual Immunotherapy in Allergic Asthma: Current Evidence and Needs to Meet. *Annals of Thoracic Medicine, 5(3),* 128-132

Jagielo, P.J., Thorne, P.S., Kern, J.A., Quinn, T.J., & Schwartz, D.A. (1996). Role of Endotoxin in Grain Dust-induced Lung Inflammation in Mice. *The American Physiological Society, 96,* 1052-1059

Jannasch, K., Guebtner, J.M., & Alves, F. (2009). Using *In Vivo* Imaging for Asthma. *Drug Discovery Today: Disease Models, 6(4),* 129-135

Jobse, B.N., Johnson, J.R., Farncombe, T.H., Labiris, R., Walker, T.D., Goncharova, S. & Jordana, M. (2009). Evaluation of Allergic Lung Inflammation by Computed Tomography in a Rat Model In Vivo. *European Respiratory Journal, 33,* 1437-1447

Johnson, J.R., Wiley, R.E., Fattouh, R., Swirski, F.K., Gajewska, B.U., Coyle, A.J., Gutierrez-Ramos, J-C., Ellis, R., Inman, M.D. & Jordana, M. (2004). Continuous Exposure to House Dust Mite Elicits Chronic Airway Inflammation and Structural Remodelling. *American Journal of Respiratory and Critical Care Medicine, 169,* 378-385

Johnson, J.R., Pacitto, S.R., Wong, J., Archer, E.W., Eirefelt, S., Miller-Larsson, A., & Jordana, M. (2008). Combined Budesonide/Formoterol Therapy in Conjunction With Allergen Avoidance Ameliorates House Dust Mite-induced Airway Remodeling and Dysfunction. *The American Journal of Physiology: Lung Cellular and Molecular Physiology, 295(5),* 780-788.

Johnson, K.A. (2007). Imaging Techniques for Small Animal Imaging Models of Pulmonary Disease: Micro-CT. *Toxicologic Pathology, 35,* 59-64

Kalender, W.A. & Kyriakou, Y. (2007). Flat-Detector Computed Tomography (FD-CT). *European Journal of Radiology, 17,* 2767-2779

Kaliste, E., Linnainmaa, M., Meklin, T., Torvinen, E., & Nevalainen, A. (2004). The Bedding of Laboratory Animals as a Source of Airborne Contaminants. *Laboratory Animals, 38, 25-37*

Karmouty-Quintana, H., Cannet, C., Zurbruegg, S., Ble, F.X., Fozard, J.R., Page, C.P., & Beckmann, N. (2007). Bleomycin-induced Lung Injury Assessed Non-invasively and in Spontaneously Breathing Rats by Proton MRI. *Journal of Magnetic Resonance Imaging, 26,* 941-949

Kasahara, K., Shiba, K., Ozawa, T., Okuda, K., & Adachi, M. (2002). Correlation Between the Bronchial Subepithelial Layer and Whole Airway Wall Thickness in Patients with Asthma. *Thorax, 57,* 242-246

Kelly, H.W. (2008). Inhaled Corticosteroid/Long-acting Inhaled β2-agonist Combination Therapy - Beyond Maintenance Medication. *US Respiratory Disease,* 45-47

Kelly, H.W. (2003). Pharmaceutical Characteristics that Influence the Clinical Efficacy of Inhaled Corticosteroids. *Analyse of Allergy, Asthma, & Immunology, 91,* 326-224

Kikuchi, S., Nagata, M., Kikuchi, I., Hagiwara, K., & Kanazawa, M. (2005). Association between Neutrophilic and Eosinophilic Inflammation in Patients with Severe Persistent Asthma. *International Articles of Allergy and Immunology, 137(1),* 7-11

Klein, M.W., Goggel, R., Westhof, A., & Erb, K.J. (2008). Development and Characterization of a Novel and Rapid Lung Eosinophil Influx Model in the Rat. *Pulmonary Pharmacology & Therapeutics, 21,* 648-656

Koningsberger, D.C., & Prins, R. (1987). X-ray Absorption: Principles, Applications, and Techniques of EXAFS, SEXAFS and XANES. John Wiley and Sons Inc., New York, NY.

Labiris, R., Ask, K., Farkas, L., Moeller, A., Froese, A., Farncombe, T., McClelland, G.B., Inman, M.D., Gauldie, J., & Kolb, M. (2008). Comparison Between Conventional and "Clinical" Assessment of Experimental Lung Fibrosis. *Journal of Translational Medicine, 6,* 16

Lalkhen, A.G. & McCluskey, A. (2008). Clinical tests: sensitivity and specificity. *Contin Educ Anaesth Crit Care Pain, 8(6),* 221-223

Lancas, T., Kasahara, D., Prado, C., Tiberio, I., Martins, M., & Dolhnikoff, M. (2006). Comparison of early and late responses to antigen of sensitized guinea pig parenchymal lung strips. J Appl Physio, 100, 1610-1616

Langheinrich, A. C., Leithäuser, B., Greschus, S., von Gerlach, S., Breithecker, A. Matthias, F.R., Rau, W.S., & Bohle, R.M. (2004). Acute Rat Lung Injury: Feasibility of Assessment with Micro-CT. *Radiological Society of North America, 233*(1), 165-171

Lederlin, M., Ozier, A., Montaudon, M., Begueret, H., Ousova, O., Marthan, R., Berger, P., & Laurent, F. (2010). Airway Remodeling in a Mouse Asthma Model Assessed by In Vivo Respiratory-gated Micro-computed Tomography. *European Radiology, 20(1)*, 128-137

Leff, J.A., Busse, W.W., Pearlman, D., Bronsky, E.A., Kemp, J., Hendeles, L., Dockhorn, R., Kundus, S., Zhang, J., Seidenberg, B.C., & Reiss, T.F. (1998). Montelukast, a Leukotriene-receptor Antagonist, for the Treatment of Mild Asthma and Exercise-induced Bronchoconstriction. *The New England Journal of Medicine, 339(3),* 147-152

Lehnert, S. & El-Khatib. (1988). The Use of CT Densitometry in the Assessment of Radiation-induced Damage to the Rat Lung: A Comparison with Other Endpoints. *International Journal of Radiation Oncology-Biology-Physics, 16(1),* 117-124

Levi, C., Gray, J.E., McCullough, E.C., & Hattery, R.R. (1982). The Unreliability of CT Numbers as Absolute Values. *American Journal of Roentgenology, 139,* 443-447

Levin, C.S. (2005). Primer on Molecular Imaging Technology. *European Journal of Nuclear Medicine and Molecular Imaging, 32(14),* 325-345

Little, S.A., Sproule, M.W., Cowan, M.D., Macleod, K.J., Robertson, M., Love, J.G., Chalmers, G., McSharry, C. & Thomson, N.C. (2002). High Resolution Computed Tomographic Assessment of Airway Wall Thickness in Chronic Asthma: Reproducibility and Relationship with Lung Function and Severity. *Thorax, 57,* 247-253

Mah, D., Hanley, J., Rosenzweig, K.E , et al. (2000). Technical aspects of the deep inspiration breath-hold technique in the treatment of thoracic cancer. *Int J Radiat Oncol Biol Phys,* 48(4),1175-85

Miller-Larsson, A., Mattsson, H., Hjertberg, E., Dahlback, M., Tunek, A., & Brattsand, R. (1998). Reversible Fatty Acid Conjugation of Budesonide : Novel Mechanism for Prolonged Retention of Topically Applied Steroid in Airway Tissue. *Drug Metabolism and Disposition, 26(7),* 623-630

Mitsunobu, F., Ashida, K., Hosaki, Y., Tsugeno, H., Okamoto, M., Nishida, N., Nagata, T., Takata, S., & Tanizaki, Y. (2003). Decreased Computed Tomographic

Lung Density During Exacerbation of Asthma. *European Respiratory Journal, 22(1),* 106-112

Morris, J.F. (1976). Spirometry in the Evaluation of Pulmonary Function. *Western Journal of Medicine, 125(2), 110-118*

Namati, E., Chon, D., Thiesse, J., Hoffman, E.A., de Ryk, J., Ross, A., & McLennan, G. (2006). In vivo micro-CT lung imaging via a computer-controlled intermittent iso-pressure breath hold (IIBH) technique. Phys Med Bio, 51(23), 6061-6075

Ng, S., Villemagne, V.L., Berlangieri, S., Lee, S.T., Cherk, M., Gong, S.J., Ackermann, U., Saunder, T., Tochon-Danguy, H., Jones, G., Smith, C., O`Keefe, G., Masters, C.L., & Rowe, C.C. (2007). Visual Assessment Versus Quantitative Assessment of ^{11}C-PIB PET and ^{18}F-FDG PET for Detection of Alzheimer's Disease. *The Journal of Nuclear Medicine, 48(4),* 547-552

Ng, S., Desai, S.R., Rubens, M.B., Padley, S.P., Wells, A.U., & Hansell, D.M. (1999). Visual Quantitation and Observer Variation of Signs of Small Airways Disease at Inspiratory and Expiratory CT. *Journal of Thoracic Imaging, 14(4),* 279-285

Noritake, S., Ogawa, K., Susuki, G., Ozawa, K., & Ikeda, T. (2007). Pulmonary Inflammation in Brown Norway Rats: Possible Association of Environmental Particles in the Animal Room Environment. *Experimental Animals, 56(5),* 319-327

Novelline, R. (1997). *Squire's Fundamentals of Radiology*. (5th Edition). Harvard University Press

Obenaus, A. & Smith, A. (2004). Radiation Dose in Rodent Tissues during Micro-CT Imaging. *Journal of X-Ray Science and Technology, 12(4),* 241-250

Okazawa, M., Muller, N., McNamara, A.E., Child, S., Verburgt, L., & Pare, P.D. (1996). Human Airway Narrowing Measured Using High Resolution Computed Tomography. *American Journal of Respiratory and Critical Care Medicine, 154,* 1557–*1562*

Pauluhn, J., & Poole A. (2010). Brown Norway Rat Asthma Model of Diphenylmethane-4,4'-diisocyanate (MDI): Determination of the Elicitation Threshold Concentration of After Inhalation Sensitization. *Toxicology, 281,* 15-24

Paulus, M.J., Gleason, S.S., Kennel, S.J., Hunsicker, P.R., & Johnson, D.K. (2000). High Resolution X-ray Computed Tomography: An Emerging Tool for Small Animal Cancer Research. *Nature: Neoplasia, 2(1-2)*, 62-70

Percy, D.H. & Barthold, S.W. (2008). Pathology of Laboratory Rodents and Rabbits, Third Edition: 155-156

Perez, A., Coxson, H.O., Hogg, J.C., Gibson, K., Thompson, & P.F., Rogers, R.M. Use of CT Morphometry to Detect Changes in Lung Weight and Gas Volume. *Chest, 128(4)*, 2471-2477

Poulsen, K. & Simonsen, J. (2007). Computed Tomography as Routine in Connection with Medico-Legal Autopsies. *Forensic Science International*, *171*, 190-197

Reinke, L.F. & Hoffman, L. (2000). Asthma Education: Creating a Partnership. *Heart and Lung: The Journal of Acute and Critical Care,* 29(3), 225-236

Rikxoort, E.M., Viergever, M.A., & Ginneken, B. (2009). Automatic Lung Segmentation from Thoracic Computed Tomography Scans Using a Hybrid Approach with Error Detection. *Medical Physics, 36(7),* 1118-1132

Rodt, T., von Flack, C., Dettmer, S., Halter, R., Maus, R., Ask, K., Kolb, M., Gauldie, J., Langer, F., Holy, L., Welte, T., Galanski, M., Maus, U.A., & Borlak, J. (2010). Micro-computed tomography of pulmonary fibrosis in mice induced by adenoviral gene transfer of biologically active transforming growth factor-β1. *Respiratory Research,* 11(181), 1-8

Rosi, E., Ronchi, M.C., Grazzini, M., Duranti, R., & Scano, G. (1999). Sputum Analysis, Bronchial Hyperresponsiveness, and Airway Function in Asthma: Results of a Factor Analysis. *The Journal of Allergy and Clinical Immunology*, 103(2), 232-237

Ryrfeldt, A., Persson, G., & Nilsson, E. (1989). Pulmonary Disposition of the Potent Glucocorticoid Budesonide, Evaluated in an Isolated Perfused Rat Lung Model. *Biochemical Pharmacology, 38(1),* 17-22

Saw, C.B., Brander, E., Selvaraj, R., Chen, H., Huq, M.S., & Huron, D.E. (2006). A review on the clinical implementation of respiratory-gated radiation therapy. *Biomedical Imaging and Intervention Journal*, 1-8

Schmid, O., Bolle, I., Harder, V., Karg, E., Takenaka, S., Schulz, H., & Ferron, G.A. (2008). Model for the Deposition of Aerosol Particles in the Respiratory Tract of the Rat. I. Nonhygroscopic Particle Deposition. *Journal of Aerosol Medicine and Pulmonary Drug Delivery, 21(3),* 291-307

Schoor, J.V., Joos, G.F., & Pauwels, R.A. (2000). Indirect Bronchial Hyperresponsiveness in Asthma: Mechanisms, Pharmacology and Implications for Clinical Research. *European Respiratory Journal, 16,* 514-533

Schuster, D.P., Kovacs, A. Garbow, J. & Piwnica-Worms, D. (2004). Recent Advances in Imaging the Lungs of Intact Small Animals. *American Journal of Respiratory Cell and Molecular Biology, 30(2),* 129-138

Schroeder, T., Melo, M.F.V., Musch, G., Harris, R.S., Venegas, J.G., & Winkler, T. (2007). Image-Derived Input Function for Assessment of 18F-FDG Uptake by the Inflamed Lung. *Journal of Nuclear Medicine, 48,* 1889-1896

Schwartz, D.A. (1996) Grain Dust, Endotoxin, and Airflow Obstruction. *Chest, 109,* 57-63

Schwarts, D.A., Thorne, P.S., Jagielo, P.J., White, G.E., Bleuer, S.A., & Frees, K.L. (1994). Endotoxin, Grain Dust and Airway Inflammation. *The American Physiological Society, 94,* 609-617

Schwartz, D. A., Thorne, P.S., Yagla, S.J., Burmeister, L.F., Olenchock, S.A., Watt, J.L., & Quinn, T.J. (1995). The Role of Endotoxin in Grain Dust-induced Lung Disease. *American Journal of Respiratory and Critical Care Medicine, 152,* 603-608

Senti, G., Graf, N., Haug, S., Ruedi, N., von Moos, S., Sonderegger, T., Johansen, P., & Kundig, T.M. (2009). Epicutaneous Allergen Administration as a Novel Method of Allergen-specific Immunotherapy. *The Journal of Allergy and Clinical Immunology, 124(5),* 997-1002

Shen, H.H. & Wang, S.B. (2005). Effects of Budesonide on Airway Inflammation and Airway Remodeling in the Ovalbumin Sensitized and Challenged Mice. *Zhonghua Jie He He Hu Xi Za Zhi. 28(3),* 154-159

Siddiqui, S., Jo, T., Tamaoka, M., Shalaby, K.H., Ghezzo, H., Bernabeu, M., & Martin, J.G. (2010). Sites of Allergic Airway Smooth Muscle Remodeling and Hyperresponsiveness are not Associated in the Rat. *Journal of Applied Physiology, 109(4),* 1170-1178

Simon, B.A. (2004). Regional Ventilation and Lung Mechanics Using X-Ray CT. *Academic Radiology, 12(11),* 1414-22

Singh, P., Daniels, M., Winsett, D.W., Richards, J., Doerfler, D., Hatch, G., Adler, K.B., & Gilmour, M.I. (2002). Phenotypic Comparison of Allergic Airway Responses to House Dust Mite in Three Rat Strains. *The American Journal Physiology: Lung Cell Molecular Physiology, 284,* 588-598

Sont, J.K., Willems, L.N., Bel, E.H., van Krieken, J.H., Vanderbroucke, J.P., & Sterk, P.J. (1999). Clinical control and histopathologic outcome of asthma when using airway hyperresponsiveness as an additional guide to long-term treatment. The AMPUL Study Group. *American Journal of Respiratory and Critical Care Medicine*, 159(part 1 of 4), 1043-1051

Southam, D.S., Ellis, R., Wattie, J., Glass, W., & Inma, M.D. (2008). Goblet cell rebound and airway dysfunction with corticosteroid withdrawal in a mouse model of asthma. *American Journal of Respiratory and Critical Care Medicine*, 178(11), 1115-1122

Stoel, B.C. & Stolk, J. (2004). Optimization and standardization of Lung Densitometry in the Assessment of Pulmonary Emphysema. *Investigative Radiology, 39(11),* 681-688

Sun, H.W., Miao, C.Y., Liu, L., Zhou, J., Su, D.F., Wang, Y.X., & Jiang, C.L. (2006). Rapid Inhibitory Effect of Glucocorticoids on Airway Smooth Muscle Contractions in Guinea Pigs. *Steroids, 72(2),* 154-159

Taylor, B.M., Kolbasa, K.P., Chin, J.E., Richards, I.M., Fleming, W.E., Griffin, R.L., Fidler, S.F., & Sun, F.F. (1997). Roles of Adhesion Molecules ICAM-1 and α_4 Integrin in Antigen-induced Changes in Microvascular Permeability Associated

with Lung Inflammation in Sensitized Brown Norway Rats. *American Journal of Respiratory Cell and Molecular Biology*, *17(6),* 757-766

Tigani, B., Cannet, C., Zurbrugg, S., Schaeublin, E., Mazzoni, L., Fozard, J.R., & Beckmann, N. (2003). Resolution of the Oedema Associated with Allergic Pulmonary Inflammation in Rats Assessed Noninvasively by Magnetic Resonance Imaging. *British Journal of Pharmacology, 140(2),* 239-246

Turi, G.J., Ellis, R., Wattie, J.N., Labiris, N.R., & Inman, M.D. (2010). The Effects of Inhaled House Dust Mite on Airway Barrier Function and Sensitivity to Inhaled Methacholine in Mice. *The American Journal of Physiology: Lung Cellular and Molecular Physiology, 300(2),* 185-190

Turkington, T.G. (2002). Introduction to PET Instrumentation. *Journal of Nuclear Medicine Technology*, *29,* 4-11

Wallau, B.R., Schmitz, A., & Perry, S.F. (2000). Lung Morphology in Rodents (Mammalia, Rodentia) and its Implications for Systematics. *Journal of Morphology, 246,* 228-248

Wang, G., Lin, T.H., Cheng, P.H., & Shinozaki, D.M. (1993). A General Cone Beam Reconstruction Algorithm. *IEEE Transactions on Medical Imaging*, *12(3),* 486-495

Werner-Klein, M., Göggel, R., Westhof, A., & Erb, K.J. (2008). Development and Characterisation of a Novel and Rapid Lung Eosinophil Influx Model in the Rat. *Pulmonary Pharmacology & Therapeutics*, *21(4),* 648-656

Whaites, E. (2002). *Essentials of Dental Radiography and Radiology: Dental Series*. (3rd Edition). Elsevier Health Sciences.

Whiteside, T.E., Thigpen, J.E., Kissling, G.E., Grant, M.G., & Forsythe, D.B. (2010). Endotoxin, Coliform, and Dust Levels in Various Types of Rodent Bedding. *Journal of the American Association for Laboratory Animal Science, 49(2),* 184-189

Whitty, S. (2011). *Comparative CT Densitometry in Murine Pulmonary Disease Models*. Unpublished MSc Thesis. McMaster University.

Xu, L., Olivenstein, R., Martin, J.G., & Powell, W.S. (2000). Inhaled Budesonide Inhibits OVA-induced Airway Narrowing, Inflammation, and Cys-LT Synthesis in BN Rats. *Journal of Applied Physiology, 89,* 1852-1858

Zheng, B., Leader, J.K., McMurray, J.M., Park, S.C., Fuhrman, C.R., Gur, D., & Sciurba, F.C. (2007). Automated Detection and Quantitative Assessment of Pulmonary Airways Depicted on CT Images. *Medical Physics, 34(7),* 2844-2852

CHAPTER 9

9 APPENDIX

Appendix I - Supplemental Materials and Methods

9.1 CT Validation – Thoracic and Lung Segmentation

The thoracic and lung segmentations used a sampling method for tissue densities with a defined region of interest.

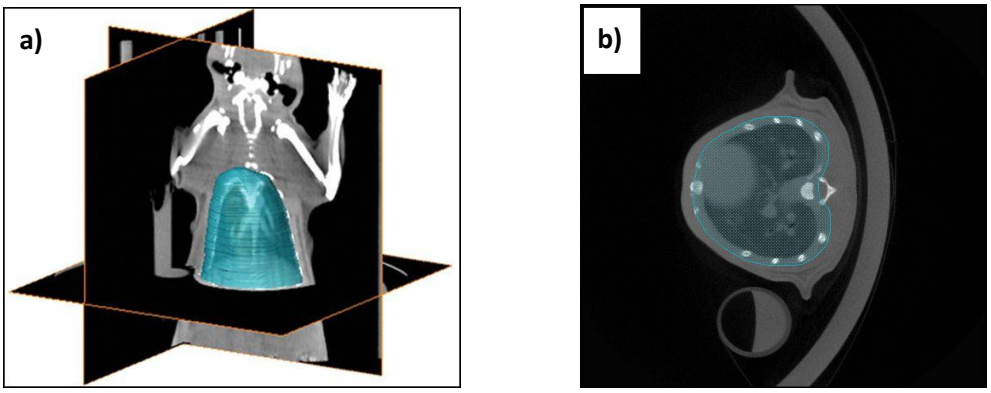

Figure 24. Thoracic Segmentation. The blue regions illustrate the location and relative size of the segmentation. **a)** 3D representation (Jobse *et al.* 2009) and **b)** Cross-sectional slice.

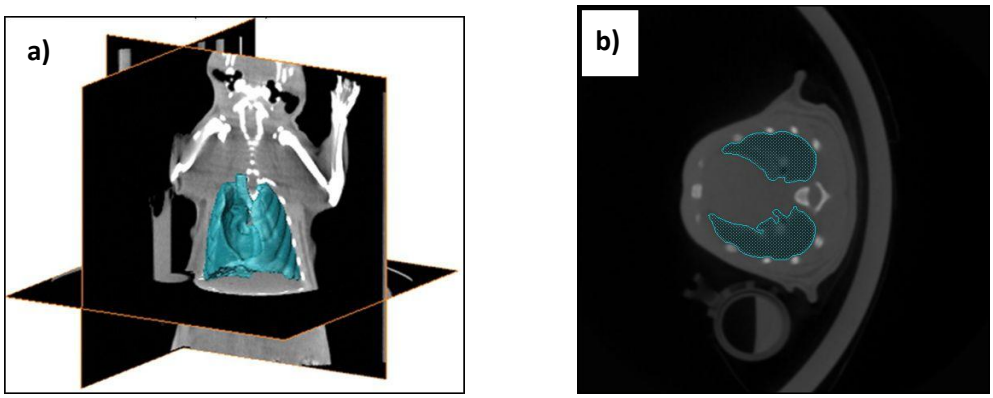

Figure 25. Lung Segmentation. The blue regions illustrate the location and relative size of the segmentation. **a)** 3D representation (Jobse *et al.* 2009) and **b)** Cross-sectional Slice.

Appendix II - Supplemental Results

9.2 Development of an Allergic Airway Inflammatory Model: Dose and Temporal Response of HDM

9.2.1 *CT Densitometry*

There were no differences in the CT density distributions between HDM_{150} and HDM_{250} at five and eight doses, nor was there a difference within the dose groups between exposures (Figure 26).

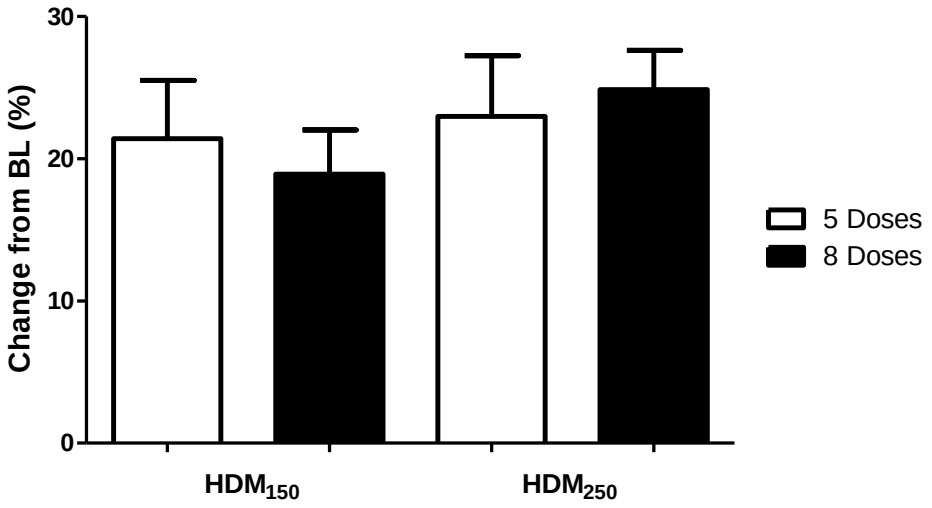

Figure 26. Change from Baseline Peribronchial CT Density Distribution. Change from baseline calculated as percent voxels above density threshold of -100HU. **a)** Post five doses, **b)** Post eight doses, **c)** HDM 150 µg at five and eight exposures, and **d)** HDM 250 µg at five and eight exposures. Data expressed as mean ± SEM.

9.3 Development of a Treatment Model: Dose and Temporal Response of Budesonide

9.3.1 *CT Densitometry*

There were no significant differences present within treatment groups between three and six administrations (Figure 27).

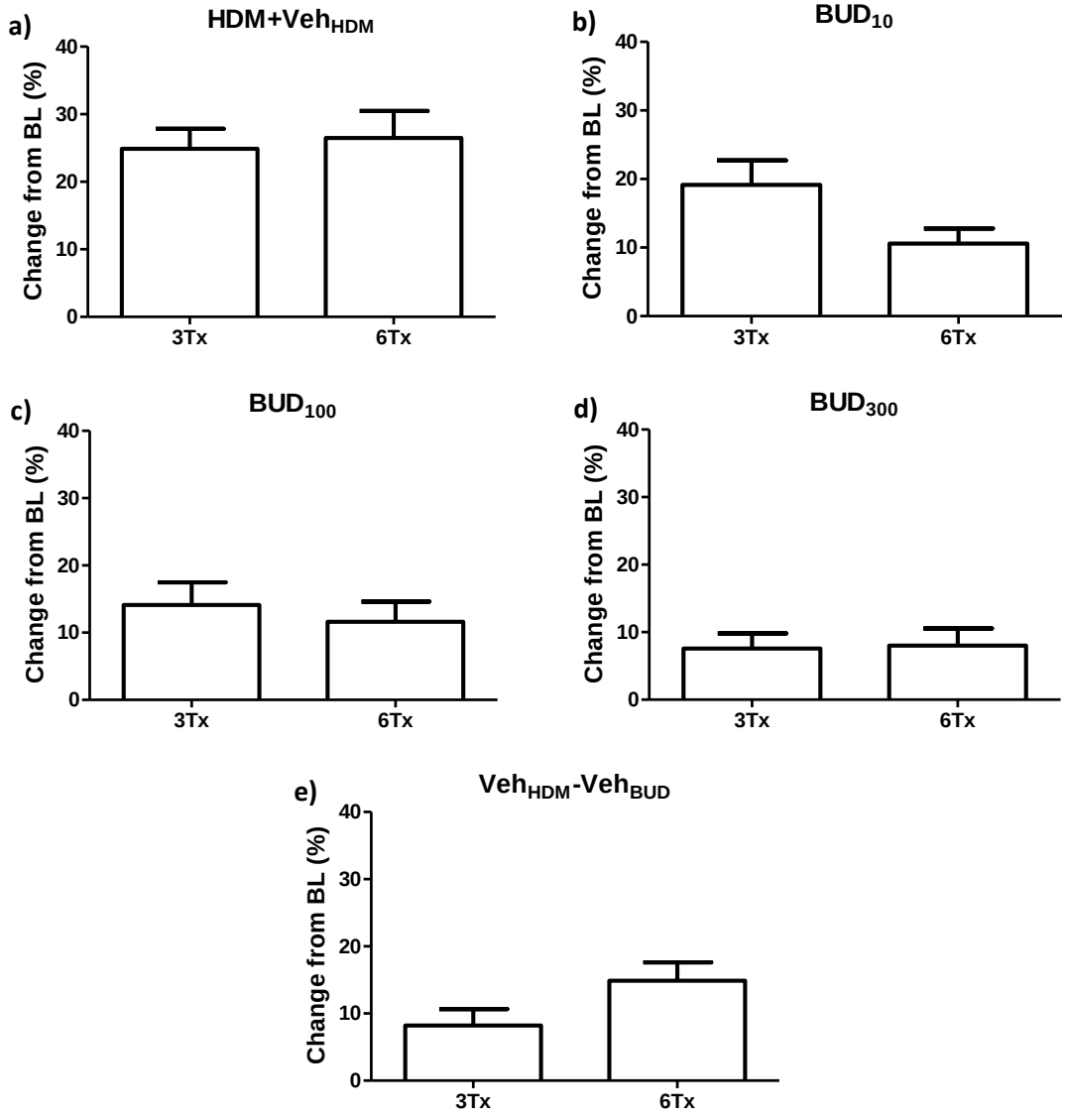

Figure 27. Change from Baseline in Peribronchial CT Density with Budesonide Treatment. Change from baseline calculation of percent voxels above density threshold of -100HU **a)** HDM 250µg, **b)** BUD 10 µg/kg, **c)** BUD 100 µg/kg, **d)** BUD 300 µg/kg, and **e)** The BUD vehicle control. Data expressed as mean ± SEM.

9.3.2 *BAL Total and Differential Cell Counts*

TCC significantly increased in the 10 µg/kg BUD group ($p<0.05$, Figure 28) while percent eosinophils significantly decreased between three and six administrations

($p<0.05$, Figure 29). The remaining groups showed no significant differences in TCC and percent eosinophils between exposures (Figures 28 & 29).

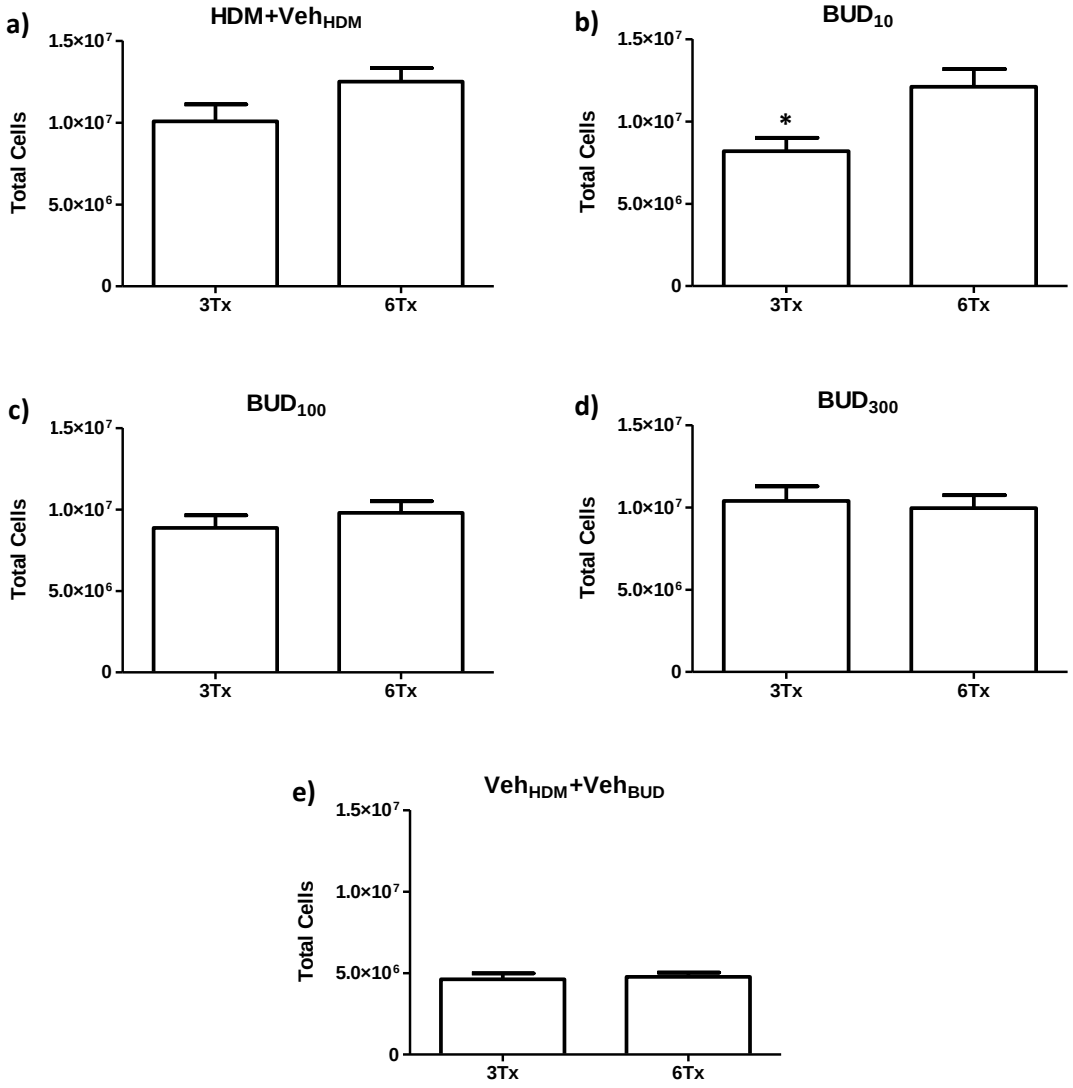

Figure 28. BAL Total Cell Counts with Budesonide Treatment. a) HDM 250 µg, **b)** BUD 10 µg/kg, **c)** BUD 100 µg/kg, **d)** BUD 300 µg/kg, and **e)** The BUD vehicle control. Data expressed as mean ± SEM. *$p<0.05$, by a two-tailed independent t-test.

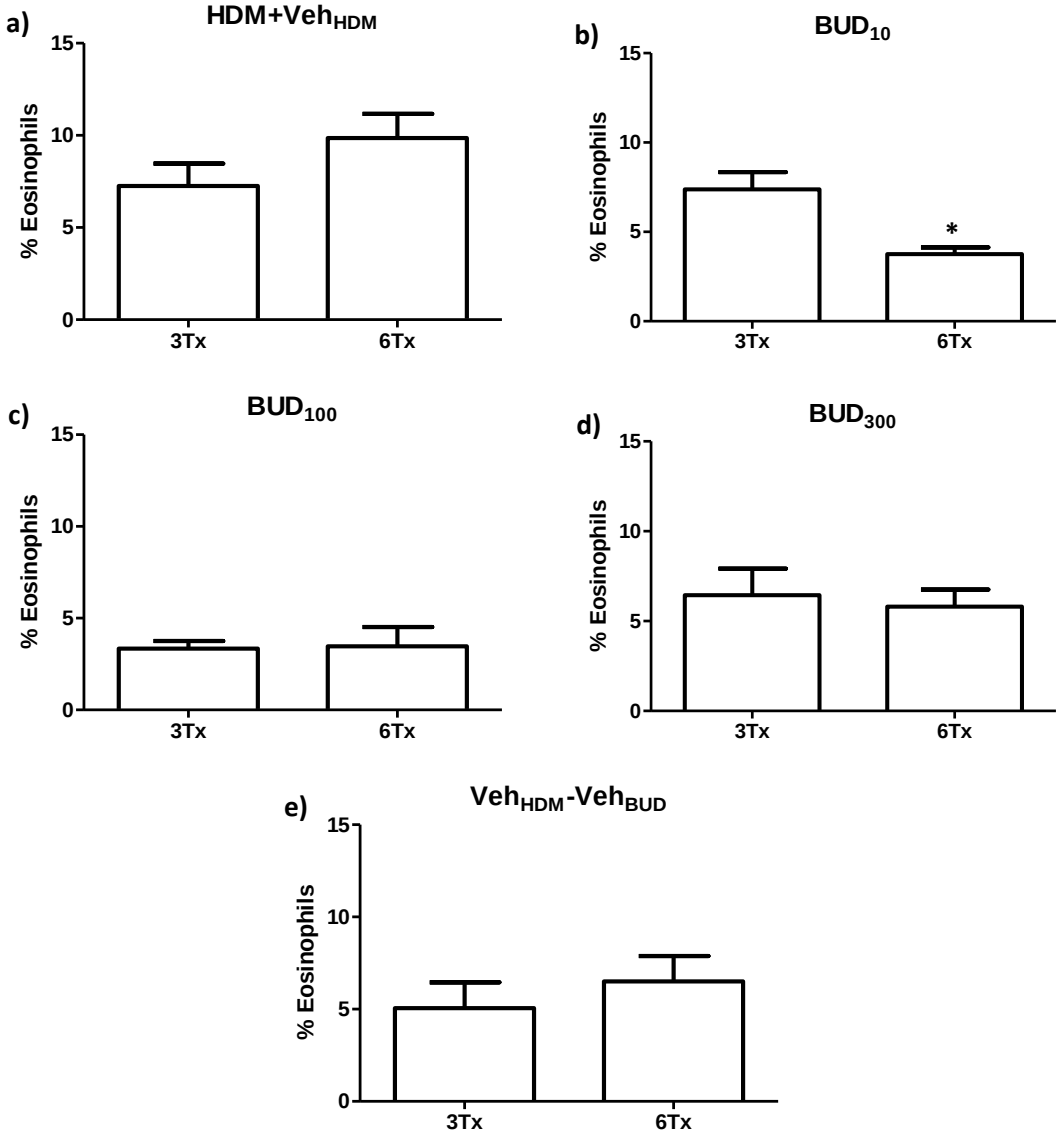

Figure 29. BAL Percent Eosinophils with Budesonide Treatment. a) HDM 250µg, **b)** BUD 10 µg/kg, **c)** BUD 100 µg/kg, **d)** BUD 300 µg/kg, and **e)** The BUD vehicle control. Data expressed as mean ± SEM. *p<0.05, by a two-tailed independent t-test.

9.3.3 *Quantitative Histology*

There was a significant decrease in inflammation within the HDM+BUD$_{100}$ group and Veh$_{HDM}$+Veh$_{BUD}$ groups between three and six administrations. The remaining groups showed no significant differences between exposures (Figure 30).

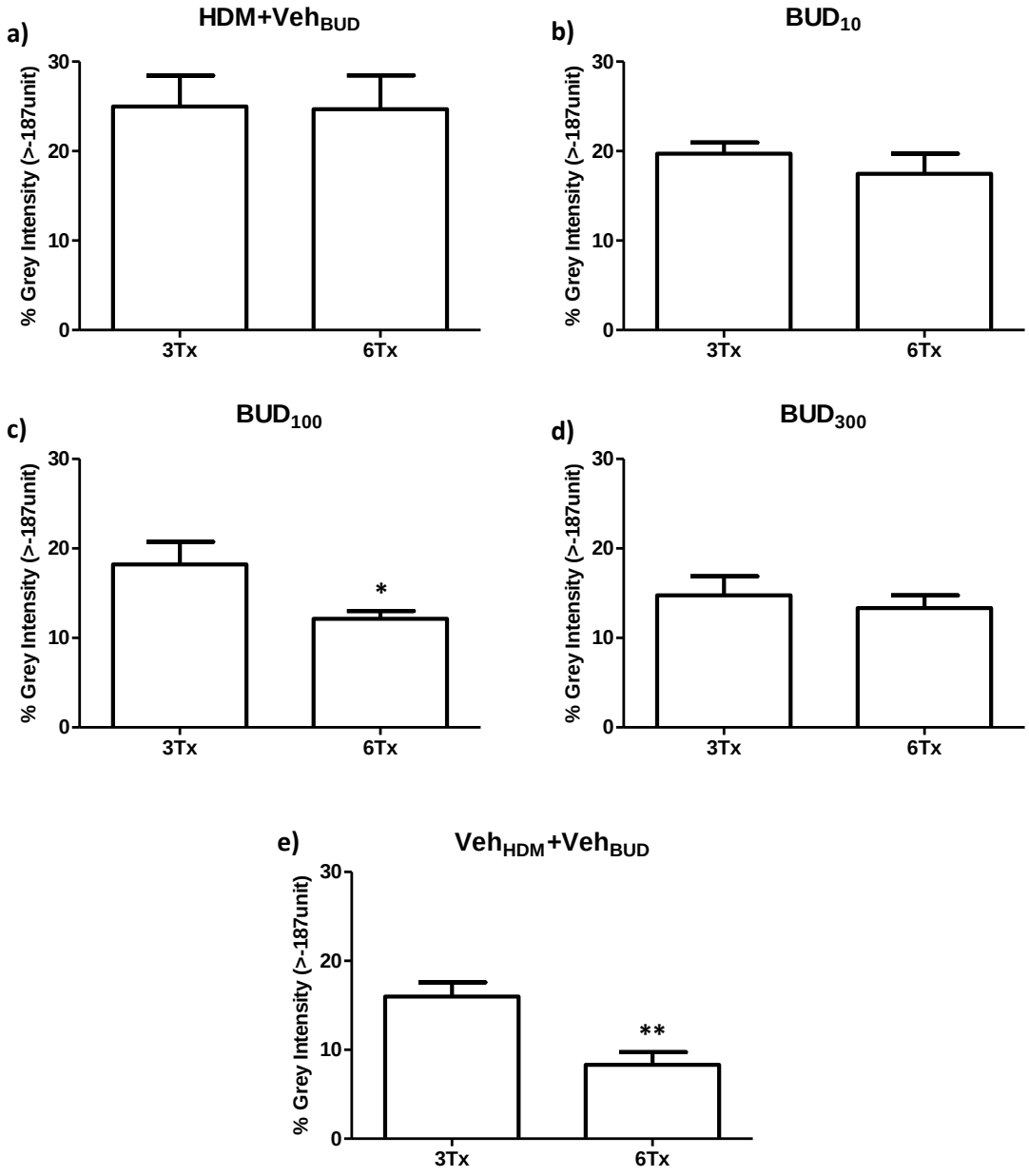

Figure 30. Quantitative Histological Analysis of Peribronchial Inflammation. Inflammation measured as percent of total area of interest above the grey intensity threshold. **a)** HDM 250 µg, **b)** BUD 10 µg/kg, **c)** BUD 100 µg/kg, **d)** BUD 300 µg/kg, and **e)** The BUD vehicle control. Data expressed as mean ± SEM. *p<0.05, **p<0.01 by a two-tailed independent t-test. Intensity threshold defined as grey intensity at where 90% of the area is below.

Appendix III – Supplemental Experimentation

9.4 Spontaneous Eosinophilic-Rich Multifocal Granulomatous Pneumonitis in the Brown Norway Rat

9.4.1 *Introduction*

Brown Norway rats have been previously used in numerous studies of respiratory disease, including asthma (Jobse *et al.* 2009, Brange *et al*. 2009, Hylkema, *et al.* 2002), but have also been documented to develop spontaneous eosinophilic rich necrotizing and granulomatous pneumonitis (Germann *et al.* 1998, Noritake *et al.* 2007, Percy *et al.* 2008). This event is found in both sexes but predominantly in females of a young age starting around 8 weeks and with recovery after 15 weeks (Percy *et al.* 2008). The lesions are multifocal to diffuse, found in the parenchyma, and characterized by a cellular infiltrate consisting of eosinophils and histiocytes; frequently, there is perivascular oedema (Noritake *et al.* 2007, & Percy *et al.* 2008). This pilot research was performed to further understand this phenomenon. The study found that the baseline CT scans of naïve animals were suggestive of increased inflammation depicted by high densities on the CT in a subset of animals we investigated the presence of spontaneous pneumonitis using CT and histopathology.

9.4.2 *Objectives*

To use CT imaging to monitor the progression and resolution of mutifocal, eosinophil-rich necrotizing and granulomatous pneumonitis found in female Brown

Norway rats and to correlate CT densitometry to histological scoring of granulomatous pneumonitis.

9.4.3 *Materials and Methods*

Female Brown Norway (BN) rats, approximately 6 weeks old weighing 80-100 g, were purchased from Harlan Global Headquarters (n=12, strain BN/SsNHsd). The animals were housed in the same system as described in Section 2.1. Animals were untreated throughout the experiment. A baseline CT was acquired for each rat (n=12) at 8 weeks old. CT scans continued every two weeks for 14 weeks (baseline, week 10, week 12, and week 14). Immediately after week 14, a subset of animals (n=5) were sacrificed to obtain histological data. The remaining animals (n=7) were CT scanned at week 16 and a final scan at week 30 followed by a sacrifice for histological samples. CT acquisition and reconstruction parameters are found in Section 2.5. The airway segmentation method and densitometry analysis was used from sections 2.6.3 and 2.7. Histopathology was performed by Dr. Jacek M. Kwiecien DVM, MSc, PhD, a veterinary research pathologist at the Central Animal Facility of McMaster University.

Based on the CT densitometry results from the HDM and BUD dose and temporal response studies, a severity scale of the percent voxels above -100HU was established based on CT density: 1 = healthy (<10%), 2 = mildly sick (11-16%), 3 = sick (17-25%), and 4 = severely sick (>26%). Histology results were scored by Dr. Kwiecien for severity of pneumonitis: 1 = healthy, 2 = minimal/mild pneumonitis, and 3 = spontaneous eosinophilic rich multifocal granulomatous pneumonitis. The Spearman rank order

correlation was used to assess the correlation between CT densitometry and histopathological scores.

9.4.4 *Results*

9.4.4.1 CT Densitometry

Baseline images from 12 rats at week 8 indicated that one animal was healthy with 6% voxels around the large airways above the -100HU density threshold, five animals were classified mildly sick (13.6% ± 1.1%), four as sick (24.5% ± 4.1%), and two as severely sick (34.7% ± 8.2%). Throughout the remaining time-points, compared to baseline, seven of the twelve rats maintained or increased CT density (6.9% ± 3.7%) and three had little change in pathology (-1.7% ± 0.3%) around the major airways (Figure 31). Only two rats demonstrated considerable resolution in airway density (19.3% ± 2.4%) from their baseline data (Figure 32).

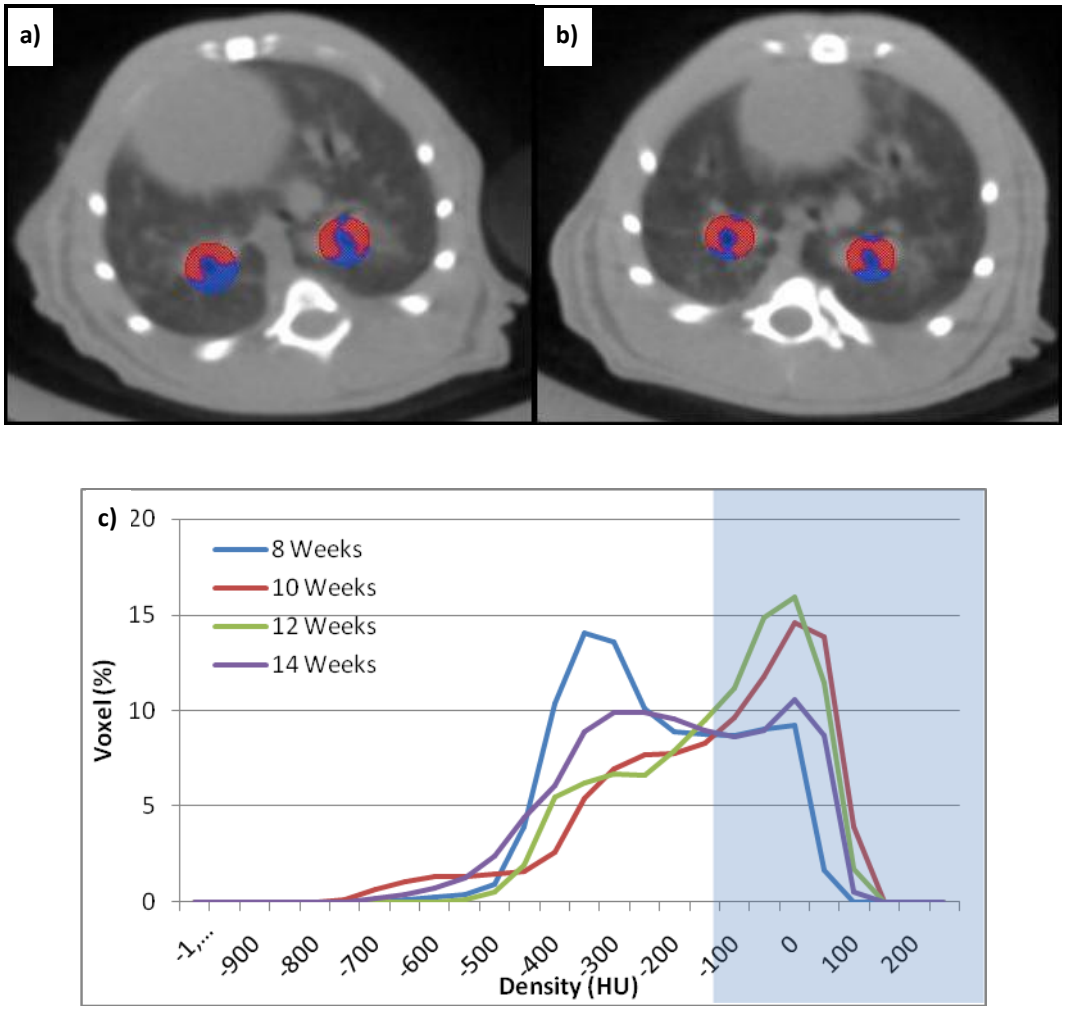

Figure 31. Representative CT from a Single Sick BN Rat Illustrating Increased Peribronchially Density with Little Resolution Over 30 Weeks. Blue area denotes values between -100 HU and -200 HU while red denotes values >-200 HU. **a)** 19.9% voxels at baseline (8 weeks), **b)** Further increase to 28.8% voxels at 30 weeks, and **c)** CT density distribution as percent voxels. Blue box: >-100 density threshold. HU: Hounsfield units.

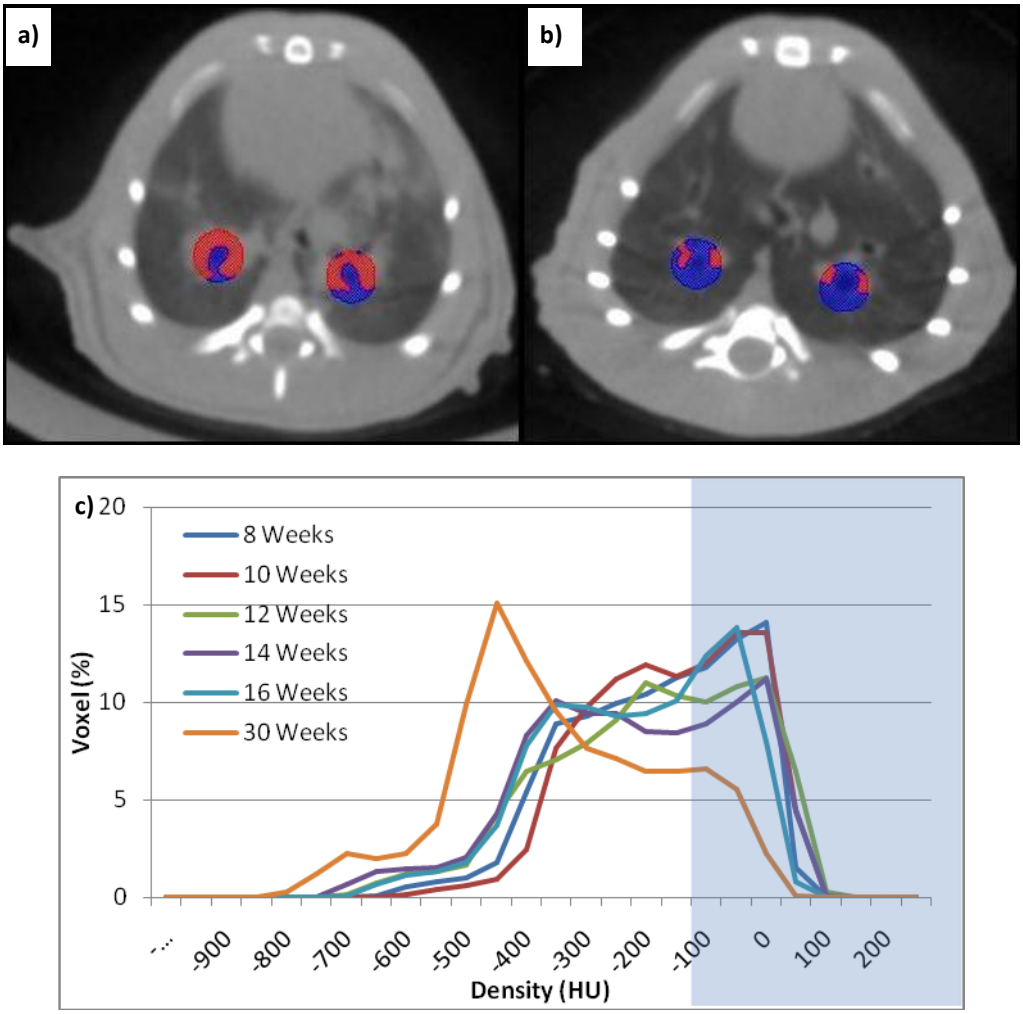

Figure 32. Representative CT from a Sick BN Rat Illustrating Resolution of Peribronchial Densities Over 30 Weeks. Blue area denotes values between -100 HU and -200 HU while red denotes values >-200 HU. **a)** 28.8% voxels at baseline (8 weeks), **b)** Resolution to 7.9% voxels at 30 weeks, and **c)** CT density distribution as percent voxels. Blue box: >-100 density threshold. HU: Hounsfield units.

9.4.4.2 Histopathology

Histopathology showed that all rats with minimal to mild pneumonitis had inflammatory cells present in the perivascular interstitium (Figure 33). This was suggestive of an active inflammatory process in the preceding weeks. Additionally, many animals expressed multifocal, eosinophil-rich necrotizing and granulomatous pneumonitis

where severe, localized inflammatory lesions were discovered within the lung lobes. Many of the lesions were believed to be the same in origin and in etiology due to the rich presence of eosinophils, epithelioid macrophages and syncytiae (Figure 34).

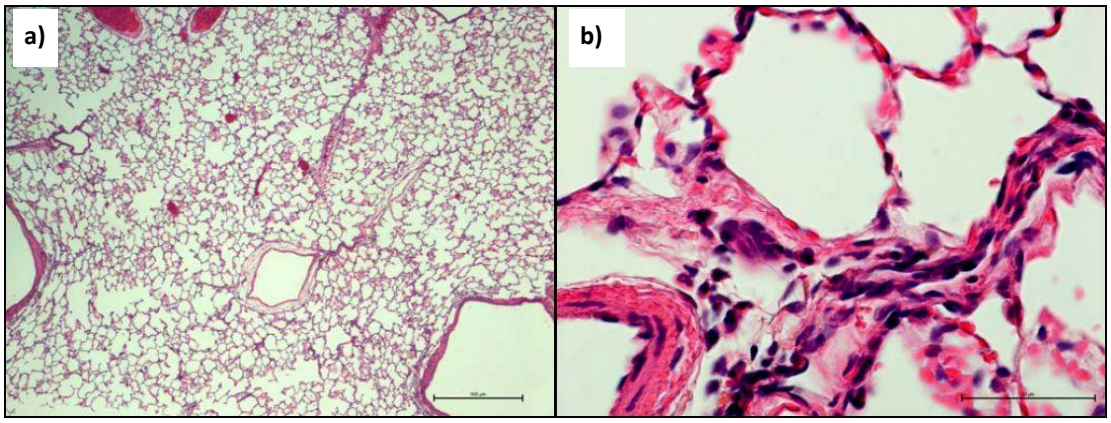

Figure 33. Representative mild pneumonitis in a female BN rat left lobe. Presence of inflammatory cells in the perivascular interstitium. **a)** 2X magnification and **b)** 60x magnification.

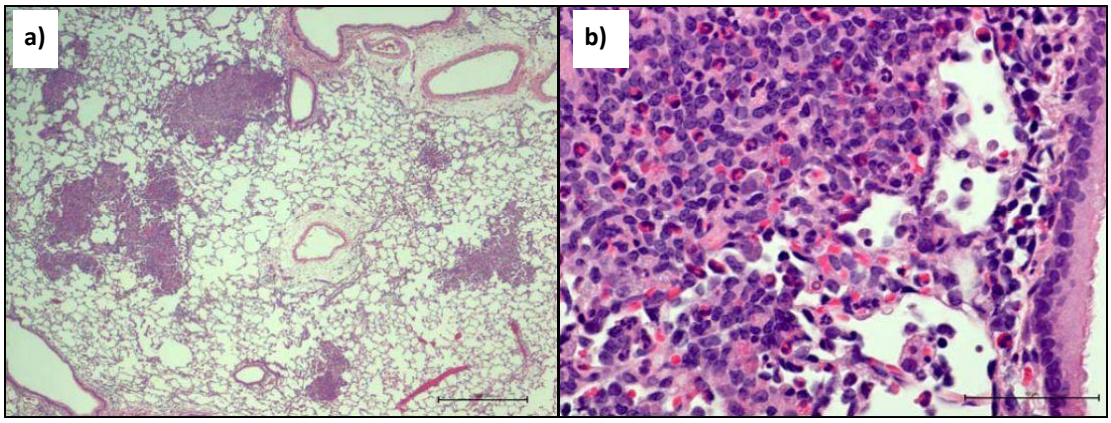

Figure 34. Representative multifocal, eosinophil-rich necrotizing and granulomatous pneumonitis in a female BN rat left lobe. Severe and localized inflammatory lesions **a)** 2X magnification and **b)** 60x magnification.

9.4.4.3 CT and Histology Correlation

The Spearman rank order correlation test showed a correlation of 0.76 between the CT airway densitometry and histology findings ($p<0.02$, Figure 35). CT densitometry had 100% sensitivity and 60% specificity in the assessment of this phenomenon.

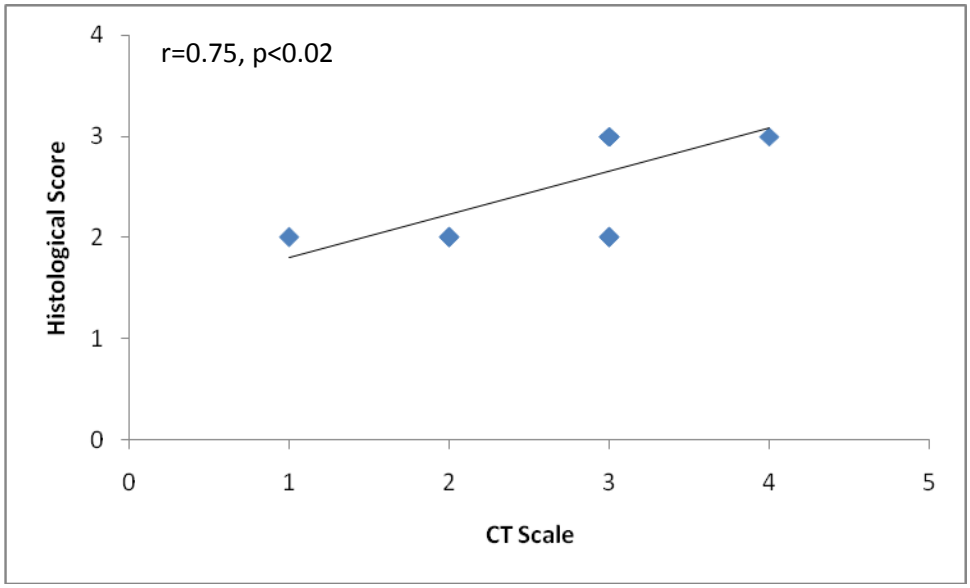

Figure 35. Correlation of CT and histology scoring in the progression and regression of mutifocal, eosinophil-rich necrotizing and granulomatous pneumonitis.

9.4.5 *Discussion and Conclusion*

CT densitometry was able to detect the inflammation of minimal and mutifocal, eosinophil-rich necrotizing and granulomatous pneumonitis found in Brown Norway rats. Visual inspection of histology showed inflammation located where CT densitometry scoring correlated with histological evidence of mutifocal, eosinophil-rich necrotizing and granulomatous pneumonitis. The CT scanning system based on the percent voxels >-100HU had a 100% sensitivity and 60% specificity in the detection of spontaneous

granulomatous pneumonitis. Three rats with mild pneumonitis assessed by histology did not correlate with the CT findings. This may be the result of the airway segmentation method used; CT density was measured around the major airways, while pathology investigated slices of the entire lung.